令和 4 年度　博士論文

Preparation of TiO_2-based thin films with improved photocatalytic activity and super-hydrophobicity by plasma-enhanced chemical vapor deposition

（プラズマ CVD 法による高い光触媒活性と超疎水性を有する TiO_2 薄膜の作製）

指導教員: 島田　学　教授

Supervisor: Manabu Shimada

Graduate School of Engineering Hiroshima University

Department of Chemical Engineering

Lang Jianghua

2022 年 9 月

Abstract

The plasma enhanced chemical vapor deposition (PECVD) process is a practical method in film deposition thanks to its simple operation step and relatively low cost. TiO_2 films with photocatalytic activity have been successfully deposited by PECVD method. In addition, different functional materials can be deposited with TiO_2 simultaneously by PECVD method. By introducing foreign materials, the TiO_2-based composite exhibits improved and new properties. In this dissertation, efforts have been made to improve the photocatalytic activity of TiO_2 thin film. In addition, a TiO_2 composite film with super-hydrophobic surface was fabricated by introducing a polymer.

Chapter 1 demonstrated the background, motivation, review of previous research and objectives of this research.

In Chapter 2, a TiO_2-CNT-Ag ternary composite film was successfully synthesized using the PECVD by simultaneously feeding a carbon nanotube (CNT)/Ag nanoparticle suspension and titanium tetraisopropoxide (TTIP) gas. Here, Ag nanoparticles were prepared from $AgNO_3$ solution by a co-precipitant in advance. During deposition, CNT/Ag suspension was spray-dried to generate those nanoparticles. The obtained CNT/Ag nanoparticles were fed with TTIP simultaneously. The as-prepared film was determined by scanning electron microscopy (SEM), transmission electron microscopy (TEM), energy-dispersive X-ray spectroscopy (EDS), X-ray photoelectron spectroscopy (XPS), X-ray diffraction (XRD), and ultraviolet (UV)-visible spectroscopy. Moreover, the Ag/Ti ratio of the film was confirmed using an inductivity coupled plasma optical emission spectrometer. The performance of the TiO_2-composite film for the degradation of Rhodamine 6G under simulated solar light irradiation was evaluated. The ternary structure that CNT and Ag nanoparticles were embedded into

TiO_2 matrix was confirmed. The rate constant of the prepared TiO_2-CNT-Ag for Rhodamine 6G degradation was approximately 1.8 times that of prepared TiO_2. This result indicates that the addition of CNT and Ag significantly improved the photocatalytic activity of the prepared films.

In Chapter 3, a TiO_2-Ag nanoparticle composite films by PECVD using a mixture of aerosolized droplets of $AgNO_3$ solution, which was used as an Ag nanoparticle precursor, and TTIP, which acted as the TiO_2 precursor. Notably, the use of PECVD eliminated the need of pre-preparing Ag nanoparticles, thus increasing the process efficiency. The structures and morphologies of the deposited films were characterized by UV-visible spectroscopy, XRD, XPS, SEM, TEM, and EDS, and the effects of the raw material concentration on the photocatalytic activity of the deposited films were determined by assessing the degradation of methylene blue under UV-light irradiation. The Ag ions were successfully reduced to metallic nanoparticles and embedded in the TiO_2 film, and the best photocatalytic activity was achieved for a TiO_2 composite film prepared by 1wt% $AgNO_3$. Importantly, the photocatalytic activity was 1.75 times that of pristine TiO_2.

Chapter 4 presents the deposition of a super-hydrophobic hybrid TiO_2/Polydimethylsiloxane (PDMS) film by supplying PDMS and TTIP vapor via PECVD method. Two different experimental conditions are performed to fabricate the composite film. It is worth noting that no curing agent was used in this work to immobilize the polymer. The prepared composite films were characterized by SEM, TEM-EDS, FTIR, XPS, and XRD. The hydrophobicity was estimated by recording the water droplets staying on the film surface using a digital microscope. The photocatalytic activity of the composite films was determined by MB degradation under UV light irradiation. The TiO_2/PDMS composite films prepared under one condition shows

almost identical photocatalytic activity with TiO_2 film, about 29% MB was degraded after 6 hours. However, many products lost their super-hydrophobicity. Under another condition, a TiO_2/PDMS composite film with durable super-hydrophobicity was obtained. And the composite film degrades 16% MB under UV light irradiation.

Chapter 5 summarizes the content of this dissertation. Suggestions for future research in film fabrication by PECVD method are also proposed.

Contents

Contents

Chapter 1

Introduction

1.1 Introduction of photocatalysts

The progress of technology drives the progress of human society, improving the ability to utilization of natural resources, and enabling human life to become more and more convenient. However, human activities have also caused severe environmental pollutants. Especially, water pollution has become an urgent problem to be solved. Numerous organic pollutants are being released from manufacturers such as textile, paint, and leather into water bodies. The aquatic systems and human health may be seriously affected by these organic effluents, which are extremely difficult to be degraded or eliminated by nature. Sustainable Development Goal (SDG) 6 is to ensure the availability of water and sustainable management of water and sanitation for all. To achieve this goal, environmentally friendly, affordable, reliable, sustainable, and modern water treatment technologies are required to be developed. Photocatalysis, which can utilize solar energy to degrade pollutant, is one of the promised technologies. The term “photocatalysis” is the acceleration of a photoreaction in the presence of a catalyst (Spasiano *et al.*, 2015).

A wide range of photocatalysts was developed. Transition-metal oxide and their composites, like TiO_2 (Yan *et al.*, 2012), ZnO (Chen *et al.*, 2017; Tian *et al.*, 2012), WO_3 (Fu *et al.*, 2015; Loka *et al.*, 2021; Song *et al.*, 2010), and SnO_2 (Chu *et al.*, 2011; Huang *et al.*, 2014; Lin *et al.*, 2012; Yuan *et al.*, 2010) are able to be active under solar irradiation and produce photoinduced electron. This ability was regarded as the key factor during the photocatalytic process. Among the above-mentioned transition-metal oxide materials, TiO_2 is notable because of its chemical stability, nontoxicity, and high

photocatalytic activity (Li *et al.*, 2019; Sobczyk-Guzenda *et al.*, 2015).

1.2 TiO_2-based photocatalysts

1.2.1 Photocatalysts

Fig. 1.1 is the common opinion of the schematic that is used for explaining photocatalysis in literature (Chong *et al.*, 2010). Photocatalytic activity was initiated when light irradiation energy is matching or greater than the bandgap (E_g) of semiconductor. The electrons (e^-) on valence band (VB) are excited to conduction band (CB) and leaving positive holes (h^+). The holes and electrons promote the reduction and oxidation, respectively, of different substance (absorbed O_2 and H_2O on TiO_2 surface). This process results in the formation of powerful oxidizing agents, like ·OH and O_2^-. These radicals play a crucial role in organic decomposition.

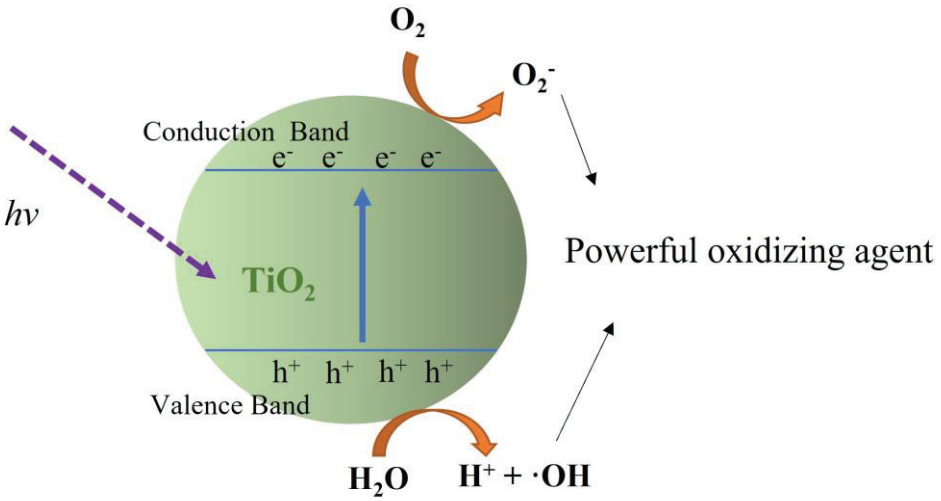

Fig. 1.1 Photo-induced mechanism of electron-hole pair in TiO_2 particle with powerful oxidizing agents.

However, its photocatalytic activity is limited by the following factors. First, due

to the large band gap (3.2 eV) of TiO_2 (anatase phase), its photocatalytic activity can be initiated only under ultraviolet light irradiation (3%–5% of the total solar spectrum) (Rapsomanikis *et al.*, 2014; Varshney *et al.*, 2016). Second, the fast recombination of electron–hole pairs results in low efficiency for photocatalytic activity (Lee *et al.*, 2005). These two challenges attract considerable attention and promote a broad range of researchers to develop heterojunction materials. Various heterojunction materials have demonstrated advantages properties such as fast charge separation, favorable electron transfer (Zhu *et al.*, 2022), hindering of electron-hole recombination (Hieu *et al.*, 2021), and a high surface area (Hao *et al.*, 2016). Hence, TiO_2-based heterojunction materials have attracted considerable attention for their improved photocatalytic activity.

Besides the research on photocatalytic activity improvement of TiO_2, efforts have been made on different applications of TiO_2. The wetting properties of droplets on TiO_2-formed surfaces can be switched under light inducing (Xu *et al.*, 2013). It becomes hydrophilic after UV light irradiation and reversible after storage in dark or heat treatment. Thus, the fabrication of TiO_2 hybrid surfaces with stable hydrophobicity gained increasing interest in recent years. These surfaces have been used in a wide range of applications, like building materials, oil-water separation, and metal protector.

1.2.2 TiO_2-based photocatalysts

Researchers have already successfully improved the TiO_2 photocatalytic activities by utilizing various materials. Especially noble metals, such as Ag, Au, Cu and non-metals such as nitrogen (N), carbon nanotubes (CNTs) are popular and common materials to collaborate with TiO_2, which can increase its capacity for visible light absorption or its reactivity in the UV spectrum (Basavarajappa *et al.*, 2020).

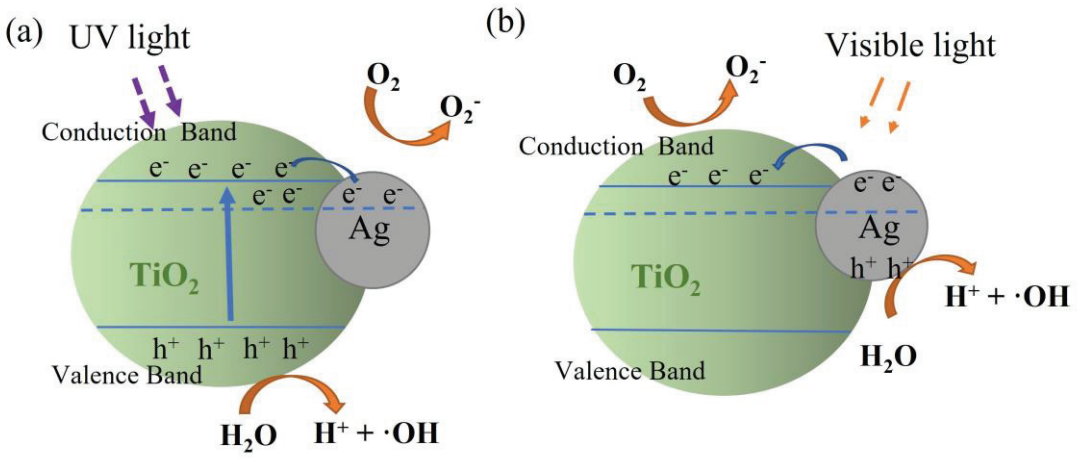

Fig. 1.2 The possible schematic of electron-hole pairs generated in TiO_2-Ag composite: (a) under UV light irradiation; (b) under visible light irradiation.

The optical properties of TiO_2 can be significantly influenced by using noble metal nanoparticles. The noble metal nanoparticles (such as Ag, Au) exhibit the localized surface plasmon resonance (LSPR) effect, which can contribute to visible light absorption after being coupled with TiO_2 (Al-Hajji *et al.*, 2020; Herderick *et al.*, 2007; Jiang *et al.*, 2012; Yang *et al.*, 2015). Among all the noble metals, Ag was a reliable candidate in terms of its relative stability, low cost, resource abundance, and nontoxic compared to other noble metals (Wang *et al.*, 2016). Researchers believe Ag nanoparticles can produce electron-hole pairs under visible light due to LSPR. The strong electron oscillating collectively on the LSPR excitation can overcome the Schottky barrier (formed on the interface between TiO_2 and Ag), thus allowing the electrons transfer from noble metal to CB of TiO_2 (Liu *et al.*, 2015). Moreover, TiO_2 can be excited under UV light irradiation and form electrons and holes on VB and CB, respectively. The CB energy level of TiO_2 is still higher than the fermi level of metal, so that electrons on CB can transfer to metal. The formation of the Schottky barrier on the interface of TiO_2 and Ag prevents the recombination of electron-hole pairs, thereby

enhancing the photocatalytic activity. Fig. 1.2 demonstrate the possible schematic of electron-hole pairs generated in TiO_2-Ag composite under different light source.

By forming an intermediate energy level between the CB of dopants and the CB of TiO_2, using non-metal, such as CNTs and nitrogen is another viable approach to improve the photocatalytic activity of TiO_2. Especially, CNTs is well-known for its unique structure, electrical, thermal and chemical properties (Koo *et al.*, 2014). It is noticed that CNTs were found to have synergistic effects in organic degradation when collaborating with TiO_2 (Cao *et al.*, 2013), which helps to enhance electron-hole separation (An *et al.*, 2007). Nevertheless, different photocatalysts mechanisms of TiO_2/CNT were reported (Woan *et al.*, 2009). The common idea believes CNTs serve as the electron scavenger when the excited electrons transfer from the conduction band of TiO_2 to CNTs, as shown in Fig. 1.3 (a). Some researchers argued that CNTs can act as photosensitizer in composite. In this model, CNTs donate the electrons to CB of TiO_2, instead of accepting the electrons from CB of TiO_2. After that, positively charged CNT attracts the electron from the VB of TiO_2, as shown in Fig. 1.3 (b). Furthermore, researchers also confirmed the existence of Ti-O-C bonds, which allows the light absorption towards to longer wavelengths, herein improved the photocatalytic activity of TiO_2 (Pyrgiotakis *et al.*, 2005), as shown in Fig. 1.3 (c).

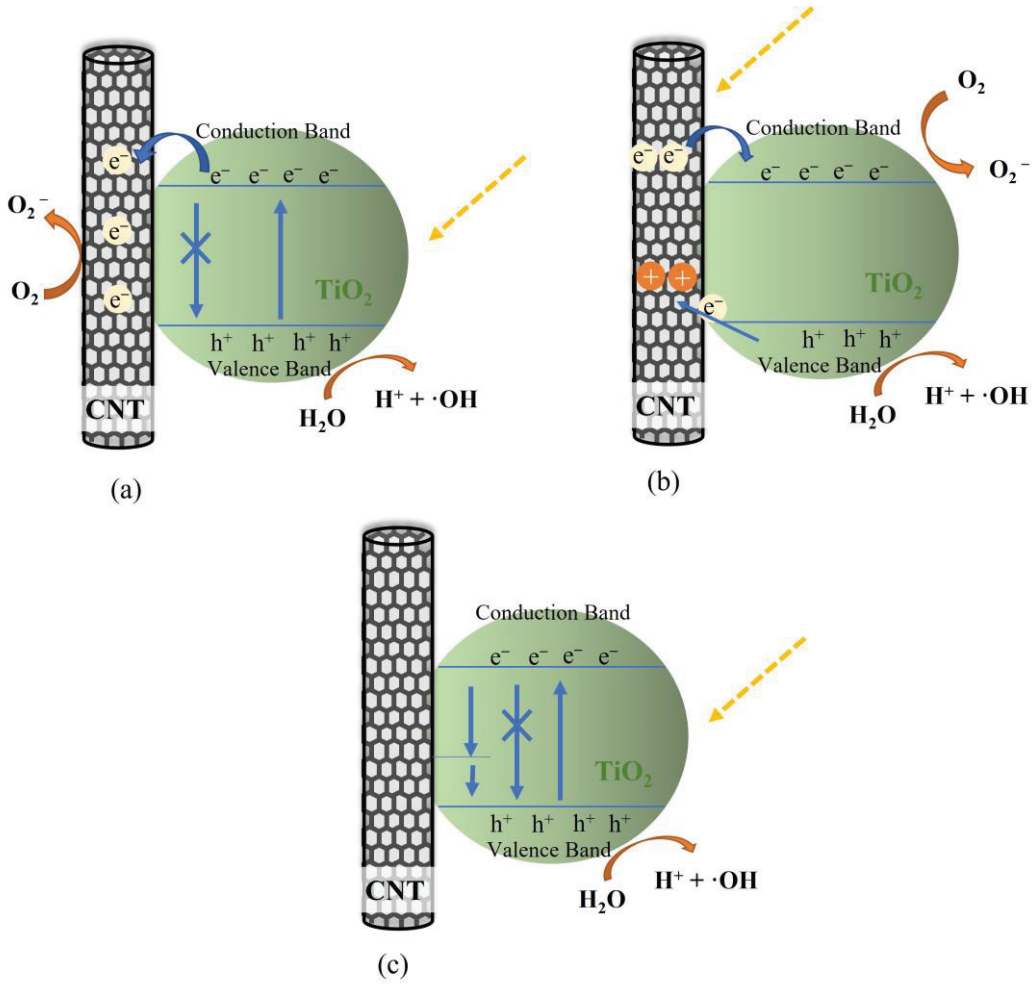

Fig. 1.3 The proposed mechanism of CNT driven improvement of photocatalytic activity: (a) CNTs act as an electron acceptor, prevent the electron-hole pair combination; (b) CNTs were regarded as a photosensitizer, generate the electron-hole pair; (c) The formation of Ti-O-C bonds.

1.2.3 TiO_2-based photocatalysts with super-hydrophobicity

The super-hydrophobic phenomenon is common in nature, which allows the water droplets rolling off the surface and take away the contaminants. However, this property becomes invalid when dealing with some organic pollutants. Photocatalysts can degrade pollutants and promise the recovery of super-hydrophobic properties.

The surface interacts with water is evaluated by measuring the contact angle

between them, as shown in Fig. 1.4. Generally, super-hydrophobic surfaces are defined as water contact angle above 150°. According to the literatures, the key factors in forming a super-hydrophobic surface are concluded as low surface energy and multiscale structure (Wang *et al.*, 2021; Wang *et al.*, 2019). Thus, the common strategies to fabricate super-hydrophobic surfaces are preparing a rough structure by low surface energy materials directly or preparing a rough structure using low surface energy as a modification. Alkyl and fluorinated alkyl groups, like CH_3 and CF_3 are typical groups that have a low energy of interaction with water (Crick *et al.*, 2010). The hydrophobic properties of polydimethylsiloxane (PDMS) have been reported and its chemical inertness is crucial for the resulting material (Wang *et al.*, 2019).

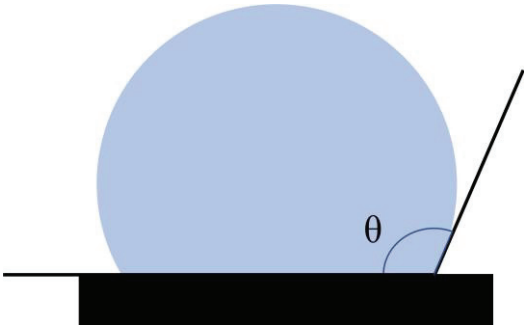

Fig. 1.4 The schematic of contact angle between the droplet and substrate.

1.3 Film deposition method

A catalyst film sometimes overcomes some drawbacks encountered with powder. For example, the form of film (1) eliminates the need for catalyst separation and filtration, (2) enables application in continuous flow systems, and (3) reduces agglomeration at various catalyst loadings (Arabatzis *et al.*, 2003; Lang *et al.*, 2022). Thus, the technologies for immobilizing the photocatalyst into the form of film draw considerable attention. Various film deposition methods have been developed which

can be classified as physical vapor deposition (PVD), Chemical vapor deposition (CVD) and solution-based chemistry. Some common preparation methods are illustrated in Fig. 1.5 (Ukoba *et al.*, 2018).

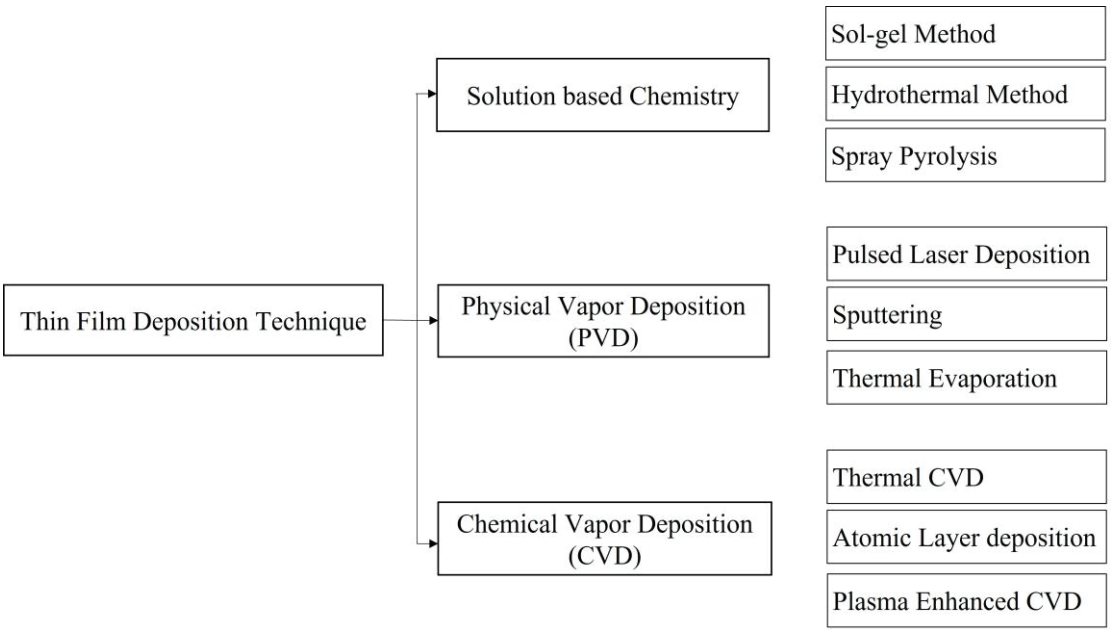

Fig. 1.5 Simple classification of some common thin film preparation method.

1.3.1 Solution-based chemistry method

1.3.1.1. Sol-gel Method

Sol-gel method was also named soft chemistry. During the process, a sol or a gel as an intermediate reactive was produced by hydrolysis and condensation from the solution precursor. Then, evaporation and heat treatment methods enable the dense ceramic to be obtained from a gel (Znaidi, 2010). Utilizing the matter transformation in this process, the sol can be immobilized on the substrate by spin coating or dip coating, resulting in a thin film.

Nanostructured titania thin films were prepared by sol-gel combinate with dip coating method (Simonenko *et al.*, 2016). A titania precursor was fabricated by using

titanium butoxide, acetylacetone, *n*-butanol and ethanol. Then, the film was formed by applying the precursor to the silica substrate via dip-coating method. The hydrolysis and polycondensation were proceeded for 60 min under air to generate the three-dimension network. A crystallized titania film was obtained after heat treatment.

1.3.1.2 Hydrothermal Method

Hydrothermal method has been widely used in recent years, which is simulated the formation of some minerals and rocks in nature. A steel pressure vessel, also called autoclave, is always used as the reactor, where the reaction process can be performed under controlled temperature and/or pressure (Yang *et al.*, 2019). In addition, stable crystalline phase films can be formed by hydrothermal treatment of a substrate solution impregnated with the substrate.

Using the hydrothermal method, Wu *et al.* (2015) grew a high-quality ZnO thin film on sapphire. In this process, ZnO buffer layer on a c-sapphire substrate is prepared by radio-frequency molecular beam epitaxy. The obtained samples were submerged in an aqueous solution of $Zn(NO_3)_2$ and HMTA in a Teflon holder. Hydrothermal process is carried out under 75 ℃ for 4 h. As a result, a large-area film with smooth surface was synthesized on a sapphire substrate.

1.3.1.3 Spray pyrolysis

Spray pyrolysis is becoming popular in thin film deposition. Spray pyrolysis entails spraying target solutions on a heated surface to form the film. The constituents of the film then react to generate a chemical compound. The chemical reactants are chosen so that undesirable products breakdown pyrolytically at the deposition temperature. In addition, ultrasonic, electrostatic and air blast are always selected as the

atomizer for the spay method.

Deyu *et al.* (2019) achieved the Al-doped SnO_2 film deposited by ultrasonic spray pyrolysis. An $SnCl_4 \cdot 5H_2O$/methanol solution was employed as the precursor. In addition, different aluminum precursor was also added in a certain concentration. Assisted by a homemade ultrasonic spray pyrolysis deposition system, the different precursor was deposited on substrates. The process was carried out under 500 ℃. The aluminum doped SnO_2 thin films with small grain size were obtained.

1.3.2 Physical vapor deposition (PVD) method

Physical vapor deposition (PVD) has been widely used in thin film deposition. Every PVD process involves three basic steps: (1) the vapor phase species creation, (2) vapor phase species transportation and (3) film growth or deposition on a substrate. In this method, the conversion of materials from solid-phase to vapor-phase can be achieved by thermal evaporation, sputtering (Abegunde *et al.*, 2019).

1.3.2.1 Thermal Evaporation

In an evaporation process, a vapor is created by heating the target materials to very high temperature, following transport of the vapor to the substrate in a vacuum. A thin film is obtained after the vapor is condensed on the substrate.

Luo *et al.* (2016) reported a PVD system for CdTe film deposition. The system pressure was maintained at about 0.9 kPa, the temperature for vaporizing CdTe powder was about 700 ℃, and the temperature of substrate was 460 ℃. Since the different temperatures between the substrate and CdTe vapor, the recrystallization occurred on the substrate. Consequently, a polycrystalline with a cubic structure film was achieved.

1.3.2.1 Sputtering

In a sputtering process, a vapor source was created by high energy ion bombardment on the target. Because of the potential difference between the negatively biased target (cathode) and a node, inert gas, most often argon gas, was charged and accelerated. The contact of the ions with the surface of the target causes the ejection of atoms that condense on a substrate to form a film (Sarakinos *et al.*, 2010).

Gao *et al.* (2004) introduced a ZnO thin films deposited in a magnetron sputtering. The deposition process was carried out in approximately 2×10^{-6} Torr. Argon was introduced into the chamber. Sputtering was performed with direct current power of 0.25 A for direct deposition form ZnO target. The resulting films have a high crystal quality and a big grain size.

1.3.2.3 Pulsed Laser deposition

Primarily, pulsed laser deposition involves focusing a high-powered laser beam on a revolving target within a vacuum chamber. Because of the high energy of the focus beam, the chemical bonds in the target were broken, which caused the particles (ions, electrons, atoms, radicals, or clusters) to "escape" from the target. After making contact with the substrate, these particles become adhered to it. Both diffusion and aggregation of particles can lead to the formation of these films (Vanalakar *et al.*, 2015).

A NiO thin film was generated using pulsed laser deposition on Si substrate (Fasaki *et al.*, 2010). The reactive pulsed laser deposition experiments were carried out in a stainless-steel vacuum chamber. Pulses with certain laser fluence was focused on the surface of Ni targets. The films grow on the Si substrates with a thermally oxidized layer of Si substrate. A film with constant thickness and less grain boundaries was deposited by controlling the substrate temperature.

1.3.3 CVD method

CVD method is a powerful technique for film deposition. It basically starts from the evaporation and activation of raw materials. Then one of two types of reactions can occur: homogeneous gas-phase reactions, which take place in the gas phase, and heterogeneous chemical reactions, which take place on/near a heated surface. After that, a film is generated on a suitable substrate (Munoz *et al.*, 2013). Thermal, laser, and plasma is common energy source for chemical reactions.

1.3.3.1 Thermal CVD

Thermal CVD (TCVD) requests the substrate to be heated to high temperature, therefore meeting the energy needed for reaction. The mixture gases including reactants and carrier gas were fed into the reaction chamber, followed by the reaction taking place and the deposition started.

Tang *et al.* (2014) reported a TCVD method for the preparation of TiO_2 coating. The $TiCl_4$ vapor was fed into the reactor with carrier gas and reactant. The film was generated with the substrate temperature upper 650 ℃. The resulting films consist of small particles and island structures.

1.3.3.2 Atomic layer deposition

Atomic layer deposition (ALD) has emerged as a widely used surface technology, which can also be regarded as pulsed CVD. Most ALD is based on the sequential alternating pulses of precursor that react with the substrate (Johnson *et al.*, 2014). For one cycle, only a finite number of reactants are allowed to be deposited on the substrate, which restricts each cycle deposit a single layer. Hence, the different cycles can be performed sequentially to deposit thickness-desired thin film.

Aaltonen *et al.* (2011) reported a Li_2O-Al_2O_3 thin film deposited by ALD. Two different alternate pulsing of precursor, trimethyl aluminum and O_3, LiOtBu and H_2O were supplied sequentially. The Al_2O_3 thin layer was generated as the base layer for Li_2O-Al_2O_3 composite film.

1.3.3.3 Plasma enhanced CVD

Plasma enhanced CVD (PECVD) is a popular technique since it inherits the benefits of CVD technology and enables the film deposition at lower temperatures. In PECVD, the temperature of a chemical initiator was instead by the free plasma radicals. These plasma radicals in the reactor chamber can decompose the precursor even at a low temperature and leads to the deposition of thin film.

Borras *et al.* (2009) reported a PECVD method for the growth of TiO_2 thin films. The Ar/O_2 gas was employed to generate the plasma with a power of 400 W. Titanium isopropoxide (TTIP) was supplied as a precursor. A TiO_2 film in the form of anatase was prepared by PECVD. The growth of the film can be described in four stages: nucleation, coalescence, column formation and column development, which is also named as Kolmogorov model.

1.3.4 Advantages and limitations of film deposition method

The preparation method and processing conditions play an essential role in morphologies and properties of the thin film. Thus, a proper method is necessary to meet the requirement. Here, the advantages and limitations of the mentioned method are summarized.

The sol-gel method is a controllable method that allows the deposition of large-area films with good reproducibility. However, the requirement of a long period and

relatively high temperature limits its application in film preparation. The hydrothermal method can produce a film with high crystallinity. However, the processes are difficult to control since it happens in an autoclave. The spray pyrolysis is a simple, cost-effective method. However, it is a challenge to deposit the film with uniform thickness.

The thermal evaporation PVD method is suitable for any metal materials, but the disadvantages such as high cost cannot be ignored. The sputtering deposition ensures the high quality of the film. However, the effect of ionic bombardment on the substrate during deposition must be considered. PLD is another simple method to deposit thin metal films. But the emission of particulates from target is the main drawback of this method.

TCVD method has some advantages such as producing a film with desired morphology and high durability. However, the requirement for high deposition temperature needs to be addressed. ALD method is exceptionally effective at depositing multilayer films with excellent adhesion. However, ALD is facing challenges like high materials waste rate. PECVD is suitable for deposition on multicomponent film in a high deposition rate and relatively low cost. However, it also faces the high materials waste rate.

1.4 Reviews of materials reported in the dissertation

1.4.1 Preparation of TiO_2-CNT-Ag ternary composite films

As mentioned in 1.2.2, CNT and Ag are reliable materials to improve the photocatalytic activity of TiO_2. Researchers found that a ternary structure utilizing CNT, Ag, TiO_2, has been proved to be more efficient than not only pristine TiO_2 but also TiO_2-based (Ag or CNT) binary structure. It is noticed that different processes always lead to different ternary structures.

Zhao *et al.* (2020) fabricated the CNTs-Ag-TiO_2 (CAT) ternary structure composite using $AgNO_3$, TiO_2 precursor and CNTs via sol-gel method. The ternary structure was obtained from three steps: functionalization and activation of CNTs; Ag nanoparticles are coated on treated CNTs by reduction of $AgNO_3$ solution; and TiO_2 nanoparticles are fabricated from precursor by sol-gel method and consequently wrapped on binary composite. The structure can be described as follows: CNT was wrapped by TiO_2 nanoparticles and Ag nanoparticles. Compared to pristine TiO_2 and CNTs-TiO_2, CAT ternary structure composite exhibits a better photocatalytic activity under visible light.

The ternary structure that CNTs decorated by TiO_2/Ag composite particles has been reported several times (Koo *et al.*, 2014; Mohammad *et al.*, 2019). In these methods, Ag doped TiO_2 nanocomposites were first prepared by reducing $AgNO_3$ where TiO_2 or TiO_2 precursor existed. Then ternary composite was fabricated by attaching this nanocomposite to activated CNTs. Moreover, Ag@TiO_2 core shell nanoparticles attached to CNTs are reported by Yang *et al.* (2014). The Ag@TiO_2 core shell can be achieved by adding Ag nanoparticles into TiO_2 precursor. Different ternary structures exhibit unique properties. However, the photocatalytic activity depends on many factors. Thus, it is a challenge to judge a composite by structure only.

It is noticed that the mentioned ternary structure can be concluded as CNTs-supported nanocomposite powders. A catalyst film sometimes overcomes some drawbacks encountered with powder. Therefore, it is valuable to fabricate a ternary composite film by utilizing TiO_2, CNT, Ag. In addition, the choice of a suitable deposition method is important for film deposition. PECVD method is suitable for the preparation of multicomponent film in a simple operation. Thus, the TiO_2-CNT-Ag ternary composite film can be deposited by PECVD method.

1.4.2 Preparation of TiO_2-Ag from $AgNO_3$ reduction

Several methods have been applied for preparing Ag/TiO_2 photocatalysts by using pure Ag or Ag precursors. Pure Ag is generally utilized in PVD method. Kim *et al.* (2015) fabricated TiO_2/Ag/TiO_2 multilayer thin films using pure Ag target via sputtering method. Kusdianto *et al.* (2017) deposited a TiO_2-Ag nanocomposite film by vaporizing the Ag granules in a PVD-PECVD system. Sliver precursor, generally silver nitrate ($AgNO_3$) is a more common Ag source of TiO_2-Ag composite. It has been widely utilized in chemistry methods. In these methods, Ag nanoparticles can be obtained from the Ag^+ by reducing agents, like sodium citrate, ascorbate and borohydride.

Nevertheless, plasma reduction method has been reported to reduce the metal ions without using any reducing agent. Mariotti *et al.* (2012) synthesized Au from $HAuCl_4$ aqueous by an atmospheric pressure plasma-liquid interactions system. In this system, He gas plasma was generated above the aqueous and then formed a plasma-liquid interface. The electrons can be injected into $HAuCl_4$ aqueous from plasma. In this process, injected electrons are considered as the reduction species to produce the metallic Au.

Gallingani *et al.* (2020) recently obtained the metallic Ag by plasma conversion of

$AgNO_3$ liquid aerosol droplets. The $AgNO_3$ aqueous solution was carried into plasma reactor by Argon gas. The precursor reacts with plasma species inside the droplets, which causes the conversion of $AgNO_3$ to metallic Ag. Since that, preparation of TiO_2-Ag composite films by supplying $AgNO_3$ aqueous directly via PECVD process are considered to be feasible.

1.4.3 Preparation of super-hydrophobic TiO_2/PDMS composites.

TiO_2 is known as a photo-induced hydrophilic material when exposed to UV light. The vacancies are formed when the oxidation reactions happen on TiO_2 surface. These vacancies will absorb the OH groups, leading to a super-hydrophilic behavior of TiO_2 surface (Neves *et al.*, 2020). However, the super-hydrophobic property is more favorable in some applications such as water-oil separation, self-cleaning and surface protection. Table 1.1 illustrates some specific applications of TiO_2-based hydrophobic material.

Table 1.1 Application of TiO_2-based composite with super-hydrophobicity

Substrate	Preparation process	Application	Reference
Filter paper	The super-hydrophobic paper was obtained by adhering the bonded TiO_2 particles with coating low energy materials.	Oil-water separation	(Gao *et al.*, 2015)
Dionysos and Thasos marbles	A sol prepared by using TEOS, TTIP and PDMS was brushed on a EtOH impregnated marble surface.	Self-cleaning marble	(Kapridaki *et al.*, 2013)
Bricks	A sol was obtained by mixing TiO_2,	Building	(Alfieri *et*

	SiO_2 and Dynasylan® F 8815, before brushed on the bricks.	preservation	*al.*, 2017)
Cotton fabric	PDMS, N-doped TiO_2 particles were mixed and coated on cotton fabric by dip-coating method with ultrasonication.	Self-cleaning textile	(Pakdel *et al.*, 2021)
Steel	A suspension contains polyaniline TiO_2 hierarchical composite particles were added dropwise on steel and dried at room temperature.	Surface anticorrosion	(Huang. *et al.*, 2020)
Marble	A TiO_2 powder was dispersed in different hydrophobic organic material. The mixture was applied on the Carrara marble.	Cultural heritage protection	(La Russa *et al.*, 2016)

Different materials have been utilized in hybrid composites with hydrophobic properties. Among them, silicones with methyl groups are industrial compatible materials for their chemically inert and resistant to harsh environments. Different processes have been developed to fabricate the TiO_2/PDMS composite films. Tavares *et al.* (2014) reported a TiO_2/PDMS nanocomposite film prepared by mixing the TiO_2 with a PDMS-polymerizing agent-hexane mixture, before spraying on glass slides. Liu *et al.* (2019) reported a PMDS-grafted TiO_2 prepared in two steps, including preparing TiO_2 film by spin coating and grafting the PDMS on the TiO_2 surface under UV illumination. The mentioned methods usually rely on multi-step and time-consuming processes necessary for nanoparticle synthesis or functionalization. Thus, develop a

simple method is available for the fabrication of TiO_2/PDMS thin film.

1.5 Objectives and outline of the dissertation

In the study of this dissertation, different raw materials such as solid particles, aqueous solution, and polymer, were employed to be co-deposited with TiO_2 by plasma-enhanced chemical vapor deposition (PECVD). The main objectives of this dissertation are: (1) Use CNT/Ag solid nanoparticles to fabricate TiO_2-CNT-Ag ternary composite films with improved photocatalytic activity. (2) Fabricate TiO_2-Ag binary composite films in a simple process by using $AgNO_3$ aqueous directly. (3) Fabricate TiO_2/PDMS composite films with super-hydrophobic and photocatalytic activity. This dissertation was divided into 5 chapters as shown in Fig. 1.6. The brief objectives in Chapters 2-5 are shown below.

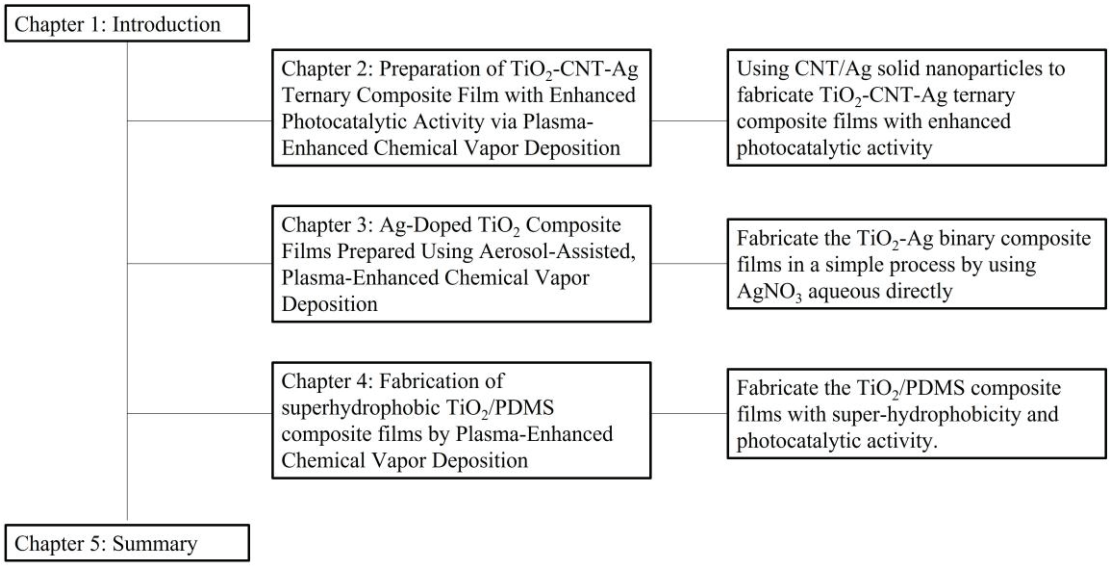

Fig. 1.6 Diagrammatic illustration of the brief objective of dissertation.

In Chapter 2, the TiO_2-CNT-Ag ternary composite films were fabricated by PECVD method. Researchers have already improved the photocatalytic activity of TiO_2

by using CNT and Ag. However, CNTs are always used as the support material for coating with TiO_2 and Ag nanoparticles. Few researchers have focused on preparing TiO_2-based composite films, utilizing TiO_2, Ag and CNTs. Among the film deposition method, PECVD has demonstrated superiority in the preparation of multicomponent films. Thus, the PECVD method is employed to fabricate TiO_2-CNT-Ag ternary composite films. In the preparation process, aqueous suspensions of CNTs and Ag nanoparticles were spray-dried to obtain aerosol particles of these solid materials. The particles were supplied into a PECVD reactor, where a TiO_2 film is prepared from titanium tetraisopropoxide vapor. The ternary structure will be described by morphology, chemical compounds, and crystal. The photocatalytic activity of as prepared composite films was evaluated.

Chapter 3 introduces a TiO_2-Ag composite film by reducing Ag^+ in PECVD. Previous research introduced that the aerosol droplets of $AgNO_3$ aqueous solution can be reduced to Ag nanoparticles in plasma. Thus, using $AgNO_3$ aqueous solution directly without pre-preparing the Ag nanoparticle is considered to be feasible. During the process, $AgNO_3$ aqueous solution was aerosolized and supplied to the PECVD reactor. In the plasma, Ag nanoparticles were obtained by the reduction of $AgNO_3$, and these were deposited with TiO_2 simultaneously. The morphology and chemical species as well as the photocatalytic activity of TiO_2-Ag was carried out.

The TiO_2/PDMS composite film with photocatalytic activity and super-hydrophobicity was investigated in Chapter 4. TiO_2 is known as a photo-induced hydrophilic material when exposed to UV light. However, researchers found that TiO_2/PDMS composite with hydrophobic properties is favorable in some applications, like self-cleaning surface. The TiO_2/PDMS composite has been generated in various processes. However, the common strategies in fabricating TiO_2/PDMS are the liquid

phase method. It is always related to complex operation steps. Recently, Thongrom *et al.* (2018) obtained PDMS film in a one-step PECVD method. Thus, it is feasible to fabricate the TiO_2/PDMS composite film in PECVD method. According to different experimental ideas, two different experimental conditions were designed to fabricate TiO_2/PDMS composite. The morphology and molecular structure of these composites and their super-hydrophobicity and photocatalytic activity were determined.

Chapter 5 highlights the summary of each chapter. Suggestions for further research on thin film preparation are also proposed.

References

Aaltonen, T., Nilsen, O., Magrasó, A., & Fjellvåg, H. Atomic layer deposition of Li_2O–Al_2O_3 thin films. *Chemistry of Materials, 23*(21), 4669-4675. (2011).

Abegunde, O. O., Akinlabi, E. T., Oladijo, O. P., Akinlabi, S., & Ude, A. U. Overview of thin film deposition techniques. *AIMS Materials Science, 6*(2), 174-199. (2019).

Al-Hajji, L. A., Ismail, A. A., Bumajdad, A., Alsaidi, M., Ahmed, S. A., Almutawa, F., & Al-Hazza, A. Construction of Au/TiO_2 heterojunction with high photocatalytic performances under UVA illumination. *Ceramics International, 46*(12), 20155-20162. (2020).

Alfieri, I., Lorenzi, A., Ranzenigo, L., Lazzarini, L., Predieri, G., & Lottici, P. P. Synthesis and characterization of photocatalytic hydrophobic hybrid TiO_2-SiO_2 coatings for building applications. *Building and Environment, 111*, 72-79. (2017).

An, G., Ma, W., Sun, Z., Liu, Z., Han, B., Miao, S., Miao, Z., & Ding, K. Preparation of titania/carbon nanotube composites using supercritical ethanol and their photocatalytic activity for phenol degradation under visible light irradiation. *Carbon, 45*(9), 1795-1801. (2007).

Arabatzis, I. M., Stergiopoulos, T., Bernard, M. C., Labou, D., Neophytides, S. G., & Falaras, P. Silver-modified titanium dioxide thin films for efficient photodegradation of methyl orange. *Applied Catalysis B: Environmental, 42*(2), 187-201. (2003).

Basavarajappa, P. S., Patil, S. B., Ganganagappa, N., Reddy, K. R., Raghu, A. V., & Reddy, C. V. Recent progress in metal-doped TiO_2, non-metal doped/codoped TiO_2 and TiO_2 nanostructured hybrids for enhanced photocatalysis. *International Journal of Hydrogen Energy, 45*(13), 7764-7778. (2020).

Borras, A., Sanchez-Valencia, J. R., Widmer, R., Rico, V. J., Justo, A., & Gonzalez-Elipe, A. R. Growth of crystalline TiO_2 by plasma enhanced chemical vapor deposition. *Crystal Growth & Design, 9*(6), 2868-2876. (2009).

Cao, Q., Yu, Q., Connell, D. W., & Yu, G. Titania/carbon nanotube composite (TiO_2/CNT) and its application for removal of organic pollutants. *Clean Technologies and Environmental Policy, 15*(6), 871-880. (2013).

Chen, X., Wu, Z., Liu, D., & Gao, Z. Preparation of ZnO photocatalyst for the efficient and rapid photocatalytic degradation of azo dyes. *Nanoscale research letters, 12*(1), 1-10. (2017).

Chong, M. N., Jin, B., Chow, C. W. K., & Saint, C. Recent developments in photocatalytic water treatment technology: A review. *Water Research, 44*(10), 2997-3027. (2010).

Chu, D. R., Mo, J. H., Peng, Q., Zhang, Y. P., Wei, Y. G., Zhuang, Z. B., & Li, Y. D. Enhanced photocatalytic properties of SnO_2 nanocrystals with decreased size for ppb-level acetaldehyde decomposition. *ChemCatChem, 3*(2), 371-377. (2011).

Crick, C. R., & Parkin, I. P. Preparation and characterisation of super-hydrophobic surfaces. *Chemistry–A European Journal, 16*(12), 3568-3588. (2010).

Deyu, G. K., Muñoz-Rojas, D., Rapenne, L., Deschanvres, J.-L., Klein, A., Jiménez, C., & Bellet, D. SnO_2 films deposited by ultrasonic spray pyrolysis: influence of al incorporation on the properties. *Molecules, 24*(15), 2797. (2019).

Fasaki, I., Koutoulaki, A., Kompitsas, M., & Charitidis, C. Structural, electrical and mechanical properties of NiO thin films grown by pulsed laser deposition. *Applied Surface Science, 257*(2), 429-433. (2010).

Fu, L., Xia, T., Zheng, Y., Yang, J., Wang, A., & Wang, Z. Preparation of WO_3-reduced graphene oxide nanocomposites with enhanced photocatalytic property. *Ceramics International, 41*(4), 5903-5908. (2015).

Gallingani, T., Abuyazid, N. H., Colombo, V., Gherardi, M., & Sankaran, R. M. Online ion mobility spectrometry of nanoparticle formation by non-thermal plasma conversion of metal salts in liquid aerosol droplets. *Journal of Aerosol Science, 150*, 105631. (2020).

Gao, W., & Li, Z. W. ZnO thin films produced by magnetron sputtering. *Ceramics International, 30*(7), 1155-1159. (2004).

Gao, Z., Zhai, X., Liu, F., Zhang, M., Zang, D., & Wang, C. Fabrication of TiO_2/EP super-hydrophobic thin film on filter paper surface. *Carbohydrate Polymers, 128*, 24-31. (2015).

Hao, R., Wang, G., Tang, H., Sun, L., Xu, C., & Han, D. Template-free preparation of macro/mesoporous g-C_3N_4/TiO_2 heterojunction photocatalysts with enhanced visible light photocatalytic activity. *Applied Catalysis B: Environmental, 187*, 47-58. (2016).

Herderick, E. D., Tresback, J. S., Vasiliev, A. L., & Padture, N. P. Template-directed synthesis, characterization and electrical properties of Au–TiO_2–Au heterojunction nanowires. *Nanotechnology, 18*(15), 155204. (2007).

Hieu, V. Q., Phung, T. K., Nguyen, T.-Q., Khan, A., Doan, V. D., Tran, V. A., & Le, V. T. Photocatalytic degradation of methyl orange dye by Ti_3C_2–TiO_2 heterojunction under solar light. *Chemosphere, 276*, 130154. (2021).

Huang, M., Yu, S., Li, B., Lihui, D., Zhang, F., Fan, M., Wang, L., Yu, J., & Deng, C. Influence of preparation methods on the structure and catalytic performance of SnO_2-doped TiO_2 photocatalysts. *Ceramics International, 40*(8), 13305-13312. (2014).

Huang., Xiao, Y. L., Huang, Z. J., Tsui, G. C. P., Yeung, K. W., Tang, C. Y., & Liu, Q. Super-hydrophobic polyaniline-TiO_2 hierarchical nanocomposite as anticorrosion coating. *Materials Letters, 258*, 126822. (2020).

Jiang, L., Zhou, G., Mi, J., & Wu, Z. Fabrication of visible-light-driven one-dimensional anatase TiO_2/Ag heterojunction plasmonic photocatalyst. *Catalysis Communications, 24*, 48-51. (2012).

Johnson, R. W., Hultqvist, A., & Bent, S. F. A brief review of atomic layer deposition: from fundamentals to applications. *Materials today, 17*(5), 236-246. (2014).

Kapridaki, C., & Maravelaki-Kalaitzaki, P. TiO_2–SiO_2–PDMS nano-composite hydrophobic coating with self-cleaning properties for marble protection. *Progress in Organic Coatings, 76*(2), 400-410. (2013).

Kim, J. H., Lee, H.-K., Na, J.-Y., Kim, S.-K., Yoo, Y.-Z., & Seong, T.-Y. Dependence of optical and electrical properties on Ag thickness in TiO_2/Ag/TiO_2 multilayer films for photovoltaic devices. *Ceramics International, 41*(6), 8059-8063. (2015).

Koo, Y., Littlejohn, G., Collins, B., Yun, Y., Shanov, V. N., Schulz, M., Pai, D., & Sankar, J. Synthesis and characterization of Ag–TiO_2–CNT nanoparticle composites with high photocatalytic activity under artificial light. *Composites Part B: Engineering, 57*, 105-111. (2014).

Kusdianto, K., Jiang, D., Kubo, M., & Shimada, M. Fabrication of TiO_2–Ag nanocomposite thin films via one-step gas-phase deposition. *Ceramics International, 43*(6), 5351-5355. (2017).

La Russa, M. F., Rovella, N., Alvarez de Buergo, M., Belfiore, C. M., Pezzino, A., Crisci, G. M., & Ruffolo, S. A. Nano-TiO_2 coatings for cultural heritage protection: The role of the binder on hydrophobic and self-cleaning efficacy. *Progress in Organic Coatings, 91*, 1-8. (2016).

Lang, J., Takahashi, K., Kubo, M., & Shimada, M. Preparation of TiO_2-CNT-Ag Ternary Composite Film with Enhanced Photocatalytic Activity via Plasma-Enhanced Chemical Vapor Deposition. *Catalysts, 12*(5). (2022).

Lee, M. S., Hong, S. S., & Mohseni, M. Synthesis of photocatalytic nanosized TiO_2-Ag particles with sol-gel method using reduction agent. *Journal of Molecular Catalysis a-Chemical, 242*(1-2), 135-140. (2005).

Li, D., Bulou, S., Gautier, N., Elisabeth, S., Goullet, A., Richard-Plouet, M., Choquet, P., & Granier, A. Nanostructure and photocatalytic properties of TiO_2 films deposited at low temperature by pulsed PECVD. *Applied Surface Science, 466*, 63-69. (2019).

Lin, C.-C., & Chiang, Y.-J. Preparation of coupled ZnO/SnO_2 photocatalysts using a rotating packed bed. *Chemical Engineering Journal, 181*, 196-205. (2012).

Liu, H., Hu, Y., Zhang, Z., Liu, X., Jia, H., & Xu, B. Synthesis of spherical Ag/ZnO heterostructural composites with excellent photocatalytic activity under visible light and UV irradiation. *Applied Surface Science, 355*, 644-652. (2015).

Liu, J., Ye, L., Wooh, S., Kappl, M., Steffen, W., & Butt, H.-J. r. Optimizing hydrophobicity and photocatalytic activity of PDMS-coated titanium dioxide. *ACS Applied Materials & Interfaces, 11*(30), 27422-27425. (2019).

Loka, C., & Lee, K.-S. Preparation and photocatalytic performance of silver nanocrystals loaded Cu_2O-WO_3 composite thin films for visible light-active photocatalysis. *Materials Research Bulletin, 137*, 111192. (2021).

Luo, R., Liu, B., Yang, X., Bao, Z., Li, B., Zhang, J., Li, W., Wu, L., & Feng, L. The large-area CdTe thin film for CdS/CdTe solar cell prepared by physical vapor deposition in medium pressure. *Applied Surface Science, 360*, 744-748. (2016).

Mariotti, D., Patel, J., Švrček, V., & Maguire, P. Plasma–liquid interactions at atmospheric pressure for nanomaterials synthesis and surface engineering. *Plasma Processes and Polymers, 9*(11-12), 1074-1085. (2012).

Mohammad, M. R., Ahmed, D. S., & Mohammed, M. K. A. Synthesis of Ag-doped TiO_2 nanoparticles coated with carbon nanotubes by the sol–gel method and their antibacterial activities. *Journal of Sol-Gel Science and Technology, 90*(3), 498-509. (2019).

Munoz, R., & Gómez-Aleixandre, C. Review of CVD synthesis of graphene. *Chemical Vapor Deposition, 19*(10-11-12), 297-322. (2013).

Neves, J. C., Mohallem, N. D. S., & Viana, M. M. Polydimethylsiloxanes-modified TiO_2 coatings: The role of structural, morphological and optical characteristics in a self-cleaning surface. *Ceramics International, 46*(8, Part B), 11606-11616. (2020).

Pakdel, E., Zhao, H., Wang, J., Tang, B., Varley, R. J., & Wang, X. Superhydrophobic and photocatalytic self-cleaning cotton fabric using flower-like N-doped TiO_2/PDMS coating. *Cellulose, 28*(13), 8807-8820. (2021).

Pyrgiotakis, G., Lee, S.-H., & Sigmund, W. Advanced photocatalysis with anatase nano-coated multi-walled carbon nanotubes. *MRS Proceedings, 876*, R5.7. (2005).

Rapsomanikis, A., Apostolopoulou, A., Stathatos, E., & Lianos, P. Cerium-modified

TiO_2 nanocrystalline films for visible light photocatalytic activity. *Journal of Photochemistry and Photobiology a-Chemistry, 280*, 46-53. (2014).

Sarakinos, K., Alami, J., & Konstantinidis, S. High power pulsed magnetron sputtering: A review on scientific and engineering state of the art. *Surface and Coatings Technology, 204*(11), 1661-1684. (2010).

Simonenko, N. P., Nikolaev, V. A., Simonenko, E. P., Generalova, N. B., Sevastyanov, V. G., & Kuznetsov, N. T. Preparation of nanostructured titania thin films by sol–gel technology. *Russian Journal of Inorganic Chemistry, 61*(12), 1505-1511. (2016).

Sobczyk-Guzenda, A., Owczarek, S., Szymanowski, H., Volesky, L., Walkowiak, B., Miszczak, S., & Gazicki-Lipman, M. Iron doped thin TiO_2 films synthesized with the RF PECVD method. *Ceramics International, 41*(6), 7496-7500. (2015).

Song, X. C., Yang, E., Liu, G., Zhang, Y., Liu, Z. S., Chen, H. F., & Wang, Y. Preparation and photocatalytic activity of Mo-doped WO_3 nanowires. *Journal of Nanoparticle Research, 12*(8), 2813-2819. (2010).

Spasiano, D., Marotta, R., Malato, S., Fernandez-Ibanez, P., & Di Somma, I. Solar photocatalysis: Materials, reactors, some commercial, and pre-industrialized applications. A comprehensive approach. *Applied Catalysis B-Environmental, 170*, 90-123. (2015).

Tang, S., Wang, J., Zhu, Q., Chen, Y., & Li, X. Preparation of rutile TiO_2 coating by thermal chemical vapor deposition for anticoking applications. *ACS Applied Materials & Interfaces, 6*(19), 17157-17165. (2014).

Tavares, M. T. S., Santos, A. S. F., Santos, I. M. G. d., Silva, M. R. S., Bomio, M. R. D., Longo, E., Paskocimas, C. A., & Motta, F. V. d. TiO_2/PDMS nanocomposites for use on self-cleaning surfaces. *Surface and Coatings Technology, 239*, 16-19.

(2014).

Thongrom, S., Tirawanichakul, Y., Munsit, N., & Deangngam, C. One-step microwave plasma enhanced chemical vapor deposition (MW-PECVD) for transparent superhydrophobic surface. *IOP Conference Series: Materials Science and Engineering, 311*, 012015. (2018).

Tian, C., Zhang, Q., Wu, A., Jiang, M., Liang, Z., Jiang, B., & Fu, H. Cost-effective large-scale synthesis of ZnO photocatalyst with excellent performance for dye photodegradation. *Chemical Communications, 48*(23), 2858-2860. (2012).

Ukoba, K. O., Eloka-Eboka, A. C., & Inambao, F. L. Review of nanostructured NiO thin film deposition using the spray pyrolysis technique. *Renewable and Sustainable Energy Reviews, 82*, 2900-2915. (2018).

Vanalakar, S. A., Agawane, G. L., Shin, S. W., Suryawanshi, M. P., Gurav, K. V., Jeon, K. S., Patil, P. S., Jeong, C. W., Kim, J. Y., & Kim, J. H. A review on pulsed laser deposited CZTS thin films for solar cell applications. *Journal of Alloys and Compounds, 619*, 109-121. (2015).

Varshney, G., Kanel, S. R., Kempisty, D. M., Varshney, V., Agrawal, A., Sahle-Demessie, E., Varma, R. S., & Nadagouda, M. N. Nanoscale TiO_2 films and their application in remediation of organic pollutants. *Coordination Chemistry Reviews, 306*, 43-64. (2016).

Wang, X., Ding, H., Sun, S., Zhang, H., Zhou, R., Li, Y., Liang, Y., & Wang, J. Preparation of a temperature-sensitive superhydrophobic self-cleaning SiO_2-TiO_2@PDMS coating with photocatalytic activity. *Surface and Coatings Technology, 408*, 126853. (2021).

Wang, X., Zhao, Z., Ou, D., Tu, B., Cui, D., Wei, X., & Cheng, M. Highly active Ag clusters stabilized on TiO_2 nanocrystals for catalytic reduction of p-nitrophenol.

Applied Surface Science, 385, 445-452. (2016).

Wang, Y., Huang, Z., Gurney, R. S., & Liu, D. Superhydrophobic and photocatalytic PDMS/TiO_2 coatings with environmental stability and multifunctionality. *Colloids and Surfaces A: Physicochemical and Engineering Aspects, 561*, 101-108. (2019).

Woan, K., Pyrgiotakis, G., & Sigmund, W. Photocatalytic carbon-nanotube–TiO_2 composites. *Advanced Materials, 21*(21), 2233-2239. (2009).

Wu, H., Hu, Z., Li, B., Wang, H., Peng, Y., Zhou, D., & Zhang, X. High-quality ZnO thin film grown on sapphire by hydrothermal method. *Materials Letters, 161*, 565-567. (2015).

Xu, Q. F., Liu, Y., Lin, F.-J., Mondal, B., & Lyons, A. M. Superhydrophobic TiO_2–Polymer nanocomposite surface with UV-Induced reversible wettability and self-cleaning properties. *ACS Applied Materials & Interfaces, 5*(18), 8915-8924. (2013).

Yan, N. N., Zhu, Z. Q., Zhang, J., Zhao, Z. Y., & Liu, Q. J. Preparation and properties of ce-doped TiO_2 photocatalyst. *Materials Research Bulletin, 47*(8), 1869-1873. (2012).

Yang, Yang, L., Hou, J., Liu, Z., & Peng, B. Synthesis and characterization of carbon nanotubes-treated Ag@ TiO_2 core–shell nanocomposites with highly enhanced photocatalytic performance. *Optical Materials, 36*(8), 1390-1395. (2014).

Yang, D., Sun, Y., Tong, Z., Tian, Y., Li, Y., & Jiang, Z. Synthesis of Ag/TiO2 nanotube heterojunction with improved visible-light photocatalytic performance inspired by bioadhesion. *The Journal of Physical Chemistry C, 119*(11), 5827-5835. (2015).

Yang, G., & Park, S.-J. Conventional and microwave hydrothermal synthesis and application of functional materials: A review. *Materials, 12*(7). (2019).

Yuan, H., & Xu, J. Preparation, characterization and photocatalytic activity of

nanometer SnO_2. *International Journal of Chemical Engineering and Applications, 1*(3), 241-246. (2010).

Zhao, C., Guo, J., Yu, C. L., Zhang, Z. J., Sun, Z., & Piao, X. Q. Fabrication of CNTs-Ag-TiO_2 ternary structure for enhancing visible light photocatalytic degradation of organic dye pollutant. *Materials Chemistry and Physics, 248*, 122873. (2020).

Zhu, Y., Liu, Y., Ai, Q., Gao, G., Yuan, L., Fang, Q., Tian, X., Zhang, X., Egap, E., & Ajayan, P. M. J. A. M. L. In situ synthesis of lead-free halide perovskite–COF nanocomposites as photocatalysts for photoinduced polymerization in both organic and aqueous phases. *ACS Materials letter, 4*(3), 464-471. (2022).

Znaidi, L. Sol–gel-deposited ZnO thin films: A review. *Materials Science and Engineering: B, 174*(1), 18-30. (2010).

Chapter 2

Preparation of TiO_2-CNT-Ag Ternary Composite Film with improved Photocatalytic Activity via Plasma-Enhanced Chemical Vapor Deposition

2.1 Introduction

Carbon nanotube (CNTs) and Ag nanoparticles has been reported to improve the photocatalytic activity of TiO_2. To fabricate a TiO_2/CNT/Ag ternary structure, various processes have been developed. Wang *et al.* (2009) reported the creation of an Ag-CNT/TiO_2 ternary composite using the sol-gel and photoreduction techniques. TiO_2 and Ag nanoparticles were employed to decorate CNTs to create the ternary structure. Ag-CNT/TiO_2 had a photocatalytic activity that was roughly twice as high as P25. Koo *et al.* (2014) reported the creation of an Ag-TiO_2-CNT composite through photochemical reduction. The TiO_2/Ag nanoparticles were evenly packed on the CNT surface. The photocatalytic activity of Ag-TiO_2-CNT ternary composites is better than that of Ag-TiO_2. Notably, CNTs are common support material to decorate with or coated by TiO_2 and Ag nanoparticles. The preparation of TiO_2-based composite films, utilizing TiO_2, Ag, and CNTs received few concentrations. Various film deposition methods have been developed to prepare composite films, as described in Chapter 1. Among these methods, PECVD is believed as the most versatile method that allows multiple materials to be deposited simultaneously. It also can produce the uniform films with adequate coverage.

In the existence literature on TiO_2/CNT/Ag ternary composites, the fabrication process always started form preparation of binary composite. However, I believed it is possible to fabricate ternary films by supply different materials simultaneously without

preparing a binary composite. Kubo *et al.* (2017) prepared TiO_2 films embedded with SiO_2 nanoparticles by PECVD, where the SiO_2 solid suspensions and vaporized TTIP were supplied simultaneously. Therefore, by supplying CNTs and Ag solid mixtures, we have shown that producing TiO_2-CNT-Ag ternary composite films is feasible.

In this chapter, TiO_2-CNT-Ag ternary composite films were fabricated using PECVD. During deposition process, the CNT/Ag solid suspensions were sprayed with a nozzle and heated to obtain an aerosol of CNTs and Ag nanoparticles. These particles and aerosolized TTIP were simultaneously supplied into a plasma reactor, where the TiO_2-CNT-Ag films were deposited on a substrate. The morphology, components and optical properties of the obtained composite films was confirmed. The degradation of Rhodamine 6G by the films under simulated solar light irradiation was recorded.

2.2. Experimental Section

2.2.1 Preparation of CNT and Ag suspensions

The CNT suspensions (0.5 wt%) were formulated using 0.5 g of CNTs (Sigma-Aldrich, St. Louis, U. S., diameter: 110–170 nm and length: 5–9 μm) dispersed in 95 mL of deionized water with Triton X-100 as the dispersant.

The Ag nanoparticle suspensions (0.1 wt%) were fabricated by co-precipitation method (Šileikaitė *et al.*, 2006). Subsequently, $AgNO_3$ aqueous solution was prepared by dissolving 0.18 g of $AgNO_3$ (Nacalai Tesque, Inc., Tokyo, Japan) into 98 mL deionized water, and trisodium citric acid aqueous solution (2 mL, 0.01 g/mL) (Wako Pure Chemical Industries, Ltd., Osaka, Japan) was added. The mixture was then stirred at 100 °C for 1 h and cooled to ~25 °C.

A solid suspension for supplying was obtained by mixing the CNT suspension, the Ag nanoparticle suspension and water with a certain concentration.

2.2.2 Experimental setup

Fig. 2.1 depicts the experimental setup consisting of different feeding systems (Kubo *et al.*, 2017). 10mL CNT/Ag mixtures suspension was supplied through a syringe pump (YSP-301, YMC. Co., Ltd., Kyoto, Japan) equipped with a capillary tube. A two-fluid nozzle was employed to spray the solid suspension, with He gas flowing at a rate of 1000 sccm. A ribbon heater was used to preheat the transport tube to dry the solid suspension. The obtained CNT/Ag aerosol particles were supplied to the plasma reactor. Meanwhile, A He gas with flow rate of 50 sccm was used to carry the vaporized TTIP (Tokyo Chemical Industry Co., Ltd., Tokyo, Japan) in a bubbler (45 °C). In addition, the vaporized TTIP was transferred by O_2 gas at a flow rate of 50 sccm and He gas aat a flow rate of 400 sccm. The quartz tube (inner diameter: 25.4 mm; length: 300 mm) act as the reactor and was supported by a cavity. Furthermore, a quartz mesh was placed on a recessed part in the middle of the quartz tube and hold a glass substrate, on which the films could be fabricated. The plasma power was setup to 190 W (2.45 GHz). The vacuum pressure in the equipment was maintained by a vacuum pump (Pascal 2025C1, Pfeiffer Vacuum, Inc., Asslar, Germany) and ~6 kPa pressure was kept during the materials feeding. The films were generated on a glass substrate (1 × 1 cm) by the simultaneous feeding of the TTIP and CNT/Ag solid mixtures for 15 min. The fabricated films were calcined at 600 °C and 700 °C with a N_2 flow rate at 200 sccm.

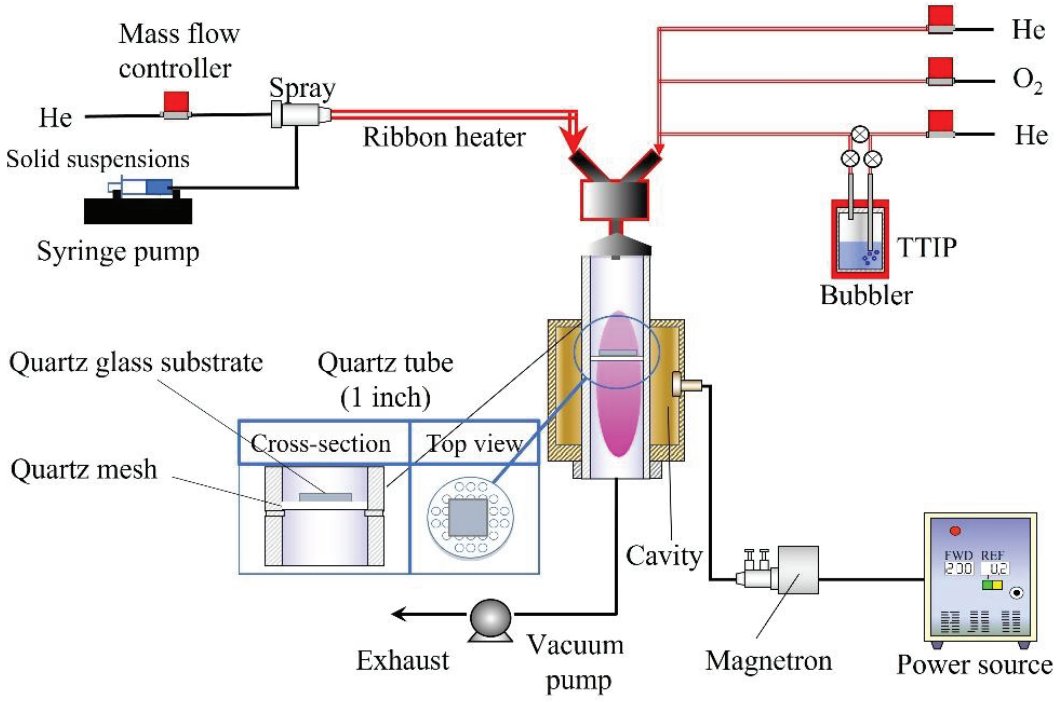

Fig. 2.1 Experimental setup for PECVD.

In addition, the mass of Ti in raw materials during deposition were estimated as follow steps:

The vapor pressure of TTIP (P_{TTIP}) was estimated by the equation (Siefering *et al.*, 1990):

$$\log_{10} P_{TTIP} = 9.837 - \frac{3193.7}{T_{Bubbler}} \quad 2.1$$

The Flow rate of TTIP (F_{TTIP} sccm) was estimated by the equation:

$$F_{TTIP} = \frac{133.3 P_{TTIP}}{P_{Bubbler}} F_{Bubbler} \quad 2.2$$

The total volume of TTIP during deposition (V_{TTIP}) was obtained from F_{TTIP}. In addition, the volume of TTIP in 20 °C (V'_{TTIP}) was estimated by the equation:

$$V'_{TTIP} = \frac{293 P_{Bubbler} V_{TTIP}}{101.325 T_{Bubbler}} \quad 2.3$$

The density of TTIP in 20 °C is 0.96g/mL. Thus, the mass of Ti during deposition (m_{Ti}) was calculated by:

$$m_{\mathrm{Ti}} = 0.96 V'_{\mathrm{TTIP}} \frac{47.9}{284.2} \quad 2.4$$

where the pressure of bubbler (P_{Bubbler}) was regarded same as that in the reactor has the unit of mmHg. The T_{Bubbler} represent the temperature of bubbler and the F_{Bubbler} represent the flow rate of bubbler.

2.2.3 Preparation of P25 film

A self-made P25 film was used as the reference. The P25 film was prepared by grinding P25 powder (commercial TiO_2 powder, Sigma-Aldrich, St. Louis, U. S.), HNO_3, and deionized water, and then spin-coated on the quartz glass substrate (Azmar *et al.*, 2019). The obtained film was annealed at 400 °C for 2 h.

2.2.4 Film characterization

The microstructure of the films was observed by SEM (S-5200, Hitachi High Technologies, Tokyo, Japan) and TEM (JEM-2010, JEOL, Tokyo, Japan), in combination with EDS (JED-2300T, JEOL, Tokyo, Japan). The elemental analysis was investigated by XPS (ESCA-3400, SHIMADAZU, Kyoto, Japan). The crystal structures of the films were determined by XRD (RINT-2100, Rigaku, Tokyo, Japan), using Cu-K_α radiation (λ = 1.5406 Å). The UV–vis spectra of the films were performed using a UV–Vis spectrophotometer V-650 (JASCO, Tokyo, Japan).

Further, an ICP-OES instrument (SPS3000, Hitachi High Technologies, Tokyo, Japan) was employed to demonstrate the elemental content of the films. The obtained films were put into a polypropylene sample tube and immersed by 1 mL of ethanol. A micro grinder equipped with an electroplated diamond burr was used to scrape the film off the substrate. Ethanol was used as a lubricant and collector for the scraped film powder. The powder was dried before dissolved in HF. H_3BO_4 was utilized to neutralize

excess HF, before solvents were filtered and used for the ICP-OES analysis.

2.2.5 Evaluation of photocatalytic activity

The degradation of Rhodamine 6G by the films under simulated solar-light irradiation was evaluated to study the photocatalytic activities of the films. A spectro multi-channel photo detector (MCPD-3000, Otsuka Electronics, Osaka, Japan) was used to record the spectrum of the light which is used to activate the film, the result is shown in Fig. 2.2. To reach adsorption equilibrium, a cuvette cell, in which the films were immersed in 3 mL of a Rhodamine 6G aqueous solution (5 mg/L), was left in the dark for 30 min. Subsequently, the catalytic process was initiated by irradiation with simulated solar light (300–800 nm). Based on the relation between the absorbance and concentration of Rhodamine 6G, the concentrations of Rhodamine 6G was converted from the maximum absorbances of Rhodamine 6G. The absorption spectrum before and after irradiation were recorded through UV–Vis spectrophotometry (V-650, Jasco) every 10 min. Furthermore, the degradation efficiency was carried out by C_t/C_0, and the rate constant k was determined by follows Eq. 2.5:

$$\ln \frac{C_0}{C_t} = kt \qquad 2.5$$

where C_0 and C_t represent the concentrations of Rhodamine 6G before and after irradiation, respectively, and t is the irradiation time.

The photocatalytic activity of the commercial photocatalyst P25 film prepared through spin coating was tested under the same conditions.

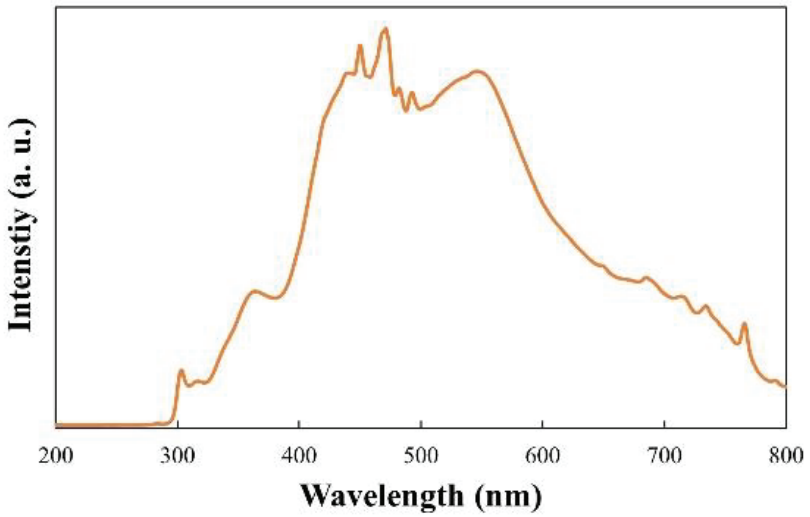

Fig 2.2 Light spectrum used to activate the films.

2.3. Results and discussion

2.3.1 Morphology

The TiO_2, TiO_2-CNT, TiO_2-Ag, and TiO_2-CNT-Ag films were prepared by supplying only TTIP, a TTIP and 0.25 wt% CNT suspension, a TTIP and 0.1 wt% Ag suspension, and TTIP and CNT/Ag mixed suspensions (0.25 wt%/0.1 wt%), respectively. The corresponding products are marked as T, T-C, T-A, and T-C-A0, respectively. Fig. 2.3 (a) shows the morphology of the CNTs. The morphology of the prepared T-C films containing cracks was shown in Fig. 2.3 (b). The cracks sometimes appear on the periphery of the annealed film surface, which could be attributed to the heat treatment. The exposed CNTs in these cracks demonstrate that they were successfully incorporated into the film.

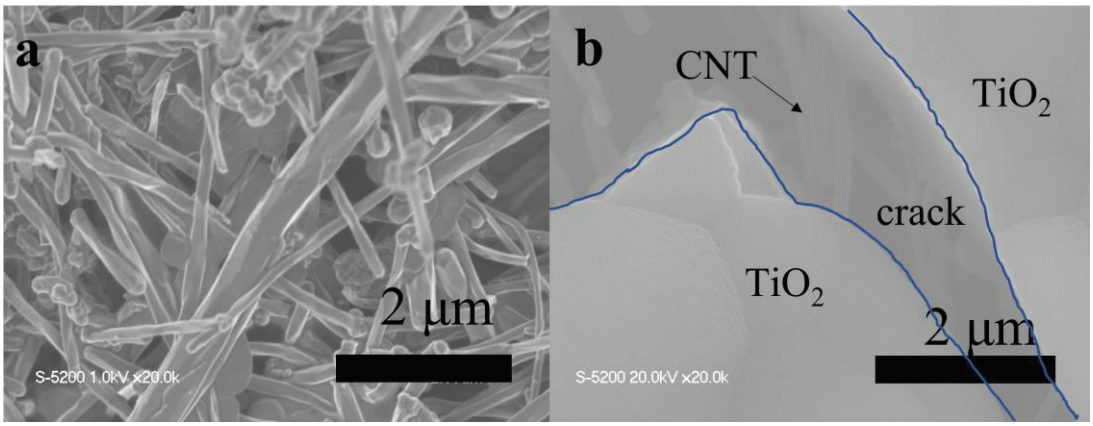

Fig. 2.3 SEM images of: (a) CNTs, (b) and (c) prepared T-C film containing cracks.

Further, Fig 2.4 shows the SEM images of the deposited T, T-C, T-A, and T-C-A films. The cross-sectional morphologies of the films were shown in Fig. 2.4 (a)–(d), which appears a dense layer with a relative uniform thickness of around 1 μm. The film thickness was not changed by the supplying of CNTs and Ag. The T films shows a relative smooth surface, while the structure of CNTs observed on surface, which are attached to the surface of T-C and T-C-A0 films (Fig. 2.4 (b) and (d)). Only few amounts of CNTs appeared, which can be attributed to a well-dispersed CNT suspension during deposition process. However, it is a challenge to confirm the presence of Ag nanoparticles in the T-A and T-C-A0 (Fig. 2.4 (c) and (d)). The observed big columnar grains in cross-sectional images of the TiO_2 film may leads to the formation of a relative regular surface, as observed on TiO_2 surface (Fig. 2.4 (e)). However, the addition of CNTs and Ag suspensions caused in some irregular structure on the film surface, like the strip structure in Fig. 2.4 (f), large aggregate particles in Fig. 2.4 (g), and both phenomena in Fig. 2.4 (e). These irregular structures may be attributed to the formation of core-shell structure of the additives.

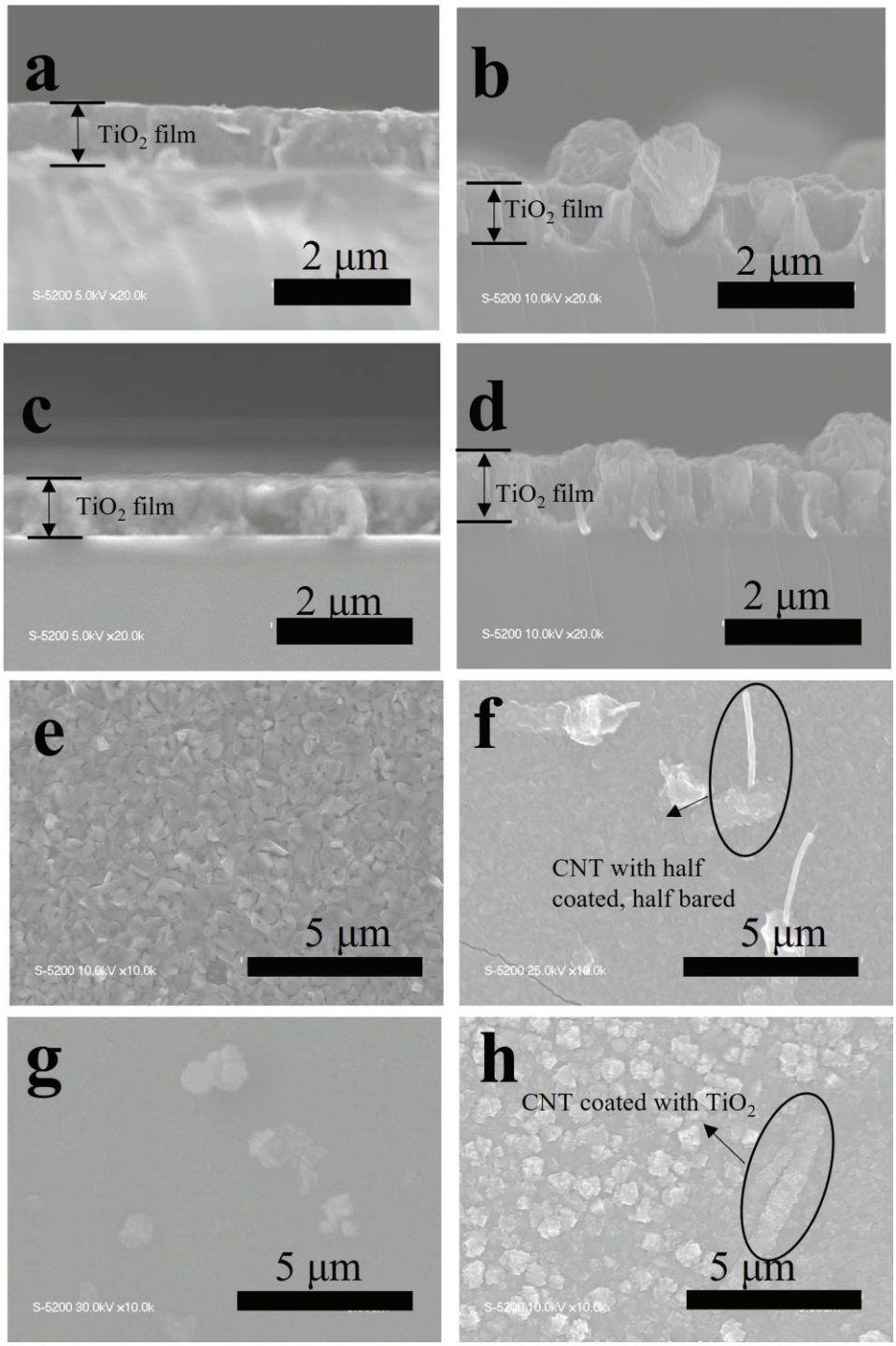

Fig. 2.4 SEM images of the prepared films. Cross-sectional morphologies of (a) T, (b) T-C, (c) T-A, and (d) T-C-A0. Surface morphologies of (e) T, (f) T-C, (g) T-A, and (h) T-C-A0.

In addition, the elements mapping of the irregular structure that appeared in the

other samples prepared under the same conditions was investigated, as shown in Fig. 2.5. The existence and distribution of Ti, O, Ag and C was confirmed. The aggregated particles contain Ag and TiO_2, and the strip structures contain CNT and TiO_2. Thus, these results confirmed the ternary structure that CNTs and Ag nanoparticles was embedded into TiO_2.

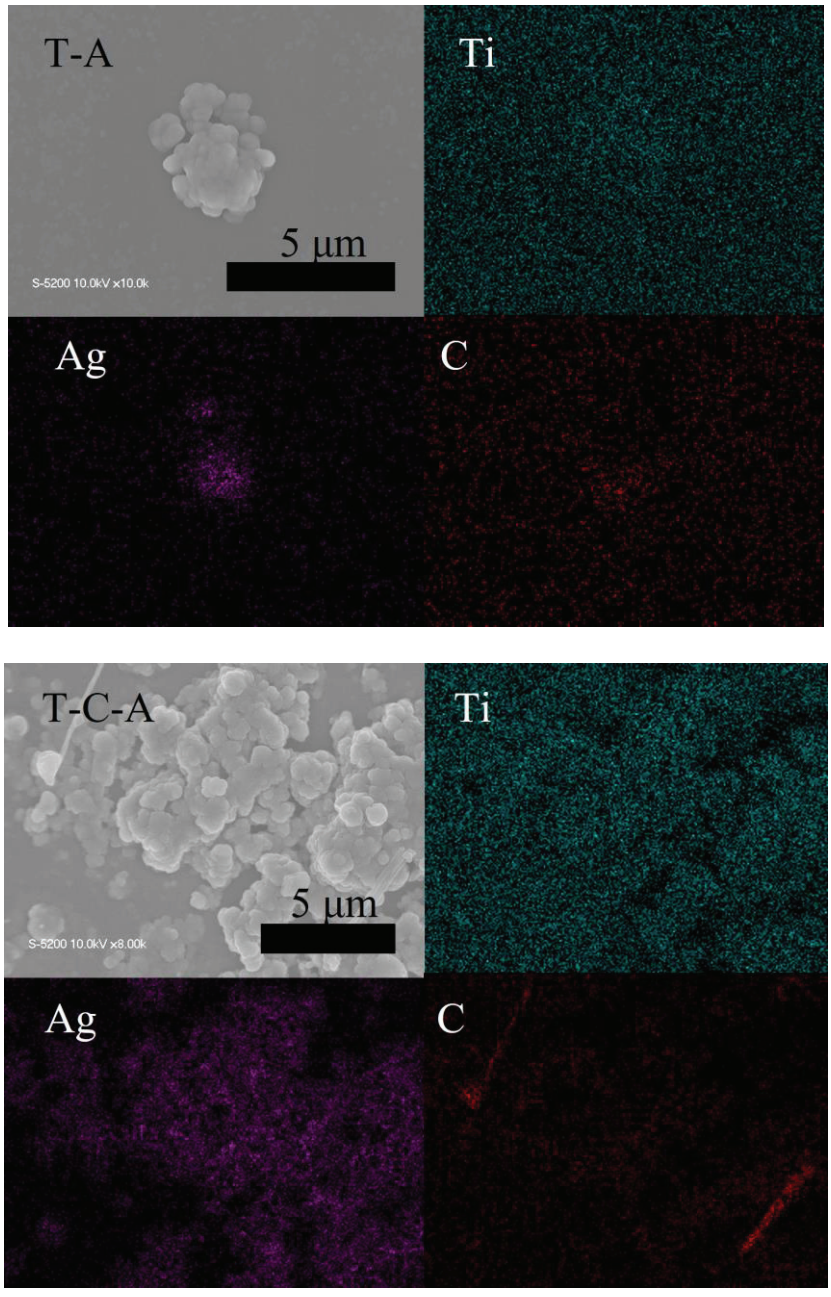

Fig. 2.5 Elemental mapping of T-A and T-C-A.

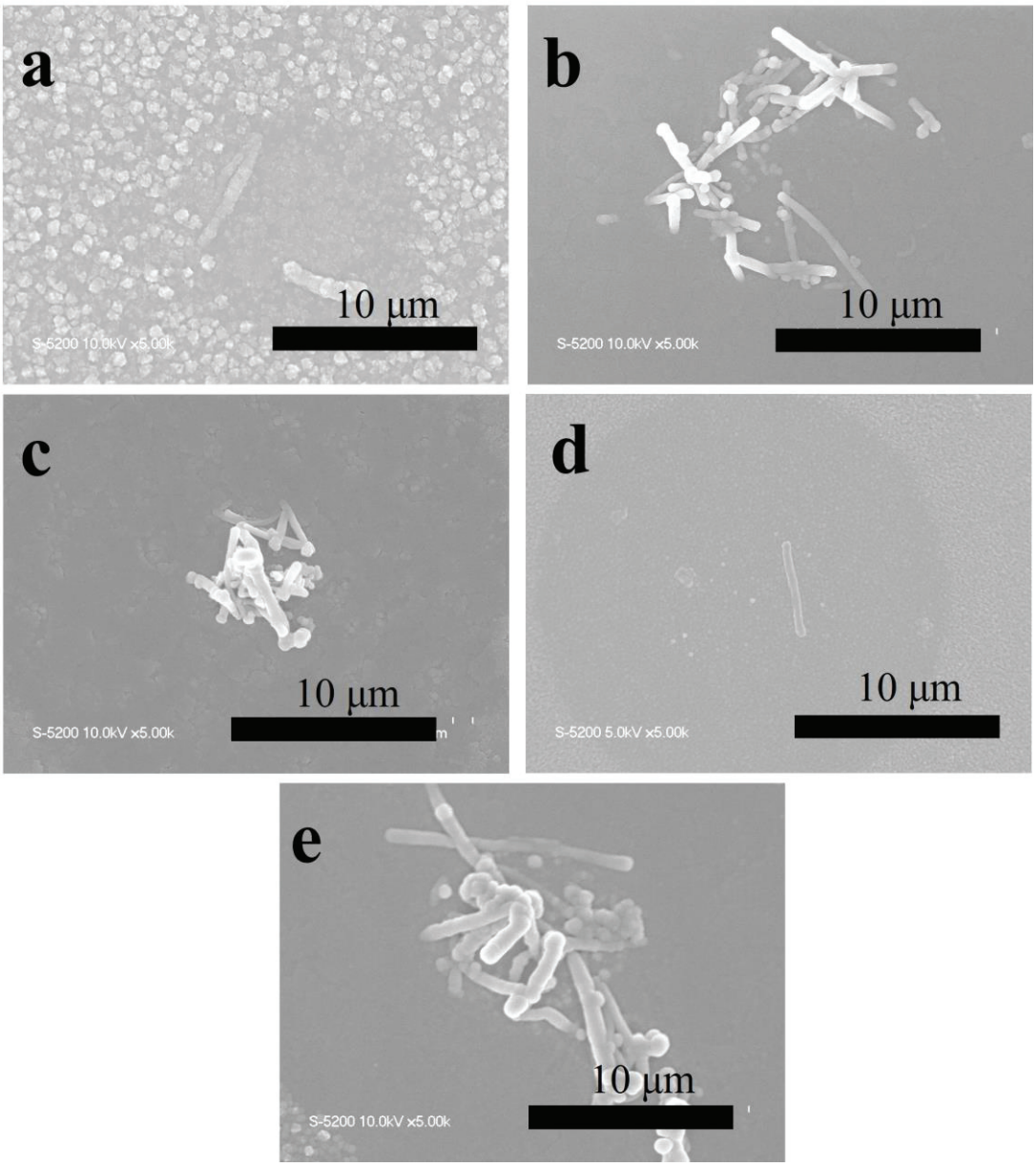

Fig. 2.6 SEM images of T-C-A films deposited using different concentrations of CNT/Ag mixed suspensions: (a) T-C-A0 (0.25 wt%/0.1 wt%), (b) T-C-A1 (0.25 wt%/0.05 wt%), (c) T-C-A2 (0.25 wt%/0.01 wt%), (d) T-C-A3 (0.01 wt%/0.1 wt%), and (e) T-C-A4 (0.5 wt%/0.1 wt%).

Furthermore, the effect of different concentrations of CNT/Ag mixed suspensions, such as 0.25 wt%/0.05 wt%, 0.25 wt%/0.01 wt%, 0.01 wt%/0.1 wt%, and 0.5 wt%/0.1 wt% concentrations, on the T-C-A films surface was investigated. The products were

remarked as T-C-A1, T-C-A2, T-C-A3, and T-C-A4, respectively. Fig. 2.6 shows the SEM images of these films. By observing the surface structure, the concentration of the mixed suspension seems to have a significant impact on the amount of CNTs on the film surface. However, referring to Fig. 2.3, it is impossible to determine the exact amount of CNTs based on the surface morphology. Additionally, due to the embedded structure and the small size of the Ag particles, it was difficult to determine the morphology of the Ag particles in all of the T-C-A films.

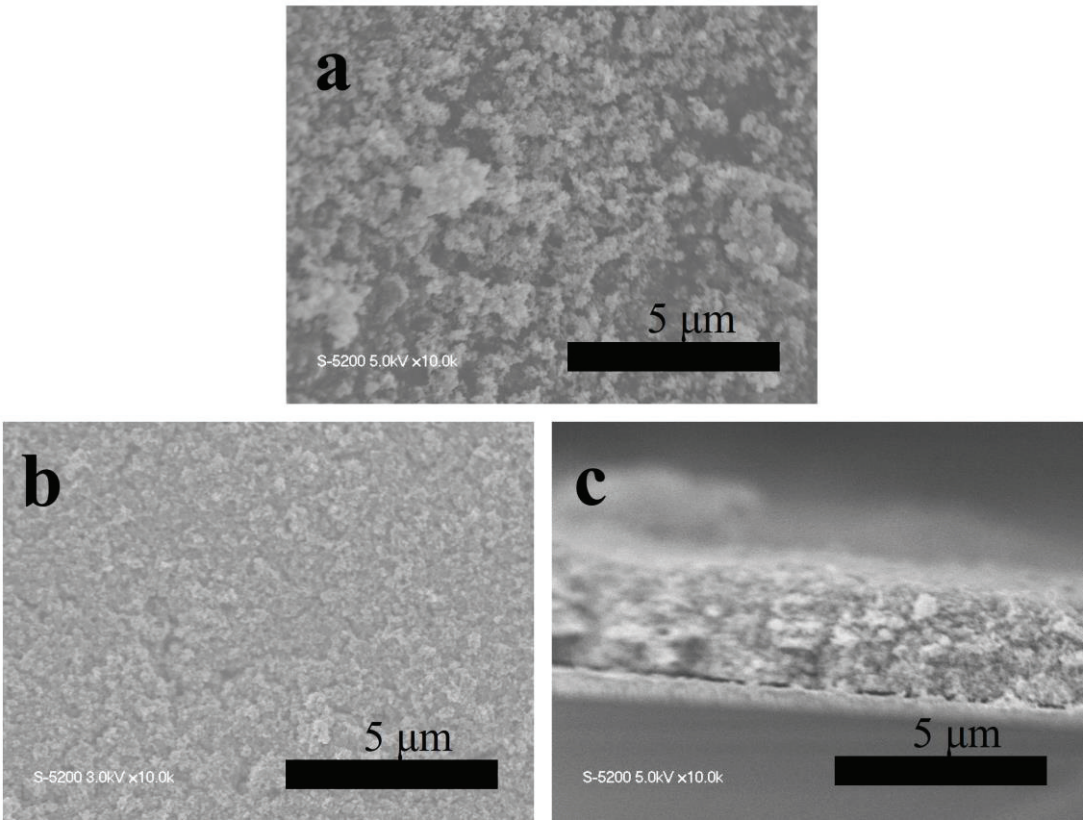

Fig. 2.7 SEM images of P25: (a) pristine P25 powder, (b) film surface, and (c) film cross-section.

Fig. 2.7 shows the SEM images of the pristine P25 powder and prepared P25 films. Fig. 2.7 (a) shows the SEM images of the pristine P25 powder stuck on carbon tape, which exhibits a random distribution. Fig. 2.7 (b) shows that the morphology of the P25

film deposited on the substrate obtained by spin coating is porous structure. Fig. 2.7 (c) shows the cross section of the P25 film, which contains a gap between the film and substrate. The porosity of the structure and the gap between the P25 film and substrate indicates that it is vulnerable to destruction.

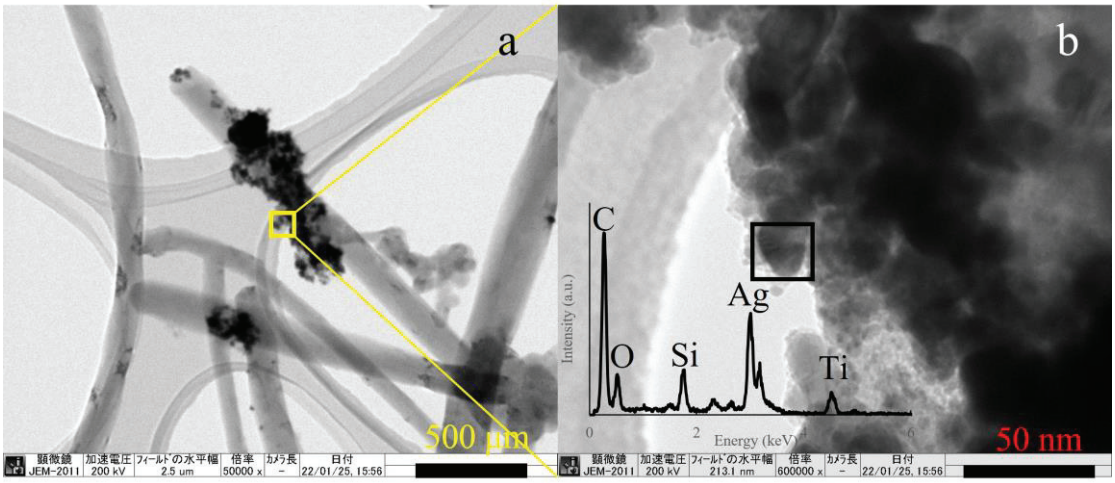

Fig. 2.8 TEM images of the prepared T-C-A0 film: (a) CNTs with Ag and TiO_2 particles attached, (b) magnified version of the area in the yellow square in (a), and EDS results corresponding to the black square in (b).

The prepared T-C-A0 film, which was chosen as a representative sample, was then subjected to TEM-EDS to confirm the presence of Ag. The original structure was not preserved since the observed sample was scraped from the films and collected by a microgrid. Fig. 2.8 (a) depicts the TiO_2 and Ag particles appeared to be attached to the CNT surface. However, as seen in Fig. 2.1, the CNTs were incorporated into the TiO_2 film. The yellow square in Fig. 2.8 (a) is shown magnified in Fig. 2.8 (b), demonstrating the aggregated TiO_2 and Ag nanoparticles. Further evidence of the presence of Ag in the film is provided by the EDS analysis of the region in the red square in Fig. 2.8 (b).

2.3.2 Elements states

The composite compounds and states in the T-C-A0 film were examined using XPS; the results are shown in Fig. 2.9. The survey spectrum of this film shows the peaks for Ti 2p, Ag 3d, C1s, and O 1s (Fig. 2.9 (a)). A typical Ti^{4+} spectrum with Ti $2p_{3/2}$ at 459.3 eV and Ti $2p_{1/2}$ at 465.0 eV was observed in Fig. 2.9(b). The presence of metallic Ag was demonstrated by Ag $3d_{5/2}$ at 368.1 eV and Ag $3d_{3/2}$ at 374.1 eV in Fig. 2.9 (c). In addition, the two decomposed peaks from the O 1s profile correspond to the lattice oxygen in TiO_2 (530.5 eV) and hydroxyl-like group (532.1 eV), respectively.

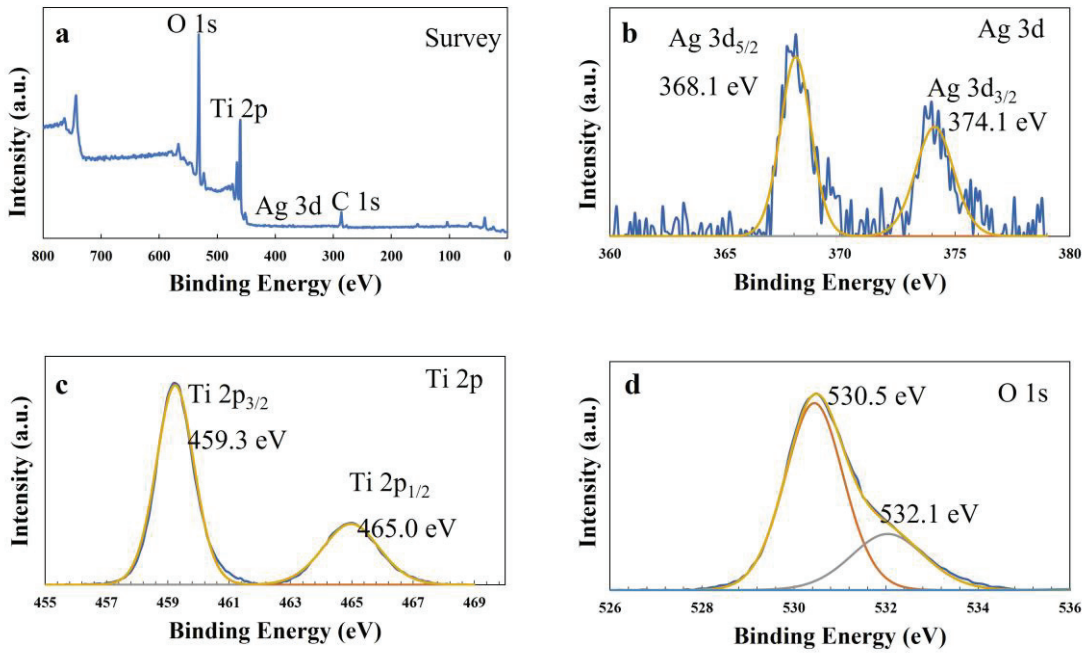

Fig. 2.9 X-ray photoelectron spectra of the T-C-A0 film: (a) survey, (b) Ag 3d, (c) Ti 2p, and (d) O 1s spectra.

2.3.3 Crystalline

The XRD patterns of the T, T-C, T-A, and T-C-A0 films are shown in Fig. 2.10 (a). The diffraction peaks marked with “A” correspond to the (101), (004), (112), (200), and (211) planes of anatase, indicating that the developed products existed in an anatase phase. The absence of an Ag peak in the patterns of the T-C-A0 and T-A films may be due to the low Ag content in these films. As a result, the main characteristic peak of Ag at 38.2° (111) coincides with the characteristic peaks of TiO_2 (Koo *et al.*, 2014). The same phenomenon occurs for the CNTs. The CNTs peak at 26.1° was shielded by anatase peak at 25.9°, suggesting that the film contained a relative low amount of CNTs compared to TiO_2 (Askari *et al.*, 2017).

The XRD analysis of the films annealed at various temperatures is shown in Fig. 2.10 (b), JCPDS cards of Ag, SiO_2, anatase and rutile were used as the reference. Additionally provided is the P25 film used in this study. Both the rutile and anatase phases can be seen in the P25 pattern. Notably, the T-C-A0 film annealed at 600 °C only exhibits the anatase phase, while annealing at 700 °C results in the presence of the rutile phase. This result is consistent with the previous observations that the phase transfer occurs between 600 and 700 °C (Choudhury *et al.*, 2013).

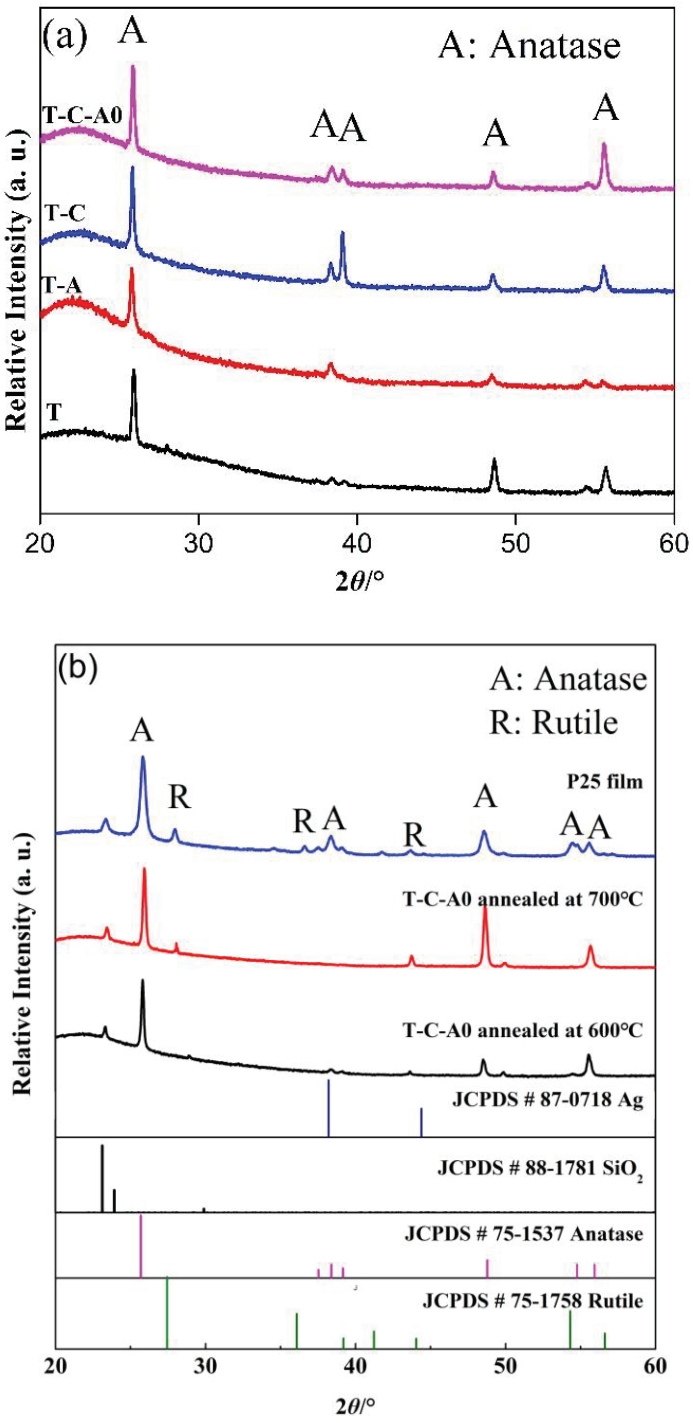

Fig. 2.10 XRD patterns of (a) T and T-composite films and (b) P25 and T-C-A0 films annealed at different temperatures.

2.3.4 Optical properties

The absorption spectra for the T, T-C, T-A, and T-C-A0 films are shown in Fig. 2.11 (a). For all the films, the light absorption below 400 nm consistent with a typical intrinsic band gap absorption of TiO_2 (Yu *et al.*, 2006). Compared to the T film, the absorption thresholds of the T-C, T-A, and T-C-A films extend to longer wavelength range. Zhao *et al.* (2020) attributed this behavior to the photosensitizing effect of CNTs and the local surface plasmon resonance (LSPR) effect of the Ag particles. Furthermore, the addition of CNTs and Ag to the composite film is thought to have aligned the energy level, which is attributed to the charge transmission between the TiO_2, Ag, and CNTs. (Aazam, 2014). The band gap energy can be estimated by employing the Tauc relation: $\alpha h\upsilon = B(h\upsilon - Eg)^{1/2}$, where $h\upsilon$ is the photon energy, α is the absorption coefficient, Eg is the optical band gap, and B is the absorption constants for direct transitions. The plot of $(\alpha h\upsilon)^2$ versus photoenergy ($h\upsilon$) was determined and the bandgap was estimated by the intercept of the tangent to the plot, as shown in Fig. 2.11 (b). The bandgap of the T film is 3.47 eV; however, it decreases to 3.39 eV, 3.31 eV, and 3.22 eV for the T-C film, T-A film, and T-C-A film, respectively. The reduction of the band gap of T-C-A nanocomposite may be attributed to the interaction between TiO_2 and CNT as a result of the C–O–Ti bond formation and the SPR effect of Ag nanoparticles (Chaudhary *et al.*, 2017). These results indicate the capability of the T-C-A samples for capturing visible light, comparatively.

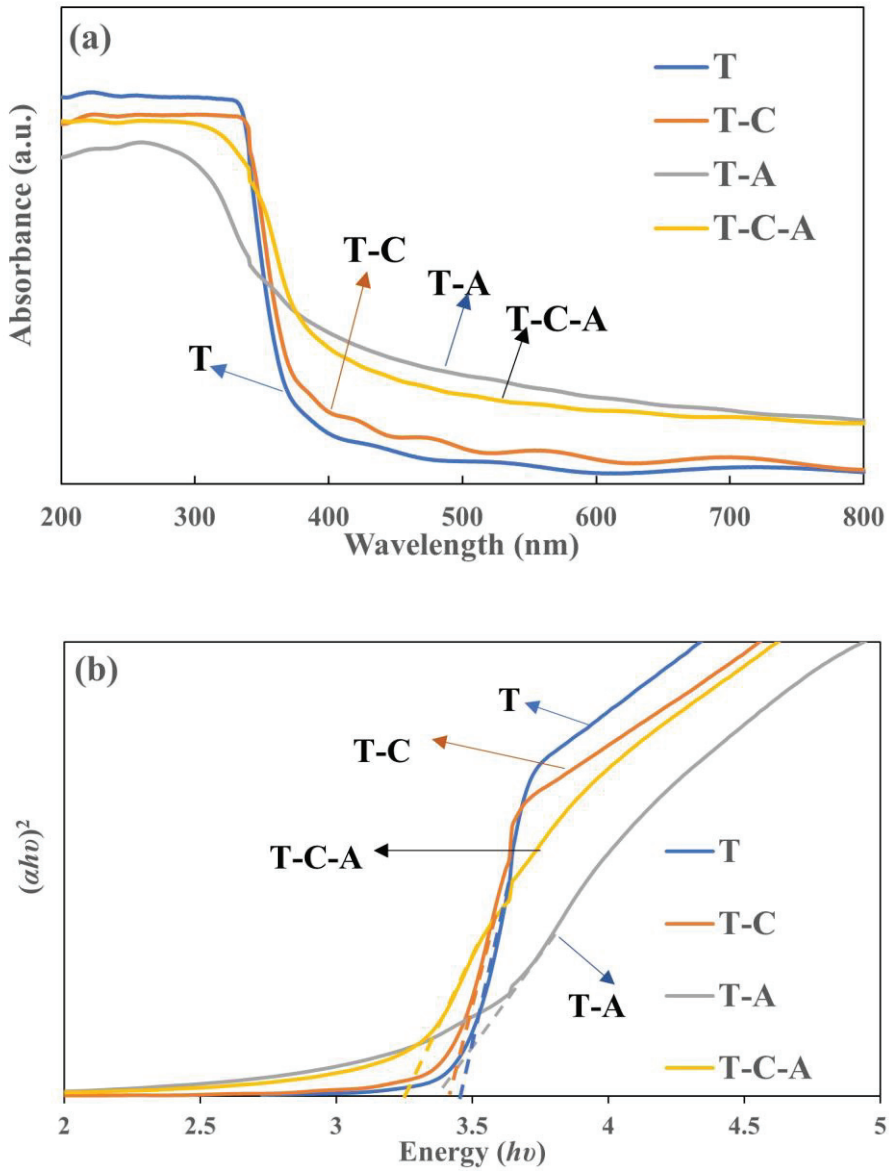

Fig. 2.11 Optical properties of the T and T-composite film: (a) absorbance spectra; (b) $(\alpha h\upsilon)^2$ versus photon energy ($h\upsilon$) plot of the prepared films.

2.3.5 Elements analysis

The ratio of Ag/Ti content in the film was analyzed by ICP-OES. The results are presented in Table 2.1. The units of Ag/Ti (g / g) refer to the raw materials (theoretical values) and correspond to the conditions when films were deposited. Ag/Ti (mg / mg) refers to the results of the ICP-OES analysis and corresponds to the content of the film (absolute values). Ag elements were present in all the T-C-A films, proving the presence

of Ag. However, decreasing Ag concentration results in a decrease of Ag/Ti ratio. This result suggests that the concentration of the raw material had a direct impact on the Ag content in the films.

Table 2.1 Ratio of Ag/Ti content in the T-C-A film

Samples	Ag and Ti in the raw materials		Ag and Ti in the films	
	Content (g/g)	Ratio	Content (mg/mg)	Ratio
T-C-A0	0.01/0.0914	0.109	0.0027/0.149	0.0182
T-C-A1	0.005/0.0914	0.0547	0.0027/0.194	0.0139
T-C-A2	0.001/0.0914	0.0109	0.0028/0.237	0.0118

2.3.6 Photocatalytic activity of the films

The photocatalytic activities of the samples were evaluated based on the decomposition of aqueous Rhodamine 6G by different films under simulated solar light. The films employed in this section were annealed at 600 °C. Fig. 2.12 (a) presents the plot of C_t/C_0 versus the correspond irradiation time (t) for different samples, Furthermore, we prepared the ln (C_t/C_0) versus t plot (Fig. 2.12 (b)) to obtain the corresponding rate constant k (Fig. 2.12(c)) from the slope of the fitting curve. The results confirmed the photocatalytic activity of the film decreased in the following order: T-C-A0 > T-A > T-C > T. Furthermore, the k of T-C-A0 is almost 1.8 times higher than that of T.

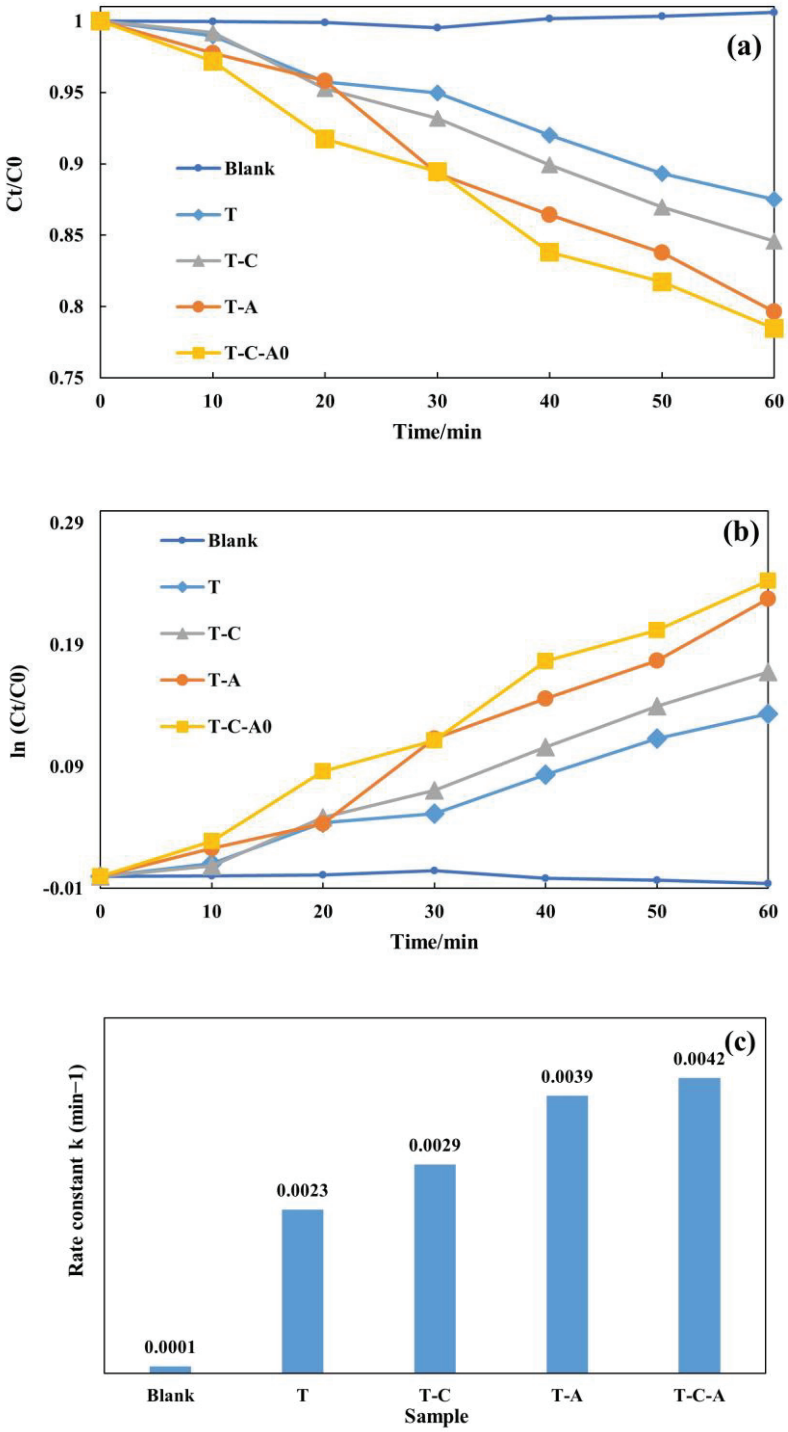

Fig. 2.12 Photocatalytic activity for the degradation of Rhodamine 6G by different films under simulated solar light: (a) degradation with respect to time, (b) ln (C_t/C_0) versus to time plot, and (c) rate constants degradation for various samples.

In addition, the photocatalytic activity of the self-prepared P25 film and T-C-A0 film annealed at different temperature was determined under the same conditions. Fig. 2.13 (a) presents the plot of C_t/C_0 versus the correspond irradiation time (t) for different samples, Furthermore, we prepared the ln (C_t/C_0) versus t plot (Fig. 2.13 (b)) to obtain the corresponding rate constant k (Fig. 2.13(c)) from the slope of the fitting curve. The higher annealing temperature resulted in the increased photocatalytic activity, one of the reasons should be the phase transfer of the crystalline phase at different annealing temperatures. Moreover, the T-C-A0 film annealed at 700 °C shows higher photocatalytic activity than the self-made P25 film. The rate constant k of T-C-A0 annealed at 700 °C is approximately 1.3 times higher than that of P25 film.

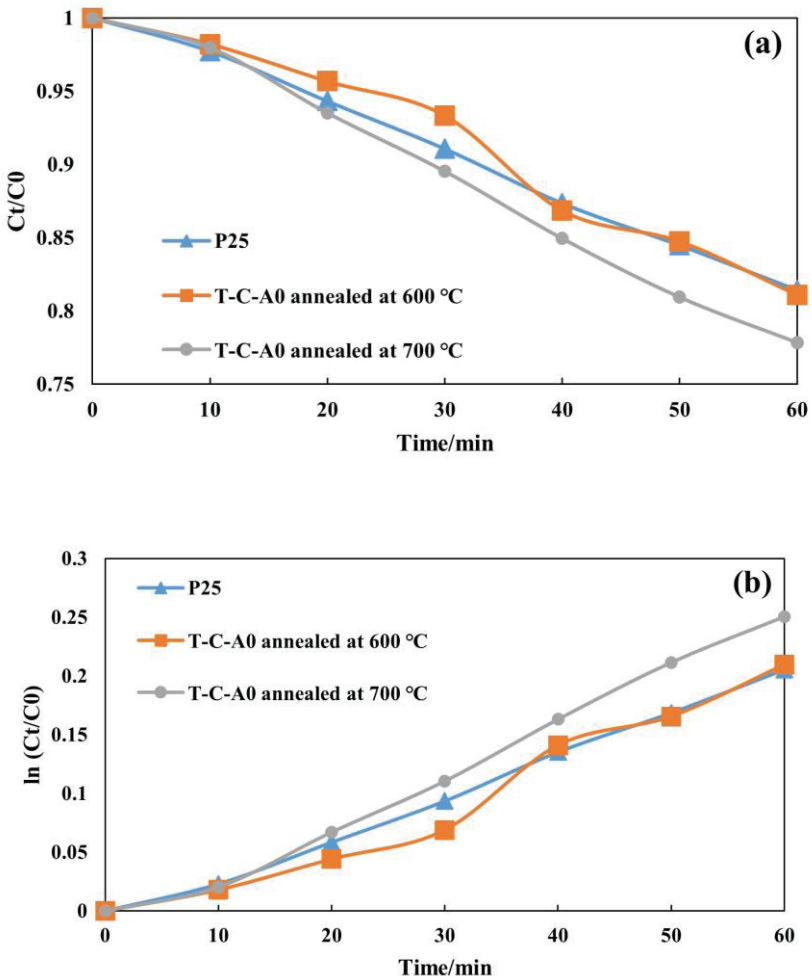

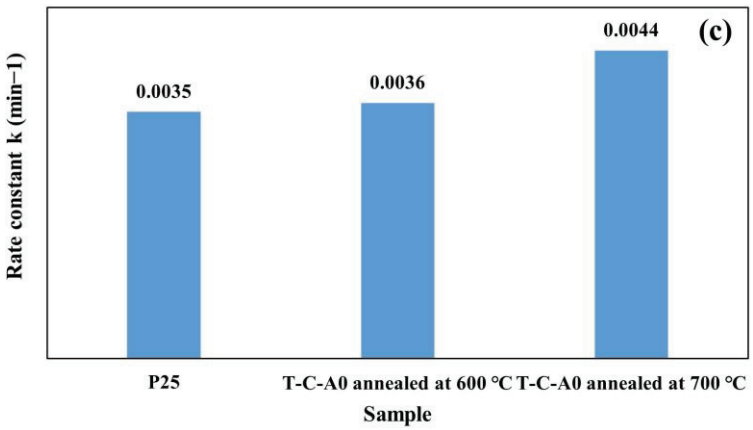

Fig. 2.13 Photocatalytic degradation of Rhodamine 6G by P25 and T-C-A films annealed at different temperatures: (a) degradation with respect to time, (b) ln (C_t/C_0) versus to time plot, and (c) corresponding rate constants of degradation for samples.

To the best of my knowledge, other researchers have also estimated the photocatalytic activity based on the rate constant. Soltanieh *et al.* (2021) prepared a TiO_2/Ag^0@MWCNTs composite with rate constant of 0.07675 min^{-1}. Wang *et al.* (2009) illustrated an Ag-CNT/TiO_2 composite with a rate constant 0.03052 min^{-1}. Numerous factors affect the photocatalytic activity, such as the concentration of dyes, power of the irradiation light, and morphology of the catalyst. Consequently, it is challenging to compare the activity of catalysts produced in different experiments. In this study, however, the photocatalytic activity of TiO_2 was successfully improved. Therefore, the developed method is useful to improve the performance of photocatalysts.

These results demonstrate that the incorporation of CNTs and Ag particles into the TiO_2 film considerably increases the photocatalytic activity of TiO_2. The mechanism of photocatalytic reaction for ternary structure is complex. The Ag particles can be activated by light irradiation due to the LSPR effect and produce photoinduced electrons. These photoinduced electrons can be transferred to the conduction band of

TiO_2. In addition, since the band gap of TiO_2 in the ternary composite has narrowed, it is hypothesized that TiO_2 can also function as a sensitizer to create electrons (Chaudhary *et al.*, 2017; de la Flor *et al.*, 2021). In addition, CNTs act as electron acceptors is a common idea, which accepts the photoinduced electrons from TiO2 and Ag, thus reducing electron-hole recombination (Wang *et al.*, 2019). In this case, the possible mechanism should be: the electrons were excited to the conduction band of TiO_2 since the narrowing band gap of ternary composite, then the activated electrons can easily be transferred to the CNTs and Ag, the recombination of electron–hole pairs was reduced, as shown in Fig. 2.14.

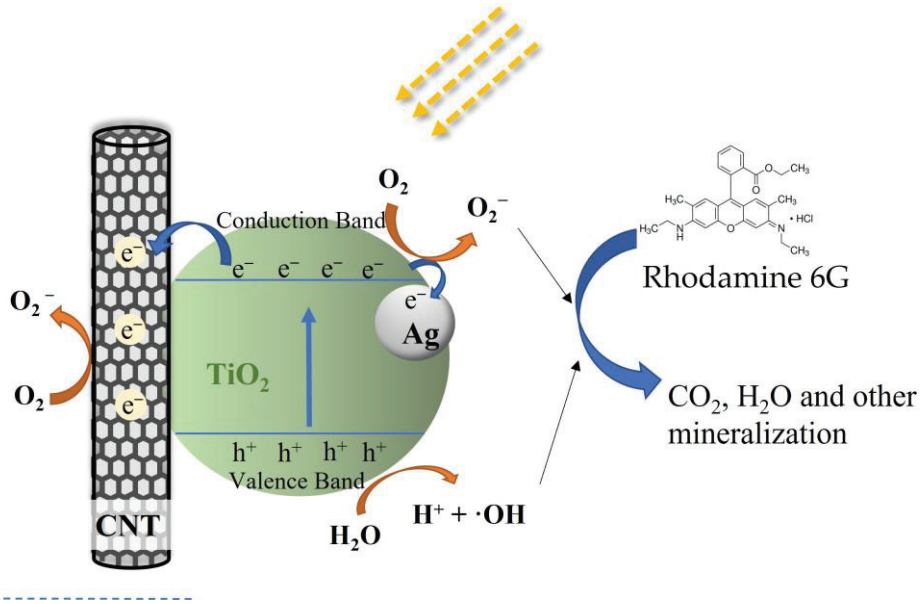

Fig. 2.14 Possible schematic explaining the photocatalytic activity of the T-C-A ternary film.

2.4 Conclusions

In this study, a T-C-A ternary composite film was successfully prepared using a novel and simple process with relatively good coverage. The characterization results confirmed the structure that CNT and Ag particles were embedded into TiO_2 matrix,

and the thickness was approximately 1 μm. The surface structures and optical properties of the films were altered by the addition of CNT and Ag. The crystal structure of the film was influenced by annealing temperature. The addition of CNT and Ag can significantly improve the performance of TiO_2, where the photocatalytic activity of T-C-A was approximately 1.8 times higher than that of T. In addition, the photocatalytic activity of T-C-A with mixed-phase was 1.3 times higher than that of self-made P25 film. The investigated process shows the immense potential for improving the photocatalytic activity of TiO_2.

References

Aazam, E. S. Visible light photocatalytic degradation of thiophene using Ag-TiO_2/multi-walled carbon nanotubes nanocomposite. *Ceramics International, 40*(5), 6705-6711. (2014).

Askari, M. B., Banizi, Z. T., Seifi, M., Dehaghi, S. B., & Veisi, P. Synthesis of TiO_2 nanoparticles and decorated multi-wall carbon nanotube (MWCNT) with anatase TiO_2 nanoparticles and study of optical properties and structural characterization of TiO_2/MWCNT nanocomposite. *Optik, 149*, 447-454. (2017).

Azmar, A., Subban, R. H. Y., & Winie, T. Improved long-term stability of dye-sensitized solar cell employing PMA/PVAc based gel polymer electrolyte. *Optical Materials, 96*, 109349. (2019).

Chaudhary, D., Singh, S., Vankar, V. D., & Khare, N. A ternary Ag/TiO2/CNT photoanode for efficient photoelectrochemical water splitting under visible light irradiation. *International Journal of Hydrogen Energy, 42*(12), 7826-7835. (2017).

Choudhury, B., & Choudhury, A. Local structure modification and phase transformation of TiO_2 nanoparticles initiated by oxygen defects, grain size, and

annealing temperature. *International Nano Letters, 3*(1), 55. (2013).

de la Flor, M. P., Camarillo, R., Martínez, F., Jiménez, C., Quiles, R., & Rincón, J. Synthesis and characterization of TiO_2/CNT/Pd: An effective sunlight photocatalyst for neonicotinoids degradation. *Journal of Environmental Chemical Engineering, 9*(5), 106278. (2021).

Koo, Y., Littlejohn, G., Collins, B., Yun, Y., Shanov, V. N., Schulz, M., Pai, D., & Sankar, J. Synthesis and characterization of Ag–TiO2–CNT nanoparticle composites with high photocatalytic activity under artificial light. *Composites Part B: Engineering, 57*, 105-111. (2014).

Kubo, M., Taguchi, T., & Shimada, M. Preparation of nanoparticle-embedded thin films by simultaneous feeding of gaseous and solid raw materials in plasma-enhanced chemical vapor deposition process. *Thin Solid Films, 632*, 55-65. (2017).

Siefering, K. L., & Griffin, G. L. Growth Kinetics of CVD TiO2: Influence of Carrier Gas. *Journal of The Electrochemical Society, 137*(4), 1206-1208. (1990).

Šileikaitė, A., Prosyčevas, I., Puišo, J., Juraitis, A., & Guobienė, A. Analysis of silver nanoparticles produced by chemical reduction of silver salt solution. *Journal of Materials Science, 12*(4), 1392-1320. (2006).

Soltanieh, A. M., Khavar, A. H. C., Ganjidoust, H., Mahjoub, A. R., & Khazaee, Z. Plasmon-induced charge separation by Ag nanoparticles between titanium dioxide and MWCNTs for natural sunlight-driven photocatalysis. *Journal of the Iranian Chemical Society*. (2021).

Wang, S., Gong, Q., Zhu, Y., & Liang, J. Preparation and photocatalytic properties of silver nanoparticles loaded on CNTs/TiO_2 composite. *Applied Surface Science, 255*(18), 8063-8066. (2009).

Wang, T., Tang, T., Gao, Y., Chen, Q., Zhang, Z., & Bian, H. Hydrothermal preparation

of Ag-TiO_2-reduced graphene oxide ternary microspheres structure composite for enhancing photocatalytic activity. *Physica E: Low-dimensional Systems and Nanostructures, 112*, 128-136. (2019).

Yu, J. G., Yu, H. G., Cheng, B., Zhou, M. H., & Zhao, X. J. Enhanced photocatalytic activity of TiO_2 powder (P25) by hydrothermal treatment. *Journal of Molecular Catalysis a-Chemical, 253*(1-2), 112-118. (2006).

Zhao, C., Guo, J., Yu, C. L., Zhang, Z. J., Sun, Z., & Piao, X. Q. Fabrication of CNTs-Ag-TiO_2 ternary structure for enhancing visible light photocatalytic degradation of organic dye pollutant. *Materials Chemistry and Physics, 248*, 122873. (2020).

Chapter 3

Ag-Doped TiO_2 Composite Films Prepared Using Aerosol-Assisted, Plasma-Enhanced Chemical Vapor Deposition

3.1 Introduction

In Chapter 2, TiO_2 composite films were fabricated by the addition of an Ag nanoparticle suspension, this process requires the pre-preparation of the nanoparticle mixture. Especially, Ag nanoparticles need to be prepared in advance by co-precipitation from $AgNO_3$ aqueous solution. Thus, the direct supply of silver precursor is considered to be a more straightforward method.

Generally, the reduction of $AgNO_3$ requires the reducing agent. However, Zou *et al.* (2006) found that metal ions can be reduced to their metallic state by plasma treatment. Recently, Gallingani *et al.* (2020) confirmed the aerosol droplets of $AgNO_3$ solution can be reduced by plasma. Therefore, in this study, to increase the process efficiency, $AgNO_3$ was supplied directly. During the process, $AgNO_3$ aqueous solutions were aerosolized and supplied to the PECVD reactor. In the plasma, $AgNO_3$ aerosol droplets were reduced to obtain Ag nanoparticles, and these particles were deposited on the substrate. Simultaneously, the species cracked from TTIP vapor was introduced by He and O_2 to form a TiO_2 film. Notably, the effect of $AgNO_3$ concentration on the morphology and photocatalytic activity of the TiO_2-Ag composite films was investigated.

3.2 Experimental section

3.2.1 Preparation method

The experimental setup for fabricating TiO_2-Ag has been described in Chapter 2. However, different raw material, $AgNO_3$ aqueous solutions instead of solid suspensions, was employed. As a precursor of Ag^+, $AgNO_3$ aqueous solutions with concentrations ranging from 0 to 4 wt% were supplied by a syringe pump. Assisted by a two-fluid nozzle, the aerosol droplets of $AgNO_3$ aqueous solutions were supplied into plasma chamber. The other experimental conditions are followed with Chapter 2. The annealing process is carried out under N_2 atmosphere at 600 °C for 12 hours.

3.3.2 Film characterization

The crystalline of the films was investigated by XRD. The morphologies of the films were observed by SEM and TEM -EDS. The chemical species and their energy states and ratio of contents were confirmed by XPS. The optical properties of the films were investigated using a V-650 spectrophotometer.

3.2.3 Evaluation of photocatalytic activity

The photodegradation of methylene blue (MB) aqueous solution was carried out under UV irradiation. The measurement was conducted in a thermostatically controlled system maintained at 25 °C. The prepared films with MB solution were held in a cuvette and left in the dark for 30 min to reach adsorption equilibrium. A UV light (365 nm, 1407 μW/cm) was employed to initiate the photocatalytic reaction. The absorption spectrum of the samples was recorded every 30 min, and the absorption maximum of MB was converted to the correspond concentration using the Beer-Lambert law. The

percent degradation of MB was calculated as $[(C_0-C_t)/C_0] \times 100\%$, where C_0 and C_t are the concentrations of MB at time $t = 0$ and after irradiation for time t, respectively. Further, the reaction rate constant k was determined by Eq. 3.1.

$$\ln \frac{C_0}{C_t} = kt \quad 3.1$$

3.3 Results and Discussion

3.2.1 Crystalline

The effect of $AgNO_3$ concentration on the crystal structure of the prepared films was investigated by XRD, as shown in Fig. 3.1. JCPDS cards of TiO_2, Ag and SiO_2 were employed as reference. Although different concentrations of $AgNO_3$ aqueous solution were supplied, only anatase phase peaks were observed in all films. The peaks located at 25.82°, 37.53°, 38.34°, 39.16°, 48.56°, 54.44°, and 55.56° correspond to the (101), (103), (004), (112), (200), (105), and (211) planes, respectively. However, it is a challenge to define the Ag peaks in the pattern, which could be attributed to the low content of Ag loading or coincidence with anatase peaks (Shi *et al.*, 2018). In addition, the peak observed at 23° may correspond to the substrate. There are still two weak peaks (35° and 43°) that cannot be identified, which may be attributed to unknown contamination.

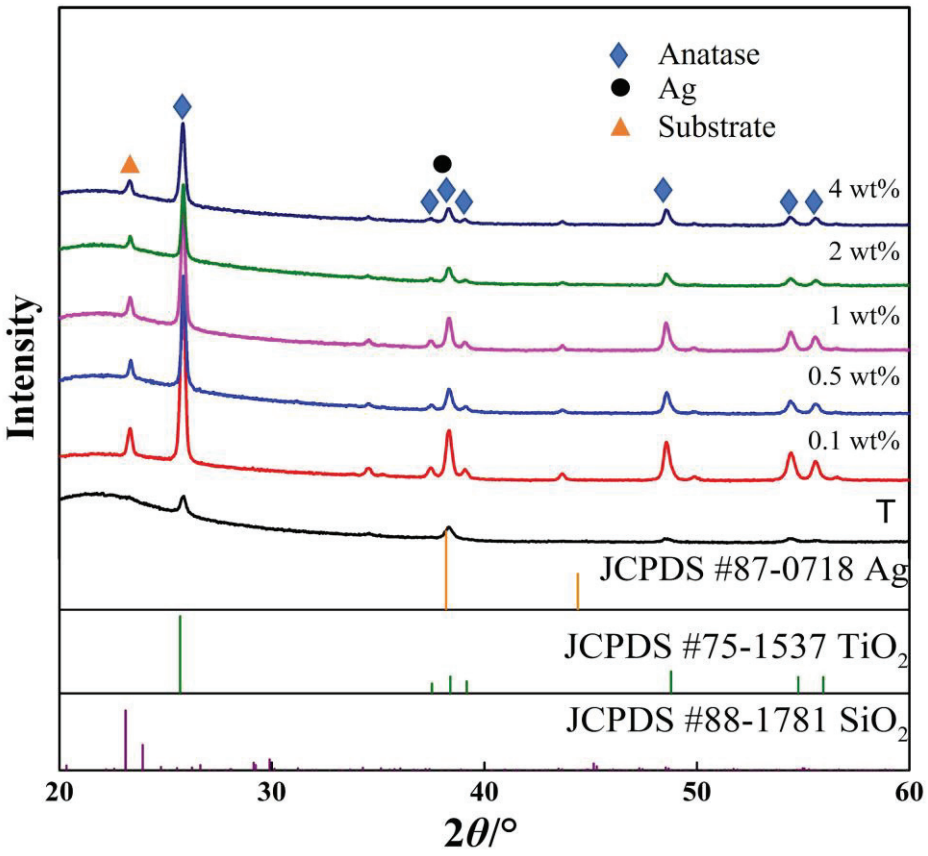

Fig. 3.1 XRD patterns of the pristine TiO_2 film and TiO_2-Ag composite films deposited using different concentrations of $AgNO_3$.

3.3.2 Morphology

The surface and cross section morphologies of the TiO_2-Ag composite films deposited using different $AgNO_3$ concentrations were shown in Fig. 3.2. Fig. 3.2(a) shows a dense surface structure in pristine TiO_2 film. The secondary spherical particles that consist of the aggregation of tiny particles was observed in TiO_2-Ag composite films; these secondary particles show a wide range of sizes. The addition of additives can leads to the formation of agglomerates during process (Chen *et al.*, 2000). In addition, the increasing concentration of $AgNO_3$ resulted in a more severe agglomeration on the surface of the films, as reported previously (Singh *et al.*, 2017; Tomas *et al.*, 2009). Moreover, the tightly packed aggregated particles indicating a good

coverage film was produced by PECVD method. Cross section images were used to determine the layer thickness. The thickness of all the films is roughly 0.7 μm. These results indicate the reproducibility of this process in film deposition.

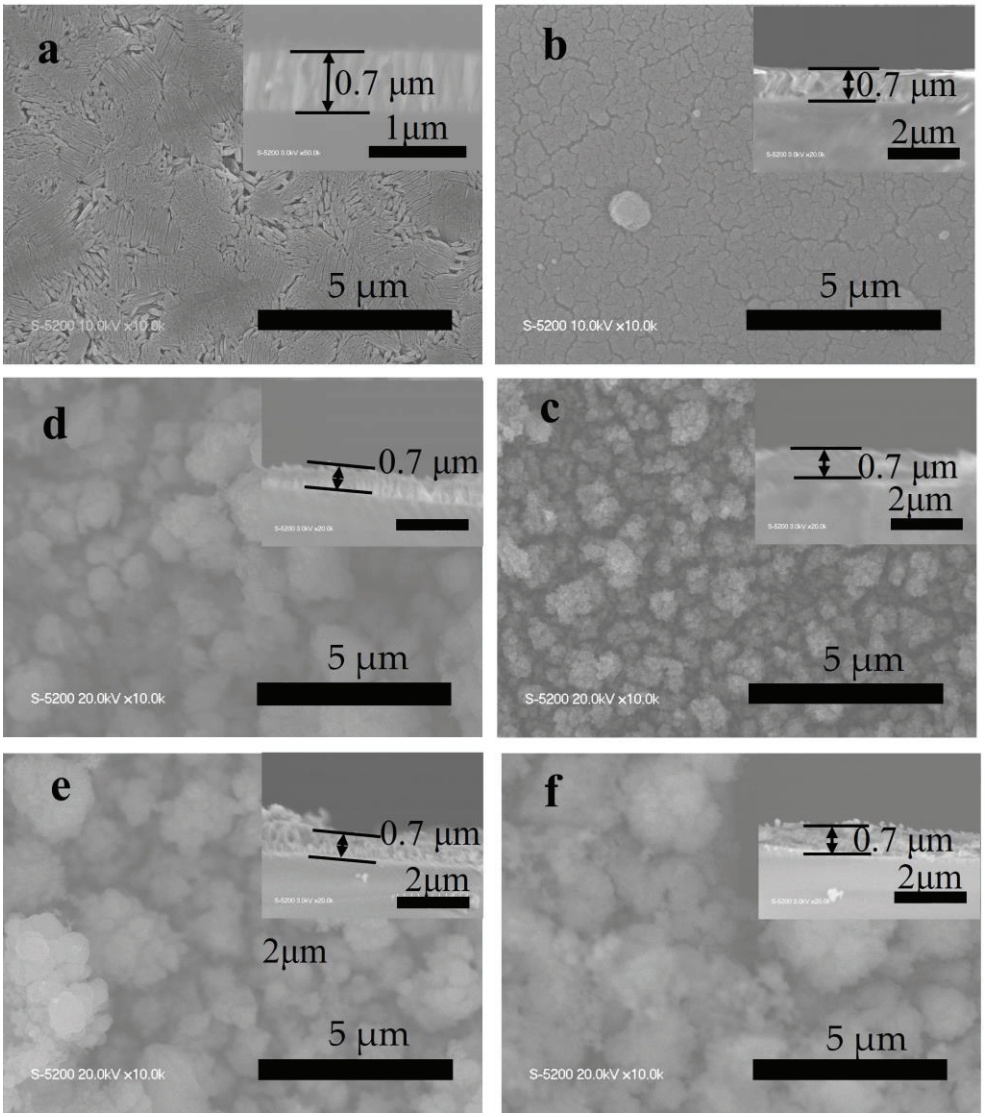

Fig. 3.2. SEM images on the surface view and cross section of (a) pristine TiO_2 film and TiO_2-Ag composite films deposited using different $AgNO_3$ concentrations: (b–f) 0.1, 0.5, 1, 2, and 4 wt.%, respectively.

The samples for TEM-EDS are scraped from the surface of the film using a microgrid. The results reflect only a very small part of the surface of the film. The

Fig.3.3 demonstrates that some very tiny TiO_2 particles were attached to a spherical Ag nanoparticle with 40–60 nm. The large size of the Ag nanoparticles may be the reason for the aggregation on the surface of the film as shown in the SEM images. A high-resolution TEM (HRTEM) images of the region enclosed in a yellow square was shown in Fig. 3.3 (b). The interplanar spacings of 0.35 and 0.24 nm correspond to the (101) plane of anatase and (111) plane of Ag, respectively. In addition,the presence of Ag in the film was also confirmed by EDS analysis.

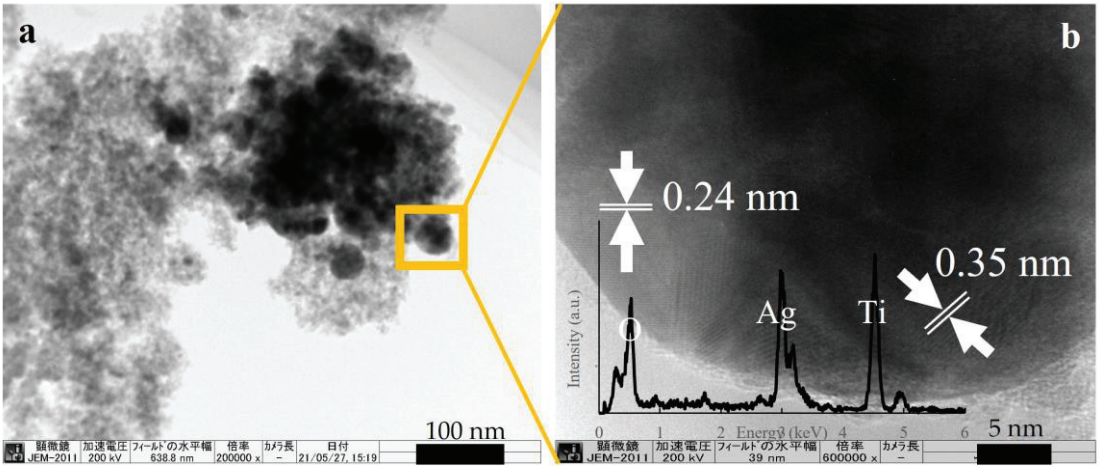

Fig. 3.3. (a) TEM image, (b) HTREM images and the corresponding EDS profile of the region in the yellow square of the TiO_2-Ag (1 wt%) film.

3.3.2 Elements analysis

Next, the chemical species and their oxidation states of the prepared 1 wt% $AgNO_3$-supplied TiO_2-Ag film were performed by XPS measurements. Fig. 3.4 (a) illustrates that the XPS survey profile contains four peaks corresponding to Ti 2p, O 1s, C1s, and Ag 3d. Fig. 3.4 (b) demonstrates the typical metallic Ag spectrum that contains Ag $3d_{5/2}$ (368.2 eV) and Ag $3d_{3/2}$ (374.1 eV) peaks; The doublet separation between the Ti $2p_{1/2}$ (464.7 eV) and $2p_{3/2}$ (459 eV) is 5.7 eV, which is consistent with binding energy

of Ti^{4+} in TiO_2, as shown in Fig. 3.4 (c). The O 1s spectrum was deconvoluted into three peaks at 530.2, 532.2, and 534.3 eV (Fig. 3.4 (d)), corresponding to the lattice oxygen in TiO_2, dissociated oxygen or hydroxyl-like group and absorbed water (Demirci *et al.*, 2016; Yu *et al.*, 2003), respectively.

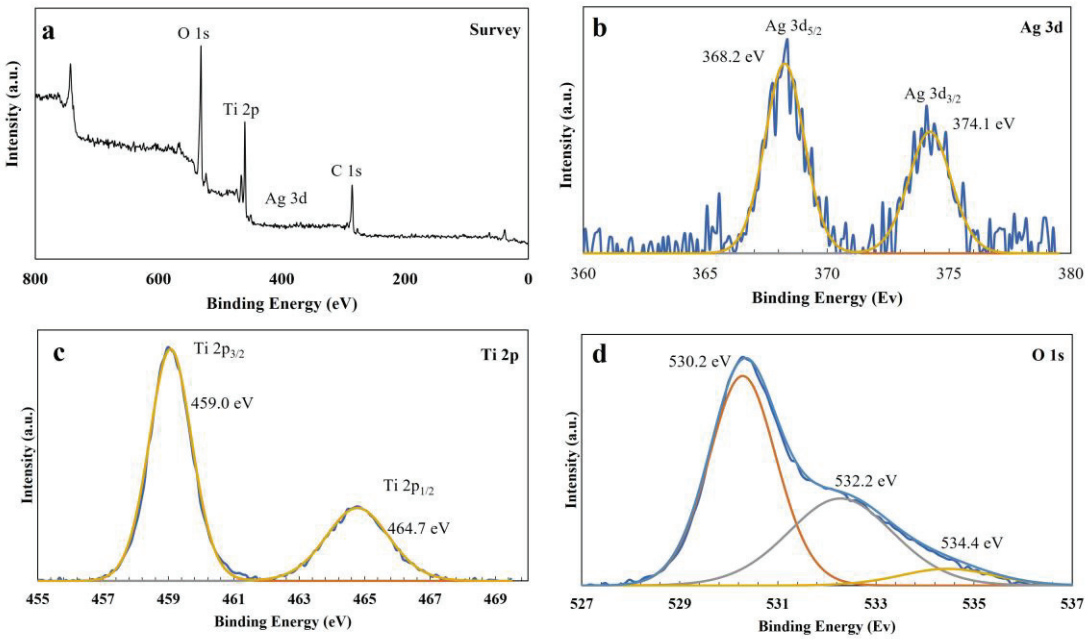

Fig. 3.4 XPS profiles of the TiO_2-Ag (1 wt.%) film: (a) Survey, (b) Ag 3d, (c) Ti 2p, and (d) O 1s spectra.

In addition, the ratio of Ag/Ti in raw materials was estimated by the method mentioned in Chapter 2. The ratio of Ag/Ti in the films was estimated by the peak area of Ag 3d and Ti 2p, the results were shown in Table 3.1. It is mentioned that the accuracy of the results deserves further study, since the thickness of the film interferes with the accuracy of XPS measurement. The results show that increasing $AgNO_3$ concentration results in an increase of Ag/Ti ratio. This result suggests that the concentration of the raw material had a direct impact on the Ag content in the films.

Table 3.1 Ratio of Ag/Ti content in the T-C-A film

Film	Ag/Ti in the raw materials	Ag/Ti in the films
TiO_2-Ag (0.1 wt%)	0.0694	0.0290
TiO_2-Ag (0.5 wt%)	0.347	0.0423
TiO_2-Ag (1 wt%)	0.694	0.0872
TiO_2-Ag (2 wt%)	1.389	0.104
TiO_2-Ag (4 wt%)	2.777	0.255

3.2.4 Optical properties

Fig. 3.5 (a) demonstrate the UV-vis spectra of the pristine TiO_2 film and the TiO_2-Ag composite films prepared using different concentrations of $AgNO_3$ (0.1–4 wt%). The threshold wavelength of pristine TiO_2 film is approximately 358 nm, which only fall in the range of UV light. The increase of the concentration of $AgNO_3$ result in a redshift of the absorption edges of the TiO_2-Ag composite films; that is, they shift toward the visible region. It suggests that the appearance of Ag can significantly improve the visible-light absorption of TiO_2. The bandgap energy was calculated as described in Chapter 2. The plots of $(\alpha h\upsilon)^2$ versus $h\upsilon$ plots for different samples are shown in Fig. 3.5 (b). The bandgap values were estimated by the tintercept of the tangent to the plot, and the results are listed in Table 3.2. The bandgap of pristine TiO_2 was 3.54 eV, while those of the TiO_2-Ag composite films decreased from 3.21 to 2.61 eV with increasing concentration of $AgNO_3$. The difference in the bandgaps of these samples probably originates from the different surface microstructures and compositions (Yu *et al.*, 2005).

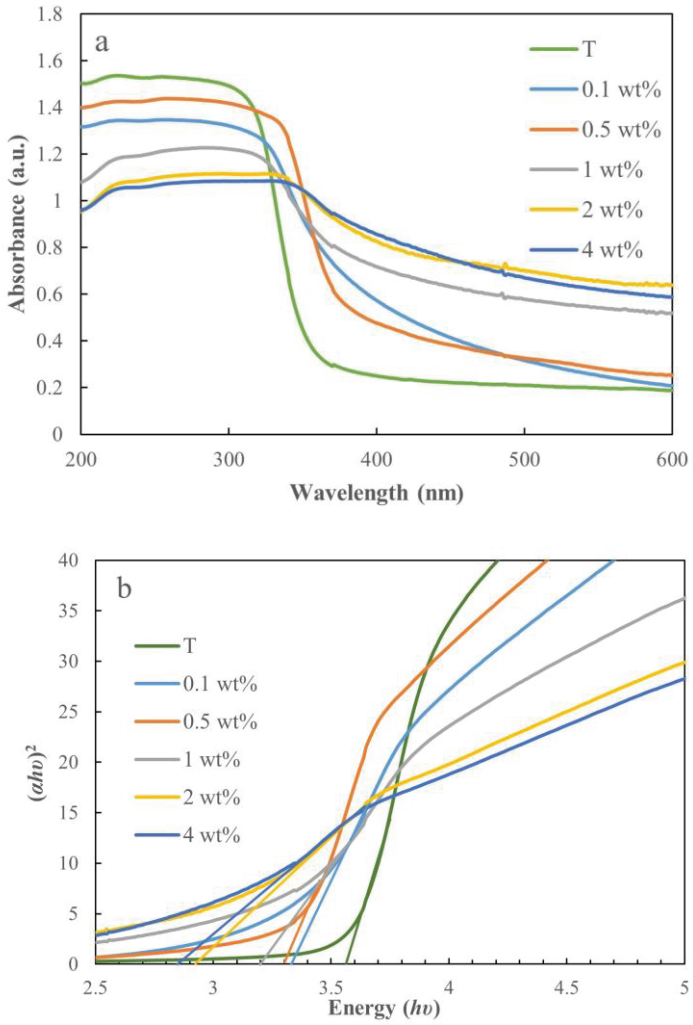

Fig. 3.5 (a) Absorbance spectra of the pristine TiO_2 film (T) and TiO_2-Ag composite films deposited using $AgNO_3$ concentrations of 0.1–4 wt.%. (b) Plot of $(\alpha h\upsilon)^2$ versus photon energy ($h\upsilon$) of the prepared films.

Table 3.2 Bandgap energies (E_g) of the films.

Film	Threshold wavelength (nm)	E_g (eV)
Pristine TiO_2	350	3.54
TiO_2-Ag (0.1 wt%)	386	3.21
TiO_2-Ag (0.5 wt%)	389	3.18
TiO_2-Ag (1 wt%)	410	3.02
TiO_2-Ag (2 wt%)	442	2.80
TiO_2-Ag (4 wt%)	457	2.61

3.3.5 Photocatalytic activity

The photocatalytic activities of the samples were evaluated based on the decomposition of MB under UV irradiation. Fig. 3.6 (a) shows the degradation of MB (C_t/C_0) with respect to time (t) for the different films under UV-light irradiation. All the films exhibited photocatalytic activities under the same conditions. However, the presence of Ag nanoparticles increased the photocatalytic activities of the TiO_2-Ag composite films, comparing to that of the pristine TiO_2 film. A possible mechanism has been introduced in Chapter 1. The photodegradation efficiency of MB degradation in 3 h was calculated using the formula $[(C_0\text{-}C_{180})/C_0] \times 100\%$, where C_0 and C_{180} are the initial concentrations and concentrations after 3 hours irradiation, respectively. The TiO_2-Ag (1 wt%) composite film demonstrated the best photocatalytic activity, resulting in an MB degradation of around 41%, while the pure TiO_2 film displayed an activity of just about 11%. Furthermore, we prepared the ln (C_t/C_0) versus t plot (Fig. 3.6 (b)) to obtain the corresponding rate constant k (Fig. 3.6 (c)) from the slope of the fitting curve. The resulting k values further demonstrate that the TiO_2-Ag (1 wt%) composite film exhibits the maximum photocatalytic activity, which was almost 1.7

times that of pristine TiO_2. However, an excessive $AgNO_3$ concentration resulted in lower activities. Researchers believe that: (1) the excess addition of Ag may increase the reflection of UV irradiation; (2) the negatively charged Ag can attract the positive holes. The high content of Ag increased the probability of trapping holes, thus making Ag a new recombination center and affecting photocatalytic ability. (Ko *et al.*, 2011).

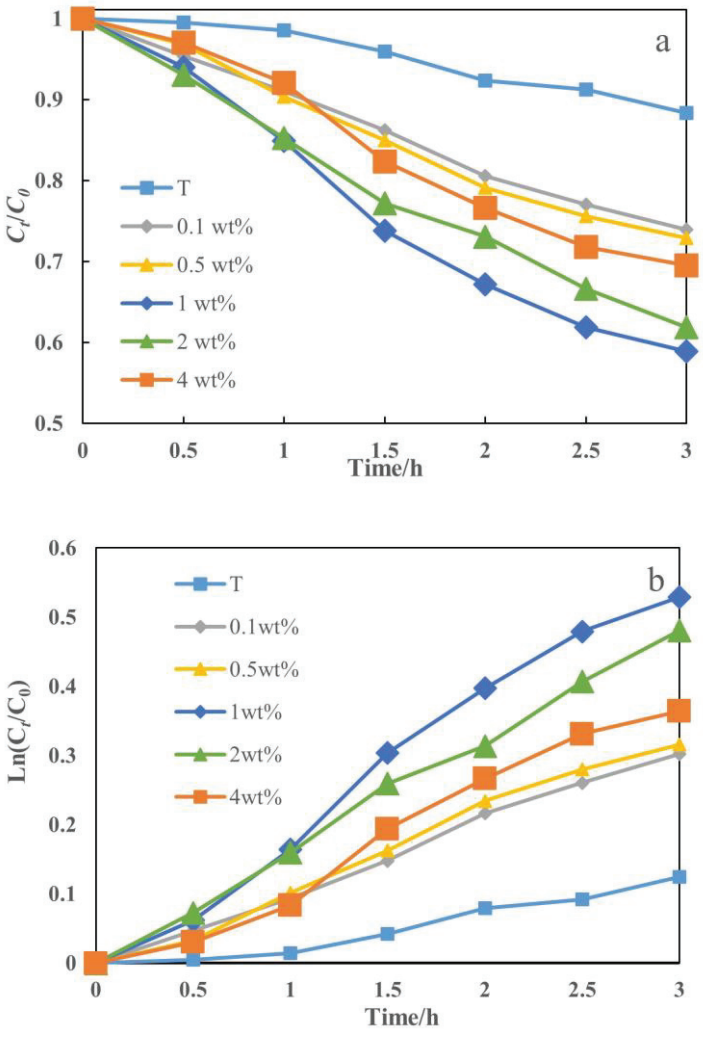

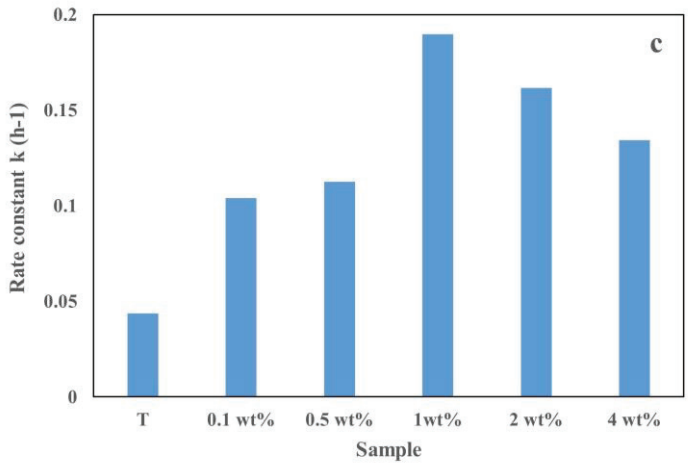

Fig. 3.6 Photocatalytic activity for the degradation of MB over different films: (a) degradation with respect to time, (b) ln (C_t/C_0) versus to time plot, and (c) rate constants degradation for various samples.

Furthermore, the photocatalytic activity of the films was also carried out by degradation of R6G under visible light. However, there is no significant difference in photocatalytic activity between films. Therefore, the photocatalytic ability of thin films on different dyes needs further study. In addition, comparing to the photocatalytic activity of T-C-A in chapter 1, T-A films in this chapter exhibit better photocatalytic activities under UV light irradiation. However, T-C-A film in chapter 1 exhibits better photocatalytic activity under simulated solar light irradiation.

3.4 Conclusions

In this work, TiO_2-Ag composite films were successfully prepared using AgNO3 as raw material. XRD patterns revealed the typical anatase phase of the film annealed at 600 °C. The existence of metallic Ag in the composite film was confirmed. The presence of Ag nanoparticles significantly altered the morphology and bandgap of the TiO_2-Ag composite films. The TiO_2-Ag composite films exhibit improved photocatalytic activities as compared to pristine TiO_2. Among them, the film prepared using 1 wt% $AgNO_3$ exhibits a best photocatalytic activity. Overall, the results

demonstrate a successful process for preparing TiO_2-Ag composite film. Compared to Chapter 2, supplying $AgNO_3$ aqueous solution instead of Ag nanoparticles ensures a simple procedure.

References

Chen, C. Y., & Tuan, W. H. Effect of silver on the sintering and grain-growth behavior of barium titanate. *Journal of the American Ceramic Society, 83*(12), 2988-2992. (2000).

Demirci, S., Dikici, T., Yurddaskal, M., Gultekin, S., Toparli, M., & Celik, E. Synthesis and characterization of Ag doped TiO_2 heterojunction films and their photocatalytic performances. *Applied Surface Science, 390*, 591-601. (2016).

Gallingani, T., Abuyazid, N. H., Colombo, V., Gherardi, M., & Sankaran, R. M. Online ion mobility spectrometry of nanoparticle formation by non-thermal plasma conversion of metal salts in liquid aerosol droplets. *Journal of Aerosol Science, 150*, 105631. (2020).

Ko, S., Banerjee, C. K., & Sankar, J. Photochemical synthesis and photocatalytic activity in simulated solar light of nanosized Ag doped TiO_2 nanoparticle composite. *Composites, Part B, 42*(3), 579-583. (2011).

Shi, H., Yu, Y., Zhang, Y., Feng, X., Zhao, X., Tan, H., Khan, S. U., Li, Y., & Wang, E. Polyoxometalate/TiO_2/Ag composite nanofibers with enhanced photocatalytic performance under visible light. *Applied Catalysis B: Environmental, 221*, 280-289. (2018).

Singh, J., Sahu, K., Pandey, A., Kumar, M., Ghosh, T., Satpati, B., Som, T., Varma, S., Avasthi, D. K., & Mohapatra, S. Atom beam sputtered Ag-TiO2 plasmonic nanocomposite thin films for photocatalytic applications. *Applied Surface Science, 411*, 347-354. (2017).

Tomas, S. A., Luna-Resendis, A., Cortes-Cuautli, L. C., & Jacinto, D. Optical and morphological characterization of photocatalytic TiO_2 thin films doped with silver. *Thin Solid Films, 518*(4), 1337-1340. (2009).

Yu, J.-G., Yu, H.-G., Cheng, B., Zhao, X.-J., Yu, J. C., & Ho, W.-K. The effect of calcination temperature on the surface microstructure and photocatalytic activity of TiO_2 thin films prepared by liquid phase deposition. *The Journal of Physical Chemistry B, 107*(50), 13871-13879. (2003).

Yu, J. G., Xiong, J. F., Cheng, B., & Liu, S. W. Fabrication and characterization of Ag-TiO_2 multiphase nanocomposite thin films with enhanced photocatalytic activity. *Applied Catalysis B-Environmental, 60*(3-4), 211-221. (2005).

Zou, J.-J., Zhang, Y.-p., & Liu, C.-J. Reduction of supported noble-metal ions using glow discharge plasma. *Langmuir, 22*(26), 11388-11394. (2006).

Chapter 4

Preparation of Super-hydrophobic and Photocatalytic TiO_2/PDMS Films by Plasma-Enhanced Chemical Vapor Deposition

4.1 Introduction

Super-hydrophobic surface has attracted considerable attention in recent years for its wide application, such as self-cleaning, oil-water separation, anticorrosion. Super-hydrophobic surface can deal with some contaminants in a wash process. The common strategies to form super-hydrophobic surfaces are create rough surface by low surface energy material; or combinate the low surface energy materials to rough surface. Polydimethylsiloxane (PDMS) with typical hydrophobicity, chemical stability and low-density surface property has been widely used in super-hydrophobic surface. However, super-hydrophobic coatings with long-term stability and sufficiently resistant to outdoor contamination needs to be developed (Xu *et al.*, 2018). Recently, scientists have developed the super-hydrophobic surfaces that consists of photocatalysis. These composites maintain good performance even in harsh environments. Titanium dioxide (TiO_2) is the most studied photocatalysis for its unique physicochemical properties, commercial availability and inexpensiveness.

TiO_2/PDMS composites for super-hydrophobic surface were prepared by different process. However, most of the literatures focused on the liquid phase method. These methods always related to a complex step. Thus, develop a simple method is available for fabrication of TiO_2/PDMS thin film. PECVD method is a relatively simple method that allows different materials to deposit simultaneously. To my knowledge, only few

reports prepare the TiO_2/PDMS composite in PECVD method. However, PECVD method has been reported to produce the PDMS films. Some researchers prepared the PDMS film by using hexamethyldisiloxane as the precursor, followed by a polymerization in plasma reactor (Pryce *et al.*, 2000). Lee *et al.* (2009) described a SiO_x thin film deposited from PDMS/curing agent in a O_2/H_2 plasma. Thongrom *et al.* (2018) demonstrate a simpler film deposition process by PECVD which supply the PDMS directly.

In this study, TiO_2/PDMS composite films was prepared by supplying PDMS directly via PECVD method. It is worth mentioning that no curing agent is used in this process. The vaporized PDMS and TTIP were fed into a plasma reactor. The morphology and component of the films was confirmed. The obtained films exhibited both super-hydrophobicity and photocatalytic activity.

4.2 Experimental Section

4.2.1 Experimental setup

The experimental setup for fabricate TiO_2/PDMS include two material supplying system as shown in Fig. 4.1. The PDMS (Sigma-Aldrich, St. Louis, U. S., average Mn 550~) was vaporized in a steel bubbler under 40° and carried by He gas. The other parts are same as described in Chapter 2 and 3. TiO_2/PDMS composite was deposited on a silicon substrate under different conditions.

Condition A: The conditions for preparation TiO_2 film have been confirmed in Chapter 2 and 3. Thus, TiO_2/PDMS is prepared based on this condition. The composite film was obtained by supplying PDMS (20 sccm) and TTIP (50 sccm) simultaneously. The effect of additional PDMS on the structure and properties of TiO_2 thin films was investigated.

Condition B: The PDMS films with super-hydrophobicity were deposited in a certain condition. The TiO_2/PDMS is prepared based on this condition. During the process, different TTIP flow rate (50 and 200 sccm) was supplied with PDMS simultaneously. The effect of additional TiO_2 on the structure and properties of PDMS films was investigated. The detail of this condition was listed in Table 4.1.

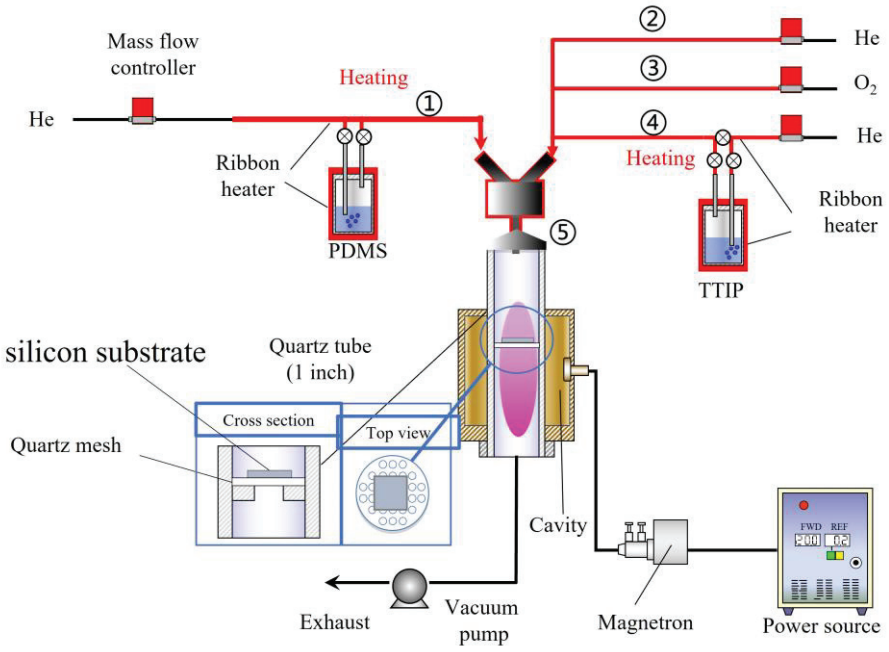

Fig. 4.1 Experimental setup of PECVD for preparing TiO_2/PDMS composite.

Table 4.1 The detail of Condition B

Experiment factor	①	②	③	④	⑤
Gas flow rate (sccm)	200	400	50	50/200	700/850
Heating temperature (°C)	40	80	80	45	80
Plasma power (W)			140		
Deposition time (min)			2		

4.2.2 Characterization

The morphology of prepared film was determined by SEM and TEM-EDX. The chemical bonds of the film were defined by XPS and FTIR. The crystal structure of the film was determined by XRD.

4.2.3 Evaluation of film properties.

The photocatalytic activity was performed by degradation of MB under UV light. A same procedure as described in Chapter 2 and 3 was performed for photocatalytic activity.

The super-hydrophobicity was determined by water contact angle. A 2 μL water droplet was kept on the film surface and recorded by a digital microscope (ViewTer-500UV, 3R Group. Co. Ltd, Fukuoka, Japan). The water contact angle was estimated by using software ImageJ. The water contact angle of the film was recorded before and after photocatalytic test.

4.3 Results and discussion

4.3.1 Film prepared under Condition A

4.3.2.1 Morphology

Fig. 4.2 (a) and (c) show the surface structure of the as-prepared films. Fig. 4.2 (b) and (d) show the cross-section morphology of the as-prepared films. It is obvious that both the surface and cross-section structure between TiO_2 and TiO_2-PDMS composite are totally different. The TiO_2 film consists of nanosized columnar grains and exhibits a relative flat surface, which has been reported in previous study (Kubo *et al.*, 2017). However, when introduced with PDMS, the columnar structure disappeared and

replaced by an impressive rough surface. The rough surface consists of huge secondary particles formed by the aggregation of tiny particles, as shown in Fig 4.2 (c). The shape of these secondary particles is corresponding to the “mountains-liked” morphology, as observed in cross-section morphology (Fig. 4.2 (d)). The hierarchical structure increased the roughness of surface, which is beneficial for hydrophobicity. The TiO_2 layer thickness is approximately 1μm and the TiO_2-PDMS films shows an increased thick layer approximately 8 μm.

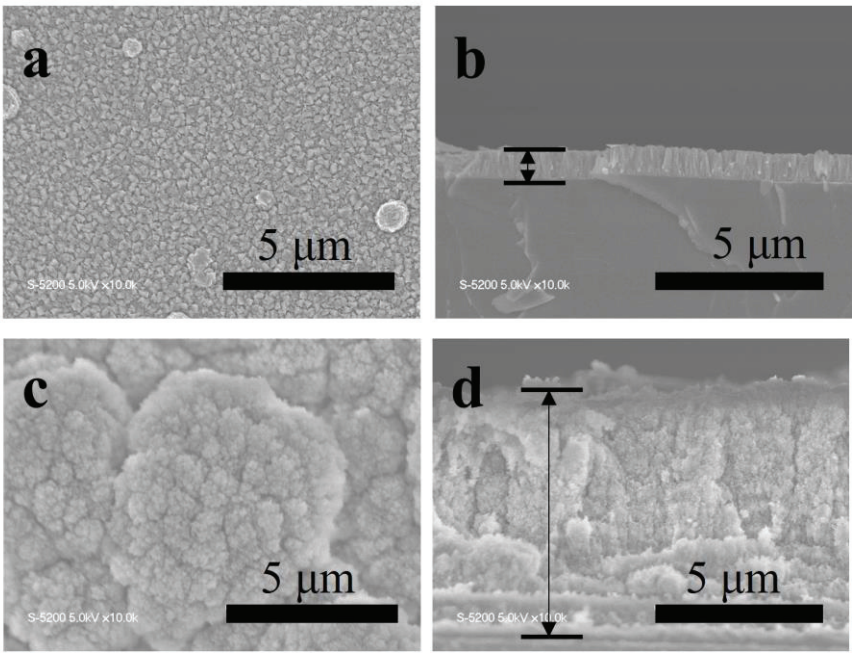

Fig. 4.2 SEM images of the prepared films. Surface morphologies of (a) TiO_2 and (c) TiO_2-PDMS. Cross sectional morphologies of (b) TiO_2 and (d) TiO_2-PDMS.

TEM-EDS is performed to analyze the composite structure in more detail. A TEM grid was employed to collect some powder form the film surface, which was subsequently investigated by TEM-EDS. Both Fig. 4.3 (a) and Fig 43 (c) are collected from the same TiO_2-PDMS composite. In Fig. 4.3 (a), only the powder with aggregation of tiny particles was observed. These particles were analyzed by EDS (Fig. 4.3 (b)), and

the results revealed the existence of a large amount of Si and a small amount of Ti. Fig. 4.3 (c) contains two different component structure, as shown in Fig. 4.3 (d) and (e). Fig 4.3 (d) depicts the aggregation of tiny particles which are almost the same components with the Fig. 4.3 (a). However, the columnar structure is mainly consisting of Ti, as shown in Fig. 4.3 (e).

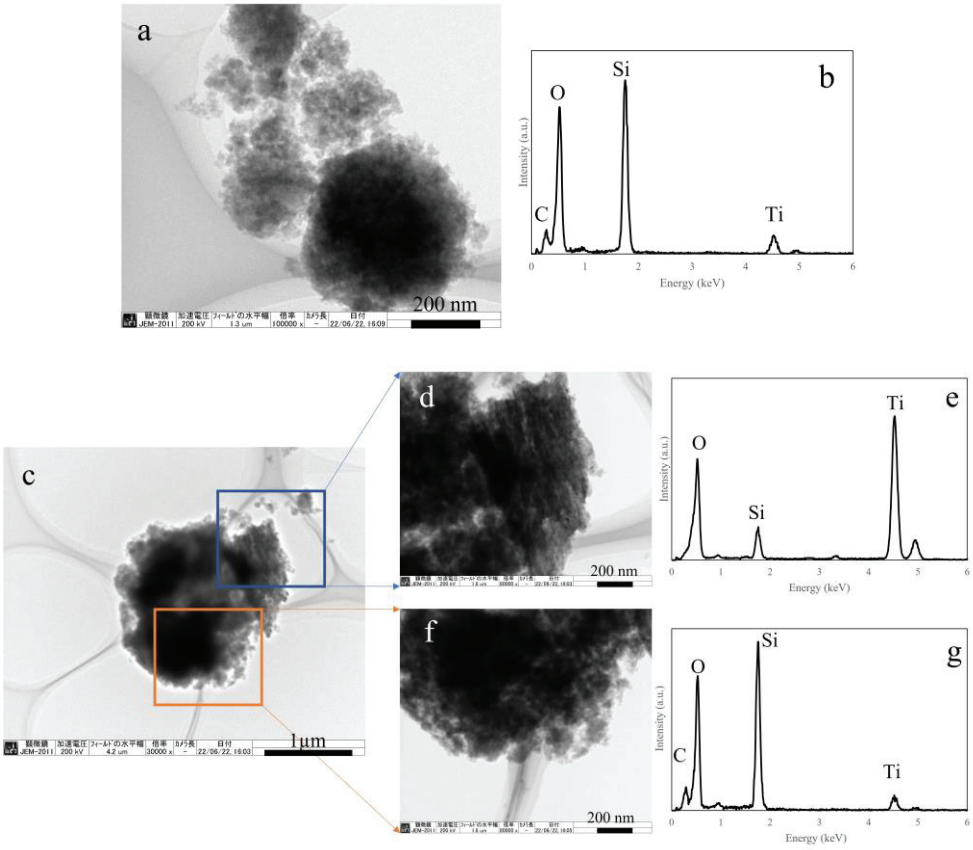

Fig. 4.3 TEM images of the prepared TiO_2/PDMS composite films. The structure of aggregation of tiny particles (a) and the corresponding EDS profile (b). The structure consists of aggregation tiny particles and columnar particles (c); The high magnification images (d) and the corresponding EDS profile (e); The high magnification images (f) and the corresponding EDS profile (g).

4.3.2.2 Molecular structure

The molecular structure of as-prepared TiO_2 film and as-prepared TiO_2-PDMS composite film was investigated by FTIR. The PDMS raw material was also performed as a reference. The obtained results were demonstrated in Fig. 4.4. The pattern of TiO_2-PDMS was compared with that of PDMS raw material. The peaks at 3446 cm^{-1} and 1637 cm^{-1} correspond to the stretching vibration of the surface-absorbed water molecules and O-H groups of samples respectively (Shao *et al.*, 2015)The absorption peak around 2964 cm^{-1} corresponds to vibration mode of the C-H stretching; The deformation of the CH_3 group leads to the absorption peak at 1398 cm^{-1}. The absorption peak at 1261 cm^{-1} is attributed to the vibration mode of Si-CH_3. The two adjacent peaks between 1100 cm^{-1} and 1000 cm^{-1} present the vibration mode of the Si-O-Si stretching (Tavares *et al.*, 2014). Another peak that corresponding to vibration mode of the asymmetric Si-O-Si stretching is located at 804 cm^{-1}. Compared to the pattern of PDMS raw material, the characteristic peak at 945 cm^{-1} presents the Si-OH or Si-O-Ti, which may suggests the formation of a three-dimensional structure with interconnected inorganic and organic component (Novotná *et al.*, 2008). In addition, the adjacent peaks between 1100 cm^{-1} and 1000 cm^{-1} transferred to a single peak at 1095 cm^{-1}, which indicates that the structure of Si-O-Si cm^{-1} network was formed. This particular spectrum suggests that the Si atoms may be bonded with more than two O atoms that involve in a three-dimensional structure (Liu *et al.*, 2015). Moreover, the relative intensity of the Si-C peak at 1261 cm^{-1} and CH_3 cm^{-1} peaks at 2964 cm^{-1} were decreased significantly, which may be attributed to the removal of methyl side groups in plasma (Pryce *et al.*, 2000) before the formation of Si-O-Si crosslink network. These results may indicate a complex crosslink structure was formed between PDMS and TiO_2. In addition, the methyl group plays an important role in super-hydrophobicity. Thus, the

structure containing the methyl group is desired.

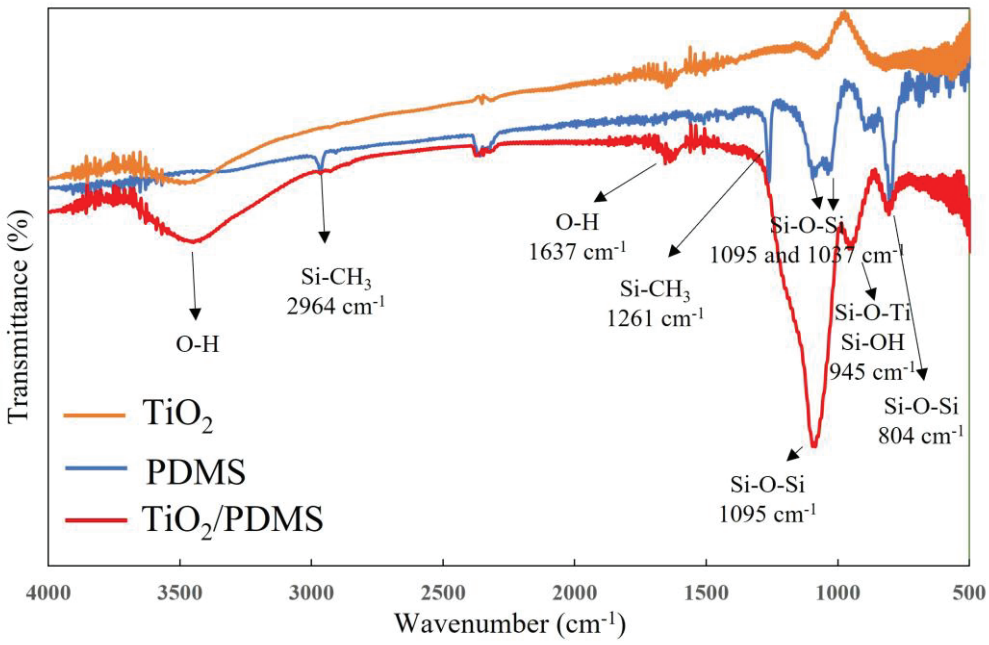

Fig. 4.4 FTIR spectrum of TiO_2, raw PDMS and TiO_2/PDMS composite films.

4.3.2.2 Elements states

The surface composition and chemical structures of as-prepared TiO_2/PDMS composite film were examined by XPS, and the results are presented in Fig.4.5. The peaks corresponding to Ti 2p, O 1s, and Si 2p are observed in the survey spectrum of TiO_2 and TiO_2/PDMS films, as shown in Fig. 4.5 (a). The Si 2p existence in TiO_2 film may be attributed to the substrate. Comparted to TiO_2 film, it is obviously that the relative intensity of Ti 2p in composite films decreased a lot. The possible reasons may be the addition of PDMS diluted the concentration of Ti during deposition, or too thick layer influence the XPS results since the XPS can only detect the approximately 1 um of the composite film. The high-resolution spectra of the Ti 2p and O 1s was shown in Fig. 4.5 (b-e). The doublet separation between the Ti $2p_{1/2}$ and $2p_{3/2}$ is 5.7 eV, which is consistent with the standard binding energy of Ti^{4+} in TiO_2, as shown in Fig. 4.5 (b) and

(d). In addition, the doublet peaks centered at 459.1 and 464.8 shifted to 459.6 and 465.3, respectively. It may be caused by the formation of Ti-O-Si (Ding *et al.*, 2021). The O 1s peak in TiO_2 spectrum consist of three components: Ti-O (530.5 eV), hydroxyl groups OH (531.8 eV), and absorbed water (532.6 eV) as shown in Fig. 4.5 (c). The O 1s peak in TiO_2/PDMS spectrum can be resolved into four peaks, Ti-O (529.6 eV), Ti-O-Si (531.4 eV), Si-O-Si (532.0 eV), absorbed water (533 eV) (Lung *et al.*, 2015), as shown in Fig. 4.5 (e). These results confirmed the formation of Ti-O-Si. And indicates the composite film with crosslink structure.

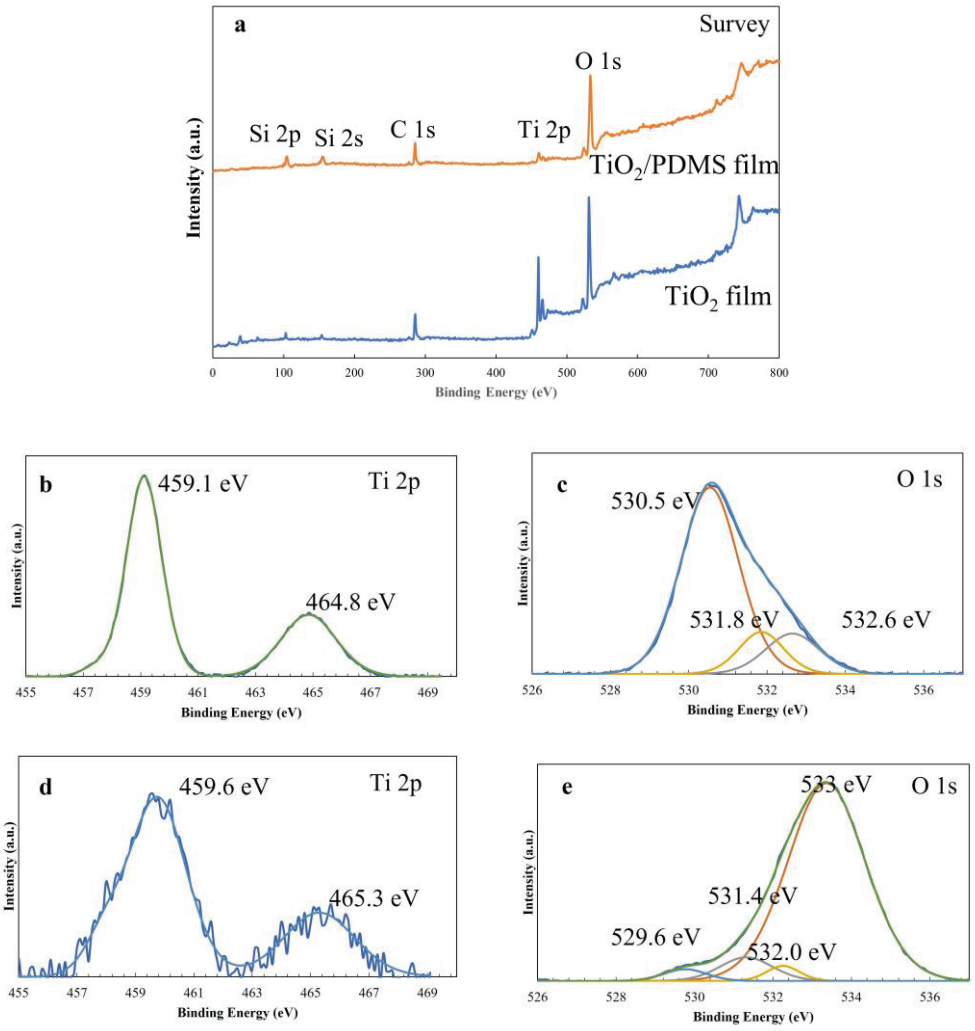

Fig. 4.5 XPS profiles of the TiO_2 and TiO_2/PDMS film: (a) Survey, (b) and (d) Ti 2p, (c) and (e) O 1s spectra.

4.3.2.4 Crystalline

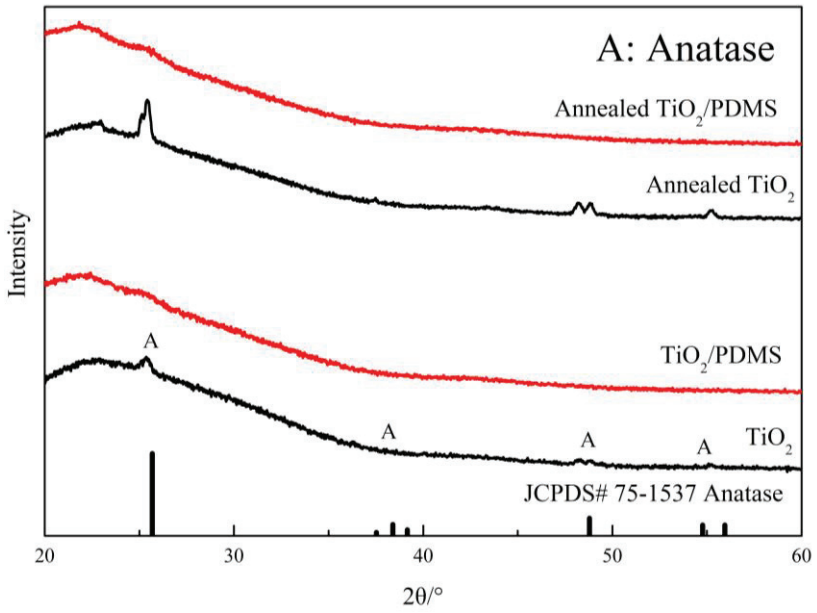

Fig. 4.6 XRD patterns of as prepared and after annealed TiO_2 film and TiO_2/PDMS composite films.

The crystalline phases of as prepared TiO_2 and TiO_2/PDMS composite films and the films annealed at 300 ℃ were determined by XRD as shown in Fig. 4.6. The as-prepared TiO_2 pattern exhibits a weak peak which is attributed to the anatase phase. However, it is observed that, the supplying of PDMS may decrease the growth and crystallization of TiO_2 particles during deposition. Li et al considered the addition of Si into TiO_2 films can hinder the formation of stable nuclei larger than the critical size. During the position process, silica atoms can prevent the diffusion of Ti atoms therefore delay the nucleation-growth of Ti crystallites (Li *et al.*, 2016). Generally, the TiO_2 film fabricated in out method is amorphous and it exhibits enhanced crystallinity after annealing. In this study, after the films annealed at 300℃, the sharper peaks appeared in TiO_2 pattern indicates that the annealing at this temperature is effective for

crystallization. However, TiO_2/PDMS composite are still amorphous. Novotná *et al.* (2008) believe that the highly dispersed SiO_2 which from PDMS decomposition inhibited the crystallization of TiO_2. Neves *et al.* (2020) also reported the same phenomenon when calcinate the TiO_2/PDMS mixture at a temperature beyond the thermal stability of PDMS. Therefore, the thermal stability of products needs to be carried out in my future work.

4.3.2.6 Water contact angle

A Digital Microscope was employed to record the water droplet contacts with the film surface. The water contact angle was estimated by the captured picture. The results are shown in Fig. 4.7. TiO_2 film shows a typical hydrophilic property (Fig. 4.7(a)), while TiO_2/PDMS shows the super-hydrophobic property with water contact angle approximately 157° (Fig. 4.7(b)).

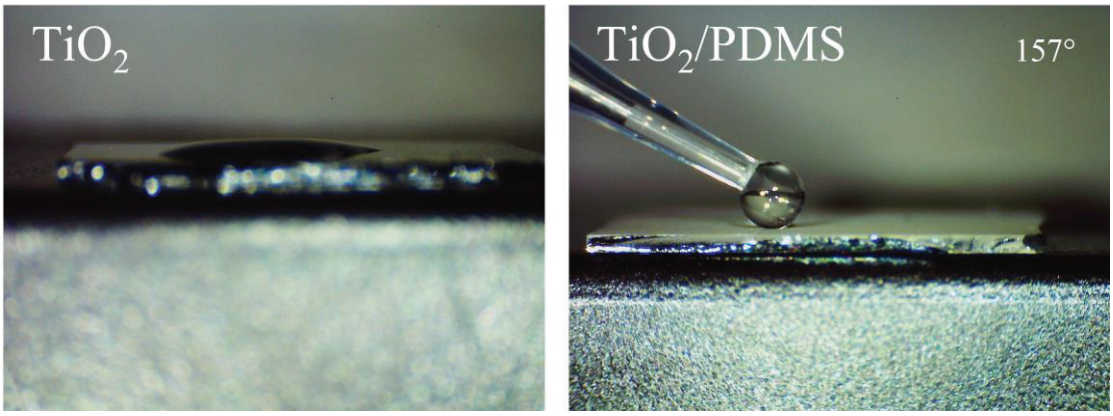

Fig. 4.7 Water contact angle of TiO_2 and TiO_2/PDMS film before photocatalytic activity test.

4.3.2.5 Photocatalytic activity

The photocatalytic activities of the samples were evaluated based on the

decomposition of MB under UV irradiation. Fig. 4.8 shows the degradation of MB (C_t/C_0) with respect to time (t) for the different films under UV-light irradiation. All the films exhibited photocatalytic activities under the same conditions. TiO_2/PDMS composite film shows almost same photocatalytic activity with TiO_2 film within 6 hours. In addition, the TiO_2/PDMS composite film yielding an MB degradation of approximately 29.3 %, whereas the pristine TiO_2 film showed an activity of approximately 29.0%.

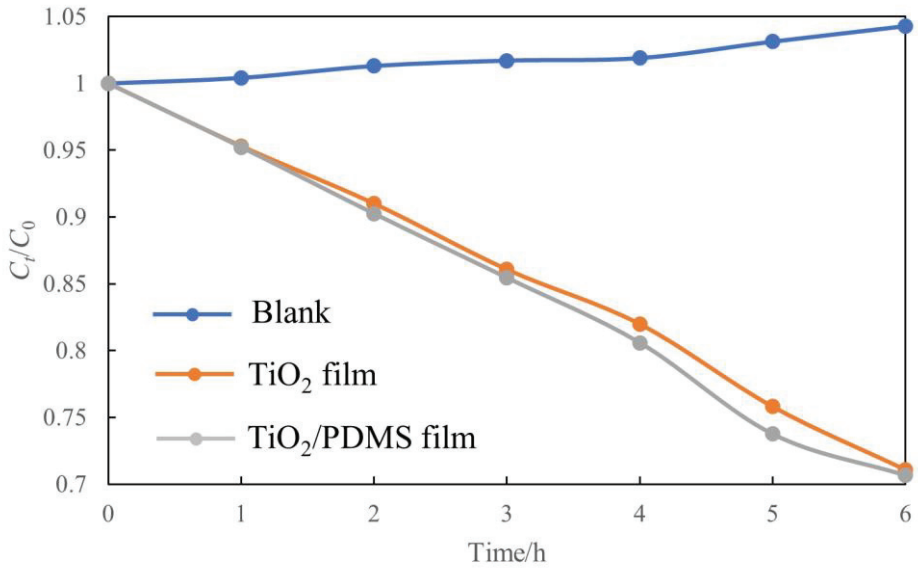

Fig. 4.8 Photocatalytic activity for the degradation of MB (C_0-C_t) with respect to time t over different films.

After photocatalytic test, the water contact angle was measured again. Unfortunately, the some of the composite films lost their super-hydrophobicity. In order to understand this phenomenon, the morphology and molecular structure of the film after photocatalytic activity test needs to be analysis again.

4.3.1 Film prepared under condition B

4.3.1.1 Morphology

Fig 4.9 shows the fabricated PDMS film with water contact angle approximately of 160°. This result proved the PDMS can be deposited as a super-hydrophobic film. The morphology of TiO_2/PDMS composite film was demonstrated in Fig. 4.10. The composite film with a relative rough surface was confirmed and the structure barely affected by varying flow rates of TTIP, as shown in Fig. 4.10 (a) and (b). Fig. 4.10 (c-f) shows the results of TEM-EDS analysis. The appeared peaks corresponding to Si and O are originated form PDMS. However, there are no peaks corresponding to Ti when TTIP flow rate is 50 sccm. When the TTIP flow rate increased from 50 to 200 sccm, the Ti was observed in the EDS spectrum. In addition, the thickness of the TiO2/PDMS composite film prepared by 200 sccm TTIP is approximately 3.5 μm. These results confirmed the composition of TiO_2/PDMS film and indicates a different structure compared to Fig. 4.2.

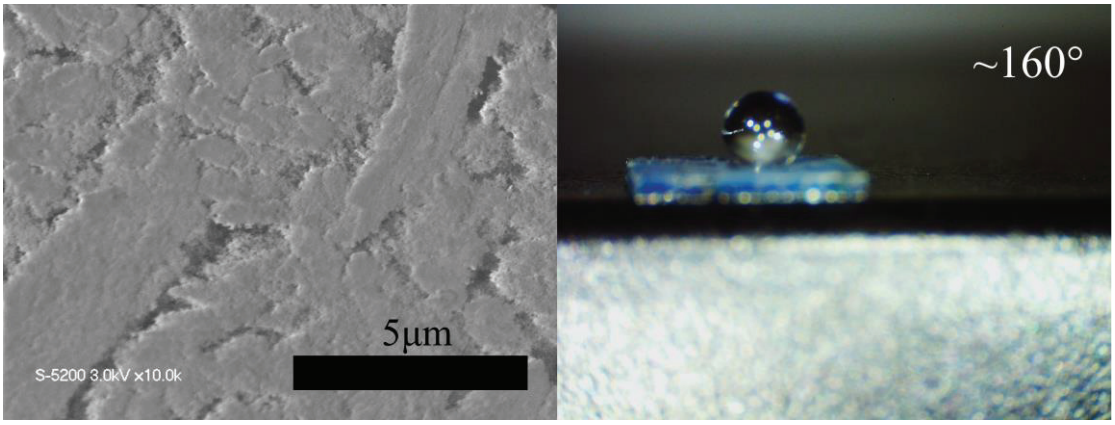

Fig. 4.9 The surface morphology of PDMS film and image of water contact angle.

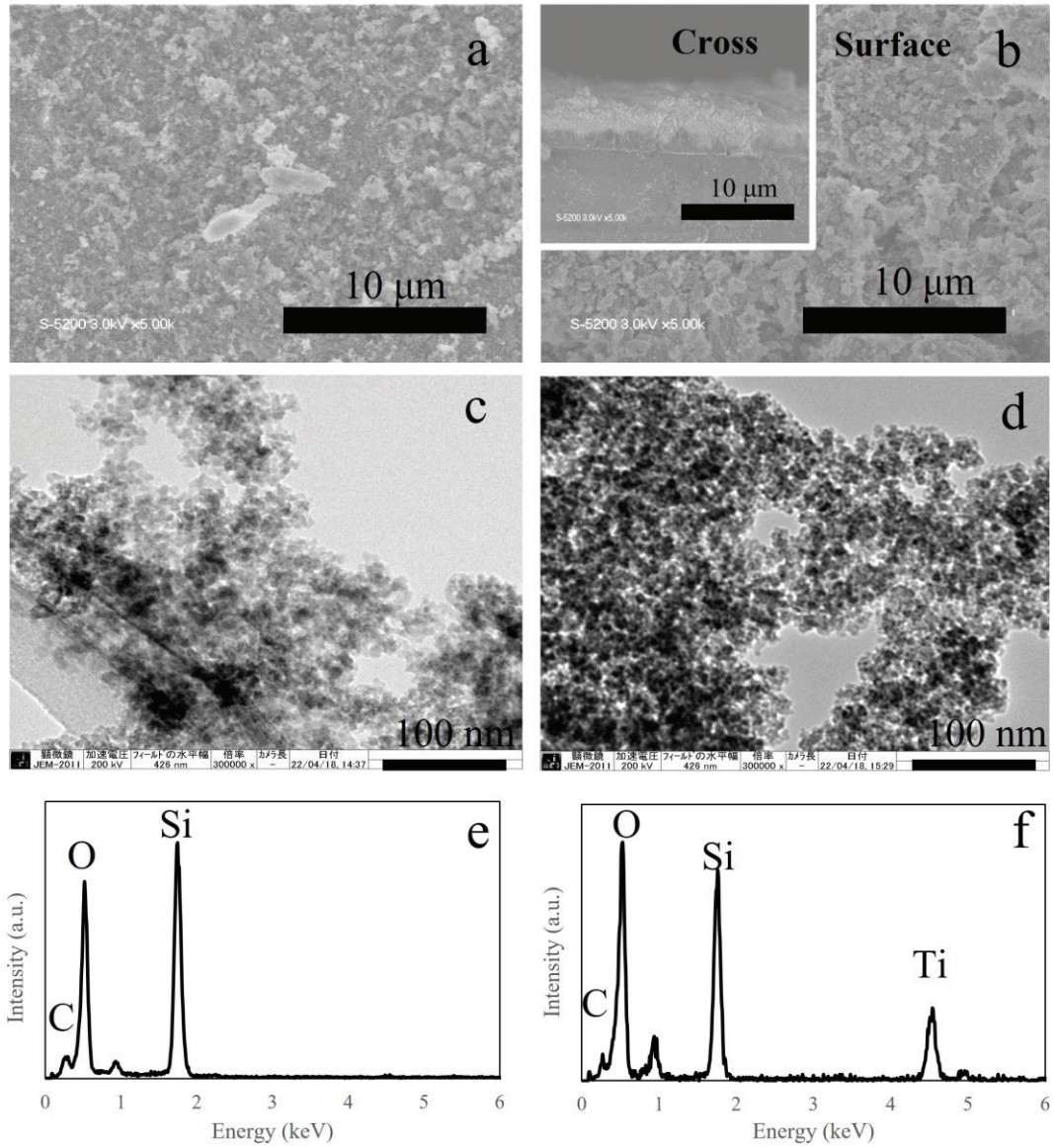

Fig. 4.10 The SEM, TEM and EDS of TiO_2/PDMS fabricated by different TTIP flow rate: 50 sccm (a) (c) and (e); 200sccm (b), (d) and (f).

4.3.1.2 Elements states

XPS analysis was employed to determine the chemical species and chemical states in TiO_2/PDMS composite prepared by TTIP with flow rate 200 sccm. The results were shown in Fig. 4.11. The survey spectrum (Fig. 4.11 (a)) illustrates contains the peaks corresponding to O 1s, Ti 2p, C1s, Si 2s and Si 2p. Among them, Fig. 4.11 (b) demonstrates the typical Ti 2p spectrum, with the 5.7 eV between two peaks, which

indicates the existence of TiO_2 in the composite film. The O 1s spectrum could be deconvoluted into three peaks at 529.9, 532.0, and 533.3 eV (Fig. 4.11 (c)), corresponding to the Ti-O band, Si-O-Si and absorbed water, respectively. Additionally, the absence of Ti-O-Si, which confirmed a different molecular structure comparing to the film prepared under Condition A.

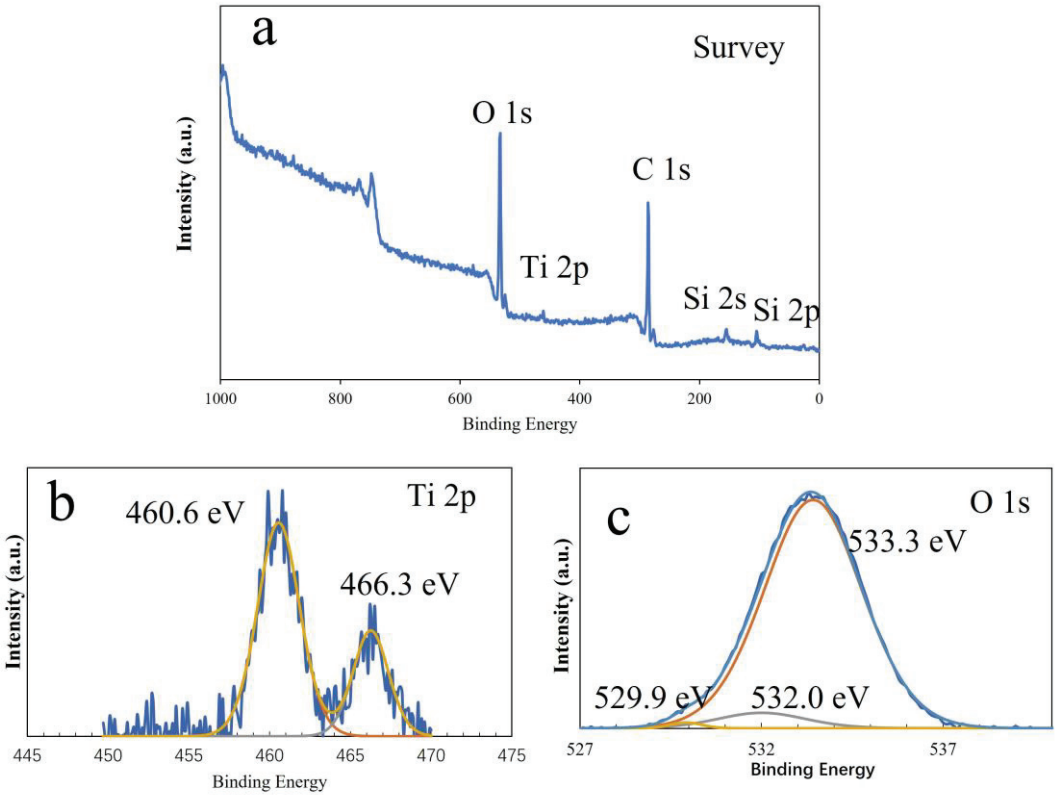

Fig. 4.11 The XPS spectrum of TiO_2/PDMS composite film: (a) survey spectrum, (b) Ti 2p spectrum and (c) O 1s spectrum.

4.3.2.3 Crystalline

The XRD pattern of as-prepared TiO_2/PDMS prepared by TTIP with 200 sccm is show in Fig. 4.12. The broaden peak at around 23° which is attributed to the amorphous SiO_2, and the peaks appeared at around 28°, 31° and 47 ° may be attributed to the Si.

There are no peaks corresponding to TiO_2, which may be attributed to the low content of TiO_2 or TiO_2 exists in an amorphous phase.

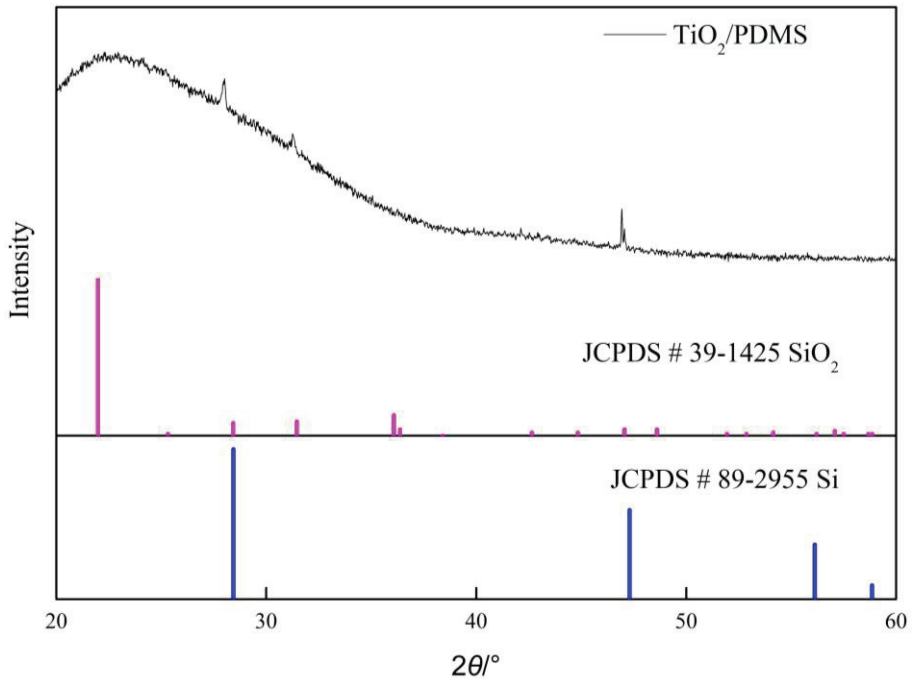

Fig. 4.12 The XRD pattern of as-prepared TiO_2/PDMS composite film.

4.3.1.3 Photocatalytic activity.

The photocatalytic activities of the samples were evaluated based on the decomposition of MB under UV irradiation. Fig. 4.13 shows the degradation of MB (C_t/C_0) with respect to time (t) for the different films under UV-light irradiation. PDMS film and TiO_2/PDMS prepared by TTIP with flow rate 50 sccm cannot degrade the MB, which is attributed to the absence of TiO_2. When increase the TTIP flow rate to 200 sccm, the obtained film exhibits the photocatalytic activity. The percent MB degradation by the different films after 6 h of irradiation was calculated using the formula $[(C_0\text{-}C_t)/C_0] \times 100\%$, where C_0 and C_t are the concentrations of MB at time t = 0 and after irradiation for time t, respectively. The TiO_2/PDMS composite film prepared

by TTIP with 200 sccm flow rate shows a photocatalytic activity which degrades 16% MB after 6 hours irradiation.

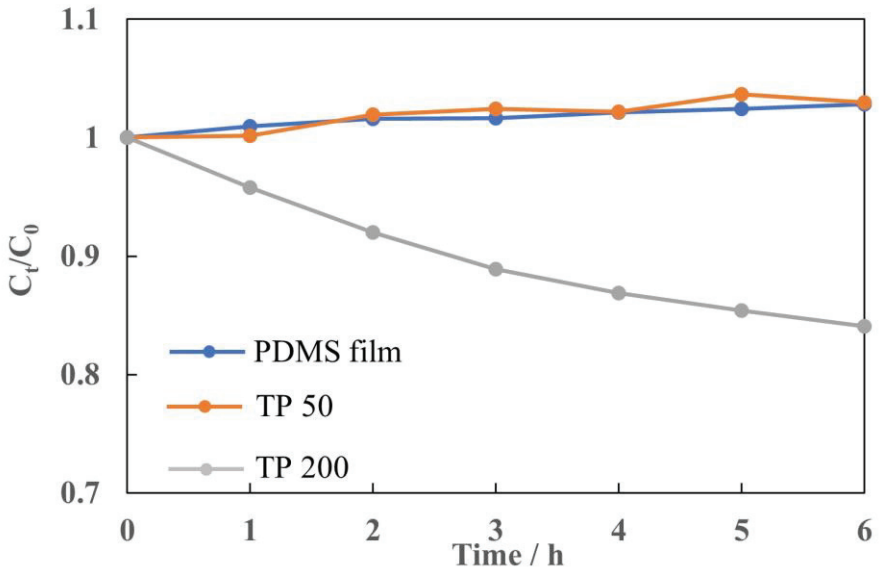

Fig. 4.13 Photocatalytic activity for the degradation of MB (C_0-C_t) with respect to time t over PDMS film, TiO_2/PDMS composite prepared by different TTIP flow rare: 50 sccm (TP 50); 200 sccm (TP 200).

4.3.2.7 Water contact angle

The water contact angle of the different film before and after photocatalytic test was estimated, the results are shown in Fig. 4.14. PDMS and TiO_2/PDMS film possess a super-hydrophobicity and this property is kept after photocatalytic activity test, that is, the film resistant to UV irradiation. The

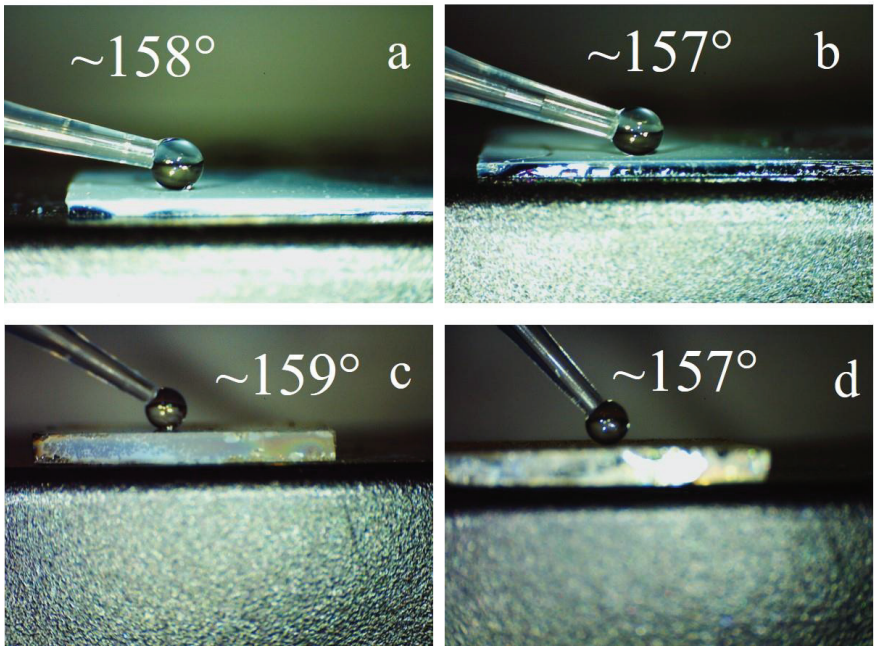

Fig. 4.14 Water contact angle of TiO_2 and TiO_2/PDMS film before photocatalytic test (a) and (c); and after photocatalytic test (b) and (d).

4.4 Conclusions

In this work, the TiO_2/PDMS composite films were prepared by PECVD method in two different experimental conditions. Under condition A, the addition of PDMS changed the morphology of the TiO_2 entirely and inhibit the crystal growth of TiO_2 heavily. The formation of Si-O-Ti indicates an interconnection between inorganic and organic component. The photocatalytic activity of the composite film decomposes approximately 29% MB, which is almost same with TiO_2 film. However, most of the samples lost the super-hydrophobicity after photocatalytic test. The potential reason will be studied in my future work. Under condition B, the presence of TiO_2 in composite film was confirmed, and it helps the film decomposing 16% MB under UV light irradiation. In addition, the durable super-hydrophobicity after UV-irradiation of the composite film was proved. Thus, the films obtained under condition B are more compliant with the expectation.

References

Ding, X., Liu, R., Zhao, J., Hu, J., Guan, H., & Tong, Y. Photocatalytic TiO_2/PDMS coating to drive self-cleaning: a facile approach for anti-stain silicone rubber surfaces. *Polymer Bulletin*. (2021).

Kubo, M., Taguchi, T., & Shimada, M. Preparation of nanoparticle-embedded thin films by simultaneous feeding of gaseous and solid raw materials in plasma-enhanced chemical vapor deposition process. *Thin Solid Films, 632*, 55-65. (2017).

Lee, J., H., Kim, Y. S., Oh, J. S., Kyung, S. J., Lim, J. T., & Yeom, G. Y. Characteristics of SiOx thin film deposited by atmospheric pressure plasma-enhanced chemical vapor deposition using PDMS/O_2/He. *Journal of The Electrochemical Society, 156*(7), D248. (2009).

Li, D., Elisabeth, S., Granier, A., Carette, M., Goullet, A., & Landesman, J. P. Structural and optical properties of PECVD TiO_2–SiO_2 mixed oxide films for optical applications. *Plasma Processes and Polymers, 13*(9), 918-928. (2016).

Liu, G., Hung, W.-S., Shen, J., Li, Q., Huang, Y.-H., Jin, W., Lee, K.-R., & Lai, J.-Y. Mixed matrix membranes with molecular-interaction-driven tunable free volumes for efficient bio-fuel recovery. *Journal of materials chemistry A, 3*(8), 4510-4521. (2015).

Lung, C. Y. K., Heinonen, M., Kukk, E., & Matinlinna, J. P. Surface modification of titanium with thermally treated polydimethylsiloxane coating and the effect on resin to titanium adhesion. *Surface and Interface Analysis, 47*(1), 105-112. (2015).

Neves, J. C., Mohallem, N. D. S., & Viana, M. M. Polydimethylsiloxanes-modified TiO_2 coatings: The role of structural, morphological and optical characteristics in a self-cleaning surface. *Ceramics International, 46*(8, Part B), 11606-11616. (2020).

Novotná, P., Zita, J., Krýsa, J., Kalousek, V., & Rathouský, J. Two-component transparent TiO_2/SiO_2 and TiO_2/PDMS films as efficient photocatalysts for environmental cleaning. *Applied Catalysis B: Environmental, 79*(2), 179-185. (2008).

Pryce, L., G., H., Edell, D. J., & Gleason, K. K. Pulsed-PECVD Films from Hexamethylcyclotrisiloxane for Use as Insulating Biomaterials. *Chemistry of Materials, 12*(11), 3488-3494. (2000).

Shao, P., Tian, J., Zhao, Z., Shi, W., Gao, S., & Cui, F. Amorphous TiO_2 doped with carbon for visible light photodegradation of rhodamine B and 4-chlorophenol. *Applied Surface Science, 324*, 35-43. (2015).

Tavares, M. T. S., Santos, A. S. F., Santos, I. M. G., Silva, M. R. S., Bomio, M. R. D., Longo, E., Paskocimas, C. A., & Motta, F. V. TiO_2/PDMS nanocomposites for use on self-cleaning surfaces. *Surface and Coatings Technology, 239*, 16-19. (2014).

Thongrom, S., Tirawanichakul, Y., Munsit, N., & Deangngam, C. One-step microwave plasma enhanced chemical vapor deposition (MW-PECVD) for transparent superhydrophobic surface. *IOP Conference Series: Materials Science and Engineering, 311*, 012015. (2018).

Xu, F., Wang, T., Bohling, J., Maurice, A. M., Chen, H., Wu, L., & Zhou, S. Extended hydrophobicity and self-cleaning performance of waterborne PDMS/TiO_2 nanocomposite coatings under accelerated laboratory and outdoor exposure testing. *Journal of Coatings Technology and Research, 15*(5), 1025-1034. (2018).

Chapter 5

Summary

5.1 Conclusions

In this thesis, different materials were employed to fabricate TiO_2-based composite films by PECVD method. By introducing these foreign materials, the TiO_2-based composite exhibit the expected improvement of photocatalytic activity and super-hydrophobicity. The conclusion of this dissertation can be described as following.

The TiO_2-CNT-Ag ternary films were successfully prepared utilizing CNTs and Ag solid mixture via PECVD method. During the process, solid nanoparticles were deposited simultaneously with TiO_2 onto the substrate. This process resulted in the nanoparticle-embedded structure, which was proved by the morphology observation. The addition of CNTs and Ag does not affect the film thickness nor the crystal structure. However, these particles influenced the surface roughness and band gap energy of the TiO_2. Furthermore, the addition of CNT and Ag significantly improved the photocatalytic activity of the prepared films.

To simplify the operation process, $AgNO_3$ aqueous solutions was supplied directly instead of being prepared as silver particles. The influence of the $AgNO_3$ concentration on the structure and photocatalytic activity of the TiO_2-Ag composite films was investigated. Results present that the addition of AgNO3 aqueous solution during preparation process caused a secondary particle on the film surface, which can be attributed to the formation of aggravated Ag nanoparticles. The addition of Ag nanoparticles significantly altered the morphology of the films owing to particle aggregation. Notably, the appearance of the Ag nanoparticles significantly decreased

the bandgap energy of the composite. In addition, appropriate $AgNO_3$ concentration (1wt% in this dissertation) leads to a higher photocatalytic activity of the films.

The TiO_2/PDMS composite film with photocatalytic activity and super-hydrophobicity was fabricated by PECVD method. Two different experimental conditions were applied for generating composite films. The different conditions resulted in different film structures and properties. The film obtained under condition A exhibits a relatively better photocatalytic activity, but unsatisfied super-hydrophobicity. The condition B yields a film with durable super-hydrophobicity, and it also exhibits the photocatalytic activity. Compared to condition A, the condition B is more conducive to the synthesis of films with super-hydrophobicity and photocatalytic activity.

Overall, the investigated process exhibited immense potential for use in the preparation of films with different materials.

5.2 Suggestions for further study

TiO_2-based composite films were successfully prepared by utilizing different raw materials via PECVD method. In response to the shortcomings of the work, the suggestion for future work can be conclude as follows:

The particle size of Ag in preparation of TiO_2-CNT-Ag ternary composite film is lack of investigation. Co-precipitation method may produce different size of Ag nanoparticles. The particle size can also significantly influence the structure and photocatalytic activity of TiO_2 film. Thus, prepare different size of Ag nanoparticle may be helpful to fabricate films with better photocatalytic activity. The use of different carbon nanotubes also deserves to be considered, as we all know the different properties between multi-walled CNT and single walled CNT.

The detail of reduction of $AgNO_3$ in plasma should be classified in future works. A controllable process for fabrication Ag nanoparticle is useful for many applications. This also facilitates the application of other metallic materials. The photocatalytic activity of composite film under visible light needs to be investigated.

The reason for the absence of hydrophobicity of the films after photocatalysis needs to be investigated, which may be helpful in preparing films with better properties. The effects of experiment factor on film structure and properties need to be explore in more detail. In addition, the composite film shows a unique structure, which may lead to different properties.

The other nanoparticles like graphene, copper as well as some ionic solution can be employed as raw material. In addition, not only TiO_2 but also other support materials like ZnO, SnO_2, WO_3 films can be deposited by PECVD method. Overall, in accordance with certain requirements, different raw material can be applied to co-deposition by PECVD.

Appendix I：List of Figures

Appendix II：List of Tables

Appendix III：List of Publications

The dissertation was partly written based on the following publications.

1. **Lang, J.**; Takahashi, K.; Kubo, M.; Shimada, M. Ag-Doped TiO_2 Composite Films Prepared Using Aerosol-Assisted, Plasma-Enhanced Chemical Vapor Deposition. *Catalysts* **2022**, *12*, 365.
2. **Lang, J.**; Takahashi, K.; Kubo, M.; Shimada, M. Preparation of TiO_2-CNT-Ag Ternary Composite Film with Enhanced Photocatalytic Activity via Plasma-Enhanced Chemical Vapor Deposition. *Catalysts* ***2022***, 12, 508.

Presentation in Conferences

1. **Lang, J.**; Takahashi, K.; Kubo, M.; Shimada, M. Photocatalytic activity and preparation of TiO_2-CNT-Ag ternary thin films via aerosol-assisted and plasma-enhanced chemical vapor deposition. *European Aerosol Conference* (*EAC 2021*), EAC2021_AT P3-9_131_Lang.pdf, virtual conference. Aug. 30–Sep. 3, **2021**.
2. **Lang, J**.; Takahashi, K.; Kubo, M.; Shimada, M. Preparation of Ag-embedded TiO_2 film by reducing metal ions via plasma-enhanced chemical vapor deposition. *SCEJ* (*The society of Chemical Engineers, Japan*) *87th Annual Meeting*, L321, Mar. 16–18, **2022**.
3. **Lang, J.**; Takahashi, K.; Kubo, M.; Shimada, M. Ag-Doped TiO_2 Composite films prepared using Aerosol-assisted, plasma-enhanced chemical vapor deposition. *12th Asian Aerosol Conference* (*AAC*) *2022*, fb1930, June 12–16, **2022**.